Center Industrial Diagnostics

Analysis of the dynamic behaviour of rotating disk-like structures submerged and confined

Doctoral Thesis

Presented to the Department of Fluid Mechanics of the

Technical University of Catalonia (UPC)

Presented by

Alexandre Presas Batllo

Under the supervision of

Professor Dr. Eng. Eduard Egusquiza i Estevez

and **Dr. Eng. Carme Valero Ferrando**

September, 2014

Barcelona

ACKNOWLEDGEMENT

Firstly, I want to express my gratitude to my thesis advisors Professor Dr. Eng. Eduard Egusquiza and Dr. Eng. Carme Valero for their time, support and advices in the crucial moments of my investigation. Without their continuous help, this work could not be possible.

Thanks to Eng. David Valentin for our discussions during the last part of my thesis which have helped to analyze the results obtained in this investigation. His work has made possible to contrast experimental results obtained with numerical simulation.

Thanks to Dr. Eng. Xingxing Huang for his friendship and help in the first years of my stay in the CDIF.

I want to have a special mention also for Paloma Ferrer and David Castañer of the CDIF for their continuous help during my thesis.

Thanks also to the other members of the CDIF and of the department for their kind treatment with me: Dr. Eng. Alfredo Guardo, Dr. Eng. Esteve Jou, Dr. Eng. Xavier Escaler and Professor Dr. Eng. Eugeni Valencia.

This project would not have been possible without the financial and human support of VOITH Hydro. I want to express my gratitude to Eng. Ulrich Seidel (Head of R&D Basic Development) and his team for our helpful meetings during these years. Their conclusions and advices after the meetings have been one of the main inspirations of this work.

Finally I want to mention the gratitude to my family, my girlfriend Laura and friends for their company during these years. Special thanks to my friends Eng. Angel Claramunt and Eng. Santiago Claramunt, with whom I shared very good and special moments at the begin of my engineering studies.

Barcelona, September 2014 **Alexandre Presas Batllo**

SUMMARY

The analysis of the dynamic behaviour of rotating turbomachinery components is of relevant interest to avoid damages or fatigue problems in these parts. To determine the dynamic behaviour of a part of a structure it is necessary to perform an analysis of the free vibration of this part and a study of the excitation characteristic. The free vibration analysis (modal analysis) determines the natural frequencies and mode shapes of the structure. The excitation analysis gives the frequency content and the shape of the excitation.

Hydraulic runners are very complex structures that are submerged and confined inside a casing. Particularly pump-turbine runners behave as disk-like structures at their first modes of vibration and they are excited with the well known Rotor-Stator Interaction (RSI) when they are under operation. In order to study the effect of the rotation, the confinement and the excitation on the dynamic behaviour of the structure in a systematic and clear way, a simplified model is needed. For this reason, in this thesis the dynamic behaviour of a rotating disk submerged in water and confined inside a casing has been analyzed analytically, experimentally and contrasted with simulation.

Firstly, an analytical model for the analysis of the dynamic behaviour is presented. The natural frequencies and mode shapes of a rotating disk considering the surrounding flow are analytically determined with a simplified model. Also the response of the disk with different excitation patterns that simulates the RSI is analyzed. Finally the transmission from the rotating to the stationary frame is discussed.

For the experimental analysis a rotating disk test rig has been developed. It consists of a rotating disk submerged and confined inside a casing. The disk has been excited from the rotating frame with piezoelectric patches (PZT) and with a special impact device. The response of the disk has been measured simultaneously from the rotating and from the stationary frame.

The first several natural frequencies and mode shapes of the disk when it rotates in air and in water have been obtained in the rotating frame with miniature accelerometers screwed on the disk and contrasted with the analytical model presented and with a numerical FEM simulation. Only the diametrical modes, which are the most relevant and similar to the real hydraulic runners, have been considered in this study.

The disk has been excited with several rotating excitation patterns that simulate the real RSI. The dynamic behaviour of the disk due to these excitation patterns has been determined experimentally and contrasted with the analytical model.

Finally, the analysis of the transmission from the rotating to the stationary frame has been performed. The natural frequencies and mode shapes of the disk have been detected with several kinds of sensors placed on the stationary frame.

RESUM

L'anàlisi del comportament dinàmic de components rotatius en turbomàquines és de gran interès per a evitar danys o problemes de fatiga en aquestes parts. Per determinar el comportament dinàmic d'una part d'una estructura és necessari dur a terme una anàlisi de la vibració lliure d'aquesta part i un estudi de la característica d'excitació. L'anàlisi de les vibracions lliures (anàlisi modal) determina les freqüències i modes propis de l'estructura. Amb l'anàlisi de l'excitació s'obté el contingut freqüencial i el mode de la excitació.

Els rodets hidràulics són estructures molt complexes que es troben submergides i confinades dins d'una carcassa. Particularment els rodets de màquines turbina-bomba es comporten com a estructures en forma de disc en els seus primers modes de vibració i estan excitats amb la coneguda interacció rotor-estator (RSI) quan estan en funcionament. Per tal d'estudiar l'efecte de la rotació, el confinament i l'excitació en el comportament dinàmic de l'estructura d'una manera sistemàtica i clara, es necessita un model simplificat. Per això, en aquesta tesi el comportament dinàmic d'un disc giratori submergit en aigua i confinat dins d'una carcassa s'ha analitzat analíticament, experimentalment i contrastat amb simulació.

En primer lloc, es presenta un model analític per a l'anàlisi del comportament dinàmic. Les freqüències i modes propis d'un disc giratori considerant el flux que l'envolta es determinen analíticament amb un model simplificat. També s'analitza la resposta del disc amb diferents patrons d'excitació que simulen la excitació RSI. Finalment es discuteix la transmissió del sistema rotatiu al sistema estacionari.

Per a l'anàlisi experimental s'ha desenvolupat un banc de proves que consisteix d'un disc giratori submergit i confinat dins d'una carcassa. El disc ha estat excitat des del sistema rotatiu amb excitadors piezoelèctrics (PZT) i amb un dispositiu d'impacte especialment dissenyat. La resposta del disc s'ha mesurat simultàniament des del sistema rotatiu i des del sistema estacionari.

Les primeres freqüències i modes propis del disc quan gira en aire i en aigua s'han obtingut des del sistema rotatiu amb acceleròmetres miniatura cargolats en el disc i s'han contrastat amb les obtingudes amb el model analític presentat i amb una simulació numèrica d'elements finits (FEM). Només els modes diametrals del disc, que són els més rellevants i similars als dels rodets hidràulics, s'han considerat en aquest estudi.

El disc ha estat excitat amb diversos patrons d'excitació que simulen el veritable RSI. El comportament dinàmic del disc a causa d'aquests patrons d'excitació ha estat determinat experimentalment i contrastat amb el model analític.

Finalment, s'ha realitzat l'anàlisi de la transmissió des del sistema rotatiu al sistema estacionari. Les freqüències i modes propis del disc s'han detectat amb diversos tipus de sensors col·locats al sistema estacionari.

RESUMEN

El análisis del comportamiento dinámico de componentes rotativos en turbomáquinas es de gran interés para evitar daños o problemas de fatiga en estas partes. Para determinar el comportamiento dinámico de una parte de una estructura es necesario llevar a cabo un análisis de la vibración libre de esta parte y un estudio de la característica de excitación. El análisis de las vibraciones libres (análisis modal) determina las frecuencias y modos propios de la estructura. Con el análisis de la excitación se obtiene el contenido frecuencial y el modo de la excitación.

Los rodetes hidráulicos son estructuras muy complejas que se encuentran sumergidas y confinadas dentro de una carcasa. Particularmente los rodetes de máquinas turbina-bomba se comportan como estructuras en forma de disco en sus primeros modos de vibración y están excitados con la conocida interacción rotor-estator (RSI) cuando están en funcionamiento. Para estudiar el efecto de la rotación, el confinamiento y la excitación en el comportamiento dinámico de la estructura de una manera sistemática y clara, se necesita un modelo simplificado. Por ello, en esta tesis el comportamiento dinámico de un disco giratorio sumergido en agua y confinado dentro de una carcasa se ha analizado analíticamente, experimentalmente y contrastado con simulación.

En primer lugar, se presenta un modelo analítico para el análisis del comportamiento dinámico. Las frecuencias y modos propios de un disco giratorio considerando el flujo que lo rodea se determinan analíticamente con un modelo simplificado. También se analiza la respuesta del disco con diferentes patrones de excitación que simulan la excitación RSI. Finalmente se discute la transmisión del sistema rotativo al sistema estacionario.

Para el análisis experimental se ha desarrollado un banco de pruebas que consiste de un disco giratorio sumergido y confinado dentro de una carcasa. El disco ha sido excitado desde el sistema rotativo con excitadores piezoeléctricos (PZT) y con un dispositivo de impacto especialmente diseñado. La respuesta del disco se ha medido simultáneamente desde el sistema rotativo y desde el sistema estacionario.

Las primeras frecuencias y modos propios del disco cuando gira en aire y en agua se han obtenido desde el sistema rotativo con acelerómetros miniatura atornillados en el disco y se han contrastado con las obtenidas con el modelo analítico presentado y con una simulación

numérica de elementos finitos (FEM). Sólo los modos diametrales del disco, que son los más relevantes y similares a los de los rodetes hidráulicos, se han considerado en este estudio.

El disco ha sido excitado con varios patrones de excitación que simulan el verdadero RSI. El comportamiento dinámico del disco debido a estos patrones de excitación ha sido determinado experimentalmente y contrastado con el modelo analítico.

Finalmente, se ha realizado el análisis de la transmisión desde el sistema rotativo al sistema estacionario. Las frecuencias y modos propios del disco se han detectado con varios tipos de sensores colocados en el sistema estacionario.

INDEX

LIST OF FIGURES

LIST OF TABLES

NOMENCLATURE

Disk parameters

h_D	Thickness
r_{out}	External radius
r_{int}	Internal radius
r_o	Averaged radius
S_{up}	Upper surface
S_{inf}	Lower surface
w, w_d	Axial displacement of the disk
r, z, θ	Cylindrical coordinates of the disk
θ, θ_d, θ_r	Angular coordinate rotating frame
Ω_{rot}, Ω_{disk}	Rotating speed of the disk
ρ_D	Density of the disk
D	Bending stiffness
D*	Parameter with units of bending stiffness
E, υ	Young and Poisson modulus of the disk material
T_p^*	Reference kinetic energy of the disk

Gaps disk-casing

H_{up}	Upper gap disk-casing
H_{down}	Lower gap disk-casing
r_{casing}	Radius of the tank

Flow parameters

U_{up}	Potential function for the upper flow
U_{down}	Potential function for the lower flow
ϕ_{up}, ϕ_{down}	Potential function simplified
$\varphi_{up}, \theta_{up}$	Angular coordinate of the upper flow
$\varphi_{down}, \theta_{down}$	Angular coordinate of the lower flow
Ω_{up}	Rotating speed of the upper flow
Ω_{down}	Rotating speed of the lower flow
p	Pressure
w_f	Axial displacement of the flow
T_F^*	Reference kinetic energy of the flow

Natural frequencies and mode shapes

n	Number of nodal diameters
m	Number of nodal circles
$\boldsymbol{\omega}_{nm}$	Natural frequency of the disk in vacuum
$\boldsymbol{\omega}_{Fnm}$	Natural frequency of the disk considering the surrounding fluid
λ_{nm}	Dimensionless natural frequency of the disk in vacuum
β_{nm}	AVMI factors
f_{nm}	Natural frequency expressed in Hz

Excitation characteristic

Z_o	Number of guide vanes
Z_b	Number of rotating blades
l,k	Harmonics
γ	Pressure pulsations
λ	Arbitrary natural number
q	Number of exciter

Nomenclature for the sensors

A-X, AR-X	Accelerometer on the disk
P-X, PR-X	Piezoelectric patch on the disk
AS-X	Accelerometer on the casing
PRES-X	Pressure sensor on the casing
LASER	Laser sensor on the stationary frame

Abbreviations

CFD	Computational Fluid Dynamics
FEM	Finite Element Modelling
FSI	Fluid Structure Interaction
PZT	Piezoelectric actuator
RSI	Rotor stator interaction

Chapter 1

1. INTRODUCTION

1.1 Background and interest of the topic

Dynamic problems in rotating components of turbomachinery are common. These problems can reduce the life of these components drastically due to fatigue cycles or due to a catastrophic failure after a short period of time [1-7]. To study the dynamic problems that occur in these kinds of components both excitation and dynamic response of the rotating part have to be studied in detail.

In turbine and pump impellers, the excitation characteristic under operation is the superposition of several frequencies, which are harmonics of the rotating speed of the machine. The harmonics that are excited depend on the number of rotating blades and number of guide vanes on the stationary part of the machine. The combination of rotating blades and guide vanes determines also the excitation shape. This kind of excitation, which is known as Rotor Stator Interaction (RSI), is well studied in many references [5, 8-10].

While the excitation is well characterized by analytical, experimental and numerical simulations, the dynamic response of impellers, especially when they are submerged and rotating, has not been deeply studied. To study the structural response of the impeller means to determine the natural frequencies, damping and associated mode shapes of the free vibration of the structure. This response has been well determined for impellers that are rotating in a low density medium, such as air[11, 12].

Nevertheless, for hydraulic impellers that are submerged in water, the influence of rotation on the natural frequencies has not been published yet. Some studies determine the added mass effect of still water on the natural frequencies [13-15]. Although the influence of still water and confinement is considered, the real operating condition of hydraulic runners, i.e. submerged, confined and rotating is not considered in these studies. To calculate the added mass effect of the surrounding water in this condition, the flow pattern inside the casing, when the runner is rotating has to be determined. Therefore a two way

FSI (Fluid-structure-interaction) problem has to be solved considering the structure and the fluid, which is a difficult task to be done analytically or numerically. Also the experimental measurement on prototypes is complicated, since the runner is inaccessible. Due to all the mentioned problems and in order to understand the effects of the rotation clearly, simplified models are needed.

An appropriate simplified model of some kind of hydraulic runners is a disk, due to the similarity of the first mode shapes of these components with the mode shapes of a disk [14]. There are many studies of rotating disks in air [16-20], but few of them for disks rotating in water [8, 21]. In [8] an analytical method to calculate the added mass effect of the rotating fluid in one side is given but without numerical results. Recently [21], conduct experiments with a stationary disk and water that is forced to rotate with respect to the disk. In this case, experimental results were provided but they were not contrasted with an analytical model or numerical simulation. Furthermore, in both mentioned cases the disk is considered stationary with the surrounding water on one side that rotates with respect to it. Nevertheless, in the real case the impeller, which is a disk-like structure, is the part that rotates inducing a water rotating flow in the upper and lower part of the structure.

Finally, since the rotating parts of the machine are usually inaccessible, it is desirable to measure their response with sensors located on the stationary frame. In this case, it has to be considered that the structural response of the rotating disk-like component viewed from the stationary frame leads to frequency shifts that depend on the rotating speed and on the mode shape [16].

Therefore, to study experimentally the effect of rotation on the natural frequencies of the rotating disk-like structure and the effect of rotation on the detection of these natural frequencies when analyzed from the stationary frame, it is necessary to develop a rotating disk test rig, that can be excited and its response measured from both, stationary and rotating frame.

1.2 State of the art

1.2.1 Free vibration of rotating disk-like structures

The vibration of rotating disk-like structures has been studied extensively in the last years due to their relevance in real engineering applications such as circular saws, cutters, hard disks or turbomachinery components. Particularly in hydraulic turbomachinery, runners are disk-like structures which are submerged and confined rotating in water.

First studies on rotating disks were developed by Campbell [22]. In this study he introduced the term critical speed, at which a standing wave appears on the disk. The effect of rotation in the dynamic behavior of the disk was introduced by Lamb and Southwell [23]. Their study was focused on a disk, which rotate about its center with constant angular velocity. Southwell [24] studied the vibration of circular disks clamped at its center. He considered the effect of a shaft that clamps the disk at its center, in the natural frequencies of the rotating disk. This effect was not considered in the previous study. Later studies [18, 25, 26] determined other effects using numerical simulation. In [25] Jin Wook Heo studied the effect of misalignment in the natural frequencies of the disk. Bauer [18]studied the effect of the attachment to the stationary part. Finally in [26], L.Pust studied bladed disk with imperfections. Although, these studies provides a good knowledge on the dynamic behavior of rotating disks, the surrounding fluid has not been considered, since in these cases this fluid was air, which has no relevant effects on the dynamic behavior of the rotating disk.

The effect of a high density surrounding fluid (such as water) in the vibration characteristics of simple structures has been considered in many cases. Assuming an infinite fluid domain, Kwak in [27]studied the hydroeleastic vibrations of circular plates. Nevertheless, the effect of nearby rigid walls, which is a very common situation in real applications, was not considered. This problem was studied firstly by Lamb [28]. He considered the contact plate-water in only one side and located in a hole of an infinite rigid wall. C.Rodriguez [29] and C.Harrison [30] studied the influence of only one nearby rigid wall in the natural frequencies of a cantilever plate. They both concluded that the distance plate-wall has a great influence on the added mass effect; i.e. the natural frequencies of the cantilever plate are generally reduced when the plate is closer to the rigid wall. The case of

immersed and confined plates, which makes the problem much more complex, has been studied recently. In [31] Askari studied a circular plate submerged in a rigid cylindrical container. He provided a very complete formulation for the flow above and under the disk. The influence of the radial gap and the influence of the free surface in the natural frequencies was also investigated. Numerical results were validated with experimentation in this study. Although the influence of the surrounding fluid, the nearby rigid walls and the free surface in the hydroelastic vibration of plates has been considered in the mentioned cases, none of them investigates the effect of the rotation of the surrounding water.

The effect of a fluid field rotating with respect to the vibrating plate on the natural frequencies is very complex to study analytically, numerically and experimentally. Nevertheless, this effect has to be considered to describe the real boundary condition in the case of hydraulic turbomachinery. Kubota in [8] investigated this problem. He proposed a model to study the effect of rotation in the natural frequencies of a rotating disk in water. Departing from a simplified Equation for the disk structure and for the fluid potential in the tank, he deduced the effect of a fluid field rotating with respect the vibrating disk. An analytical expression was deduced in that paper in order to calculate the natural frequencies of the disk. This analytical solution was provided for the case that only one surface of the disk is in contact with a high density fluid (water) and all the fluid is moving at the same rotating speed with respect to the disk. The influence of the viscosity of the fluid was not considered and the case of a submerged and completely confined disk in rotation was not studied. Furthermore, no experimental results were shown in the study.

Recently Hengstler in [21] conduct experimental tests with a disk in contact in water with a rotating flow pattern. Experimental results show the same effect than in the previous case [8]. Although an interesting physical explanation of the effect of rotation of the surrounding water is given in that study, results are not validated with an analytical model or with numerical simulation.

1.2.2 Excitation characteristic and dynamic behaviour of disk-like structures

To consider the dynamic behaviour of a structure, both free vibration and excitation has to be considered. The analysis of the free vibration of the structure or modal analysis has the objective to determine the natural frequencies and mode shapes of the structure, i.e. which frequencies and under which excitation patterns could be excited under operation. The study of the excitation characteristic has the objective to determine which frequencies are really excited when the machine starts its operation.

The main excitation on impellers with small gap from the rotating blade to the stationary guide vane is the RSI [32]. In this case the perturbations originated by the static parts (guide vanes) superposed with the perturbations originated in the rotating parts (rotating blades) lead to a pressure pulsation [33, 34] . The pressure pulsation can be discomposed in harmonic excitations, where the frequency content depends on the rotating speed of the machine and the number of static guide vanes (when analyzed from the rotating structure) and the corresponding excitation pattern that depends also on the number of rotating blades [35].

The parameters that could have an effect in the amplitude of the RSI have been studied in some papers. In [36] Iino determined the influence of the angle of the blades and in [37] Arndt quantified the importance of the distance between the stationary and moving blades under different working conditions. To the determine if a resonance can occur in the runner or not it is necessary to know the natural frequencies of the runner (dynamic response) and the frequency content of the excitation, in this case the RSI. This characteristic of the excitation was firstly studied by Kubota in[35].He determined the harmonics of the blade passing frequency. Tanaka [5] continued with the study and developed a very practical method to determine the complete frequency content, viewed from the rotating and from the stationary frame, with the combination of guide vanes and blades. Also recent studies have simulated the RSI by means of CFD and experimentation[10, 38], which confirm the frequency content of the RSI predicted in[5]. These studies are normally focused on the flow characteristic itself but not on the dynamic behaviour of the structure under this

excitation, which needs also to consider the information obtained by the analysis of the structural response.

To study the dynamic behaviour in a simplified model (rotating disk) it is advantageous to use an excitation and measurement system placed on the rotating system (rotating disk-like part of the machine), since stationary sensors and actuators could affect the flow characteristic around the rotating part of the machine.

To excite the disk with a rotating excitation, light exciters (that do not affect the mass of the disk) have to be attached on the rotating frame. Because electromagnets or shakers are very heavy and may affect the mass of the structure, light and thin piezoelectric patches can be used in this case. PZT's are used in many cases as exciters [17, 39-43]. Zengtao Yang [39] studied the governing equation of an elastic plate due to the excitation of one PZT. He modeled also the dynamic behavior of the actuator. In [40], Oriol Gomis presented a control law for a piezoelectric actuator considering the hysteresis. Also some studies have been found with more than one piezoelectric patch acting. C.Cheng [41] placed several patches on a plate and studied the effect of the added mass of the actuators. In [42] El Mostafa Sekouri used piezoelectric patches to excite a thin circular plate. Finally, Xingzhe Wang [17] and Tianhong Yan [43] studied the feasibility to suppress aerodynamic flutter of a rotating disk. In both studies the disk was rotating but the actuators were placed on the stationary frame. Although in some of the mentioned studies, PZTs actuators are used to excite a rotating disk, the exciters are placed in the stationary frame and no studies have been found with multiple PZTs actuators placed on the rotating structure acting as modal exciters. Furthermore, in the mentioned studies PZT actuators are used to excite very thin rotating disks (thicknesses less than 1mm), which is in the range of rotating disks such as CD drives, DVD drives and other data storage disks, and no studies have been found with PZTs actuators exciting thick and submerged disks in water.

1.2.3 Measurement from the stationary frame

Some kind of impellers are large disk-like structures which are confined and not accessible when they are in operation. Furthermore, in case of hydraulic turbomachinery they are submerged. Therefore, to measure the natural frequencies of this part in this condition is a difficult task. To perform measurements from the rotating frame, means to

install small sensors that do not affect the normal operation of the machine and to transmit the signals to the stationary frame. For this reason, it may be easier to perform the measurements from the stationary frame. In this case, the frequency content of the signals acquired from the stationary frame is more difficult to be interpreted, due to the difference within measured and instrumentation frame.

For disk-like structures that are rotating in air, the correlation between natural frequencies in the rotating frame and in the stationary frame is well known. This relation depends on the rotating speed of the impeller and also on the mode shape as deduced mathematically and proven experimentally in [16, 44].

Nevertheless, in both cases the study was conducted in air. The only studies that deal with dynamic response of disks submerged in water and with flow that rotates with respect to the disk have been mentioned in chapter 1.2. Since in those studies the disk is considered stationary with water that rotates with respect to it, the measurement of the natural frequencies of the rotating disk from the stationary frame is not studied.

1.3 Objectives

The state of the art and the points to be solved regarding the analysis of the dynamic behaviour of rotating disk-like structures with surrounding fluid have been presented in the previous sections.

In order to study some of the remaining points, in this thesis an analysis of the dynamic behaviour of a rotating disk considering the surrounding fluid has been performed analytically and experimentally.

An analytical model for the structural response of a disk rotating in air and in water has been presented. Furthermore, the RSI excitation characteristic that is suffered by many rotating turbomachinery components is considered and the dynamic behaviour of the disk analyzed. Finally practical rules for the detection of the natural frequencies and mode shapes of the disk but viewed from the stationary system are given.

For the experimental study a rotating disk test rig has been developed. The disk was rotating inside a tank with air and with water. The disk has been excited from the rotating frame with piezoelectric patches and with a special impact device. Its response has been

measured from the rotating frame with miniature accelerometers and from the stationary frame with several kinds of sensors.

1.4 Outline of the thesis

In Chapter 2, the analytical model for the study is presented. The natural frequencies and mode shapes of a rotating disk considering the surrounding flow are analytically determined with a simplified model. Also the response of the disk with different excitation patterns that simulates the RSI is analyzed. Finally the transmission from the rotating to the stationary frame is discussed.

In Chapter 3, the test rig and the experiments performed are described. The disk, the casing and the instrumentation used (sensors and actuators) is presented. Also the different procedures to excite the disk are commented.

In Chapter 4, the analysis of the natural frequencies and mode shapes of the rotating disk submerged in water is performed. Previously, the analysis when the disk is rotating in air, i.e. when the density of the surrounding fluid is negligibly small, has been performed for a range speed of 0-10Hz. With the natural frequencies obtained, some of the parameters of the analytical model are calibrated. With these parameters the natural frequencies and mode shapes of the rotating disk submerged in water are calculated analytically and compared with the experimental results and with a numerical FEM simulation.

In Chapter 5, the results of the excitation of the disk with different excitation patterns that simulate the RSI are presented. The response of the disk under resonance (excited frequency equal to a natural frequency of the disk) is analyzed and compared with the analytical model.

Chapter 6 presents the detection of the natural frequencies and mode shapes of the disk from the stationary frame, when the disk is rotating in air and when the disk is rotating in water. To note here is that the results from Chapter 4 and Chapter 5 are all analyzed from the rotating frame and only in this chapter they are studied from the stationary frame.

Finally, in Chapter 7 the main conclusions obtained in this study and the remaining work are summarized.

Chapter 2

2. ANALYTICAL MODEL

In this section an analytical model to study the dynamic behaviour of a rotating disk submerged in water is presented. A simplified model is used to predict the natural frequencies and mode shapes for the disk submerged inside a cylindrical tank. The dynamic behaviour of the disk when it is excited with a rotating excitation pattern, that simulates the RSI, is discussed. Finally, a model to study the transmission to the stationary frame of the natural frequencies and mode shapes of the disk is deduced here.

2.1Analytical model for a rotating disk submerged and confined

The problem of circular plates vibration in contact with fluid is studied in many cases [27, 28, 45-47]. Generally, in most of them there is assumed that the mode shapes of the plate in contact with fluid are the same than those ones with the plate in Vacuum. This assumption is used to simplify the problem in case that the plate is in contact with fluid.

The case of study is shown in *Figure 2.1*.

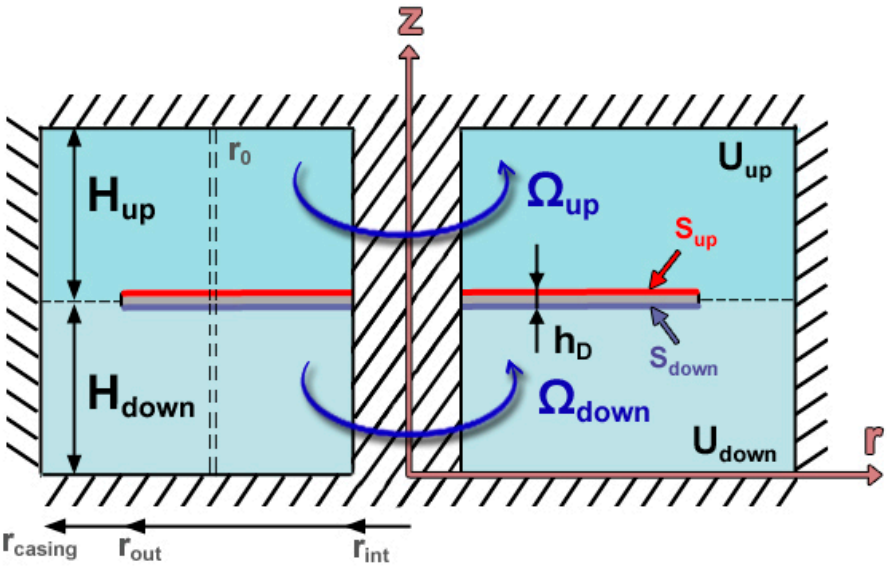

Figure 2.1: Model of a totally confined disk with rotation of the flow

An annular disk is considered to be submerged and stationary inside a casing. The fluid field is separated in two fluid fields "up" and "down". Both fields are considered to rotate as a solid rigid with a constant speed Ω_{up} and Ω_{down} with respect to the disk. θ,φ_{up} and φ_{down} (not shown in *Figure 2.1*) are the angular coordinates referred to the disk, the upper fluid field and the down fluid field. They are positive definite in counterclockwise direction and therefore the relation between them is:

$$\boldsymbol{\theta = \varphi_{up} + \Omega_{up} t} \quad \& \boldsymbol{\theta = \varphi_{down} + \Omega_{down} t} \tag{2.1}$$

2.1.1 Vacuum

It is considered that the disk shown in *Figure 2.1* with thickness h_D has a density of mass ρ_D and it is made of linear, homogeneous and isotropic material. The effects of rotating inertia, effects of shear deformation are neglected. The transverse displacement of the annular plate *w* can be described for the annular disk as [48, 49]:

$$\boldsymbol{\rho_D h_D \frac{\partial^2 w}{\partial t^2} + D\left[\frac{\partial}{\partial r^2} + \frac{1}{r}\frac{\partial}{\partial r} + \frac{1}{r^2}\frac{\partial^2}{\partial \theta^2}\right]^2 w = 0} \tag{2.2}$$

In this equation $D = {Eh_D^3}/{12(1-\upsilon^2)}$ is the bending stiffness of the disk, with E and υ the Young and Poisson modulus of the material.

The exact solution for w is given also in the mentioned references:

$$\boldsymbol{w = w(r,\theta,t) = \sum_{n=0}^{\infty}\sum_{m=0}^{\infty} W_{nm}(r)\cos(n\theta)\, e^{j\omega_{nm}t}} \tag{2.3}$$

In this solution n is the number of nodal diameters and m the number of nodal circles in the mode shape. $W_{nm}(r)$ is a function that involves the use of Bessel functions[48, 49] . Combining Eq. (2.3) and Eq. (2.2) the natural frequencies ω_{nm} can be obtained as:

$$\boldsymbol{\omega_{nm} = \frac{\lambda_{nm}^2}{r_{out}^2}\sqrt{\frac{D}{\rho_D h_D}}} \tag{2.4}$$

In this expression λ_{nm} depends on the relation of the inner to the outer radius of the disk and also on the mode shape n, m. A table with different values of λ_{nm} can be found in both references [48, 49].

2.1.2 Annular disk in contact with fluid that rotates with respect to the disk

To obtain the natural frequencies of the plate in contact with fluid, generally the added virtual mass incremental (AVMI) β_{nm} factors [27, 28, 45-47] are calculated. These factors depend on the characteristics of the disk and also on the boundary conditions of the fluid. They relate the natural frequencies in vacuum and the natural frequencies in contact with fluid as Eq. (2.5) shows.

$$\boldsymbol{\omega_{Fnm} = \frac{\omega_{nm}}{\sqrt{1+\beta_{nm}}}} \tag{2.5}$$

The calculus of the AVMI factors β_{nm} implies the calculus of the reference kinetic energy of the plate and the reference kinetic energy of the fluid [45]. The reference kinetic energy of an annular plate T_P^* can be calculated by use of the motion characteristic expressed in (2.3)[50]:

$$\boldsymbol{T_P^* = \frac{1}{2}\rho_D h_D \int_{r_{min}}^{r_{max}} \int_0^{2\pi} W_{nm}{}^2\,(r) cos^2(n\theta) r dr d\theta} \tag{2.6}$$

To calculate the reference kinetic energy of the fluid the velocity potentials $U_{up}(r, \varphi_{up}, z, t), U_{down}(r, \varphi_{down}, z, t)$ are used [50].

$$\begin{cases} \boldsymbol{U_{up}(r, \varphi_{up}, z, t) = \emptyset_{up}(\mathrm{r,z})\cos(n\varphi_{up})\dot{g_{mn}}(t)\ \ with\ g_{nm}(t) = e^{j\omega_{nm}t}} \\ \boldsymbol{U_{down}(r, \varphi_{down}, z, t) = \emptyset_{down}(\mathrm{r,z})\cos(n\varphi_{down})\dot{g_{mn}}(t)\ \ with\ g_{nm}(t) = e^{j\omega_{nm}t}} \end{cases} \tag{2.7}$$

Where $\emptyset_{up}, \emptyset_{down}$ satisfy the Laplace equation (Eq. (2.8)) in the fluid domains defined in Fig. 1. In cylindrical coordinates:

$$\begin{cases} \boldsymbol{\frac{\partial^2 \emptyset_{up}}{\partial r^2} + \frac{1}{r}\frac{\partial^2 \emptyset_{up}}{\partial r} + \frac{\partial^2 \emptyset_{up}}{\partial z^2} - \frac{m^2}{r^2}\emptyset_{up} = 0} \\ \boldsymbol{\frac{\partial^2 \emptyset_{down}}{\partial r^2} + \frac{1}{r}\frac{\partial^2 \emptyset_{down}}{\partial r} + \frac{\partial^2 \emptyset_{down}}{\partial z^2} - \frac{m^2}{r^2}\emptyset_{down} = 0} \end{cases} \tag{2.8}$$

The boundary conditions of the shown case in Figure 2.1 can be separated in the boundary conditions at the rigid surfaces and the boundary conditions at the disk and interface. At the rigid surfaces these are:

$$\begin{cases} \left.\frac{\partial \emptyset_{up}}{\partial z}\right|_{z=H_{down}+H_{up}} = \left.\frac{\partial \emptyset_{up}}{\partial r}\right|_{r=r_{casing}} = \left.\frac{\partial \emptyset_{up}}{\partial r}\right|_{r=r_{int}} = 0 \\ \left.\frac{\partial \emptyset_{down}}{\partial z}\right|_{z=0} = \left.\frac{\partial \emptyset_{down}}{\partial r}\right|_{r=r_{casing}} = \left.\frac{\partial \emptyset_{down}}{\partial r}\right|_{r=r_{int}} = 0 \end{cases} \quad \textbf{(2.9)}$$

The boundary conditions expressed in Eq. (2.9) mean that the fluid in the rigid boundaries has no velocity perpendicular to the surface. On the disk surface and on at the interface between two regions, the boundary conditions can be expressed as:

$$\begin{cases} \left.\frac{\partial \emptyset_{up}}{\partial z}\right|_{z=H_{down}} = \left.\frac{\partial \emptyset_{down}}{\partial z}\right|_{z=H_{down}} = \frac{\partial w}{\partial t} \quad for \;\; r_{int} \le r \le r_{out} \\ \left.\frac{\partial \emptyset_{up}}{\partial z}\right|_{z=H_{down}} = \left.\frac{\partial \emptyset_{down}}{\partial z}\right|_{z=H_{down}} \quad and \;\; \emptyset_{down} = \emptyset_{up} \;\; for \; r_{out} \le r \le r_{casing} \end{cases} \quad (2.10)$$

This problem when Ω_{up}=$\Omega_{down} = 0$ is solved in [31] by use of the Galerkin method. In that case:

$$\boldsymbol{\theta = \varphi_{up} = \varphi_{down}} \quad \textbf{(2.11)}$$

In the present case (Figure 2.1), also Eq. (2.1) has to be used to get $\emptyset_{up}, \emptyset_{down}$ since the angular coordinates in Eq. (2.7) and Eq. (2.3) are different. If $\emptyset_{up}, \emptyset_{down}$ are expressed in their respective angular coordinates, the reference kinetic energy of the fluid can be calculated as [31]:

$$\boldsymbol{T_F^* = \frac{1}{2}\rho_F \left(\iint_{S_{Down}} \emptyset_{Down} \frac{\partial \emptyset_{Down}}{\partial z} r dr d\varphi_{down} + \iint_{S_{Up}} \emptyset_{Up} \frac{\partial \emptyset_{Up}}{\partial z} r dr d\varphi_{up} \right)} \quad \textbf{(2.12)}$$

S_{up} and S_{down} are shown in Figure 2.1. The factors AVMI β_{nm} for each mode shapes can be easily calculated as [45]:

$$\boldsymbol{\beta_{nm} = \frac{T_F^*}{T_P^*}} \quad \textbf{(2.13)}$$

2.1.3 Similarity to the rotating disk case

When the disk rotates with respect to the surrounding flow, a rotational velocity component is induced on the flow apart from the dynamic motion produced by the disk vibration. Unfortunately, since the flow is assumed to be inviscid, the real flow pattern cannot be represented with potential flow. The real flow pattern of the disk can be obtained by using the Navier-Stokes equations analytically [51] or numerically (CFD simulation).

In [8] a rotating disk problem in contact with fluid is studied with a flow where all the particles of the fluid are moving as a solid rigid with an averaged rotating speed. Under this assumption, the averaged rotating speed of the real flow pattern with respect to the disk can be calculated and the problem can be considered as a stationary disk with a flow rotating with respect to them as shown in *Figure 2.1*.

2.1.4 Simplified model in the averaged radius

The complexity of the mentioned problem in *chap. 2.1* makes the analytical solution of $\emptyset_{up}, \emptyset_{down}$ very complex. For this reason Kubota and Ohashi in [8], tried to simplify this problem by representing the motion of the disk in an averaged radius. The flow is also represented by a potential flow in the averaged radius with a constant rotating speed with respect to the disk. Instead of calculating the reference kinetic energy of the surrounding fluid, in this case the pressure that the fluid exerts on the disk is considered in Eq. (2.2) to represent the fluid-structure interaction.

In this study the solution given by Kubota and Ohashi in [8] is extended to two fluid fields that can rotate at different rotating speeds.

The case of study in *Figure 2.1* is characterized now in the averaged radius r_0. It is assumed that the differential coefficients of the fluid and of the disk vibration in the radial direction are negligible small and that the fluid and disc are vibrating uniformly in radial direction. For this reason, the upper field and the lower field are two separate fields that are axially delimited by the disk and by a rigid surface. With this assumptions only the modes with no diametrical modes (m=0) have been considered. To simplify the nomenclature in this section, the natural frequencies will be defined as $\omega_{n0} = \omega_n$.

If the disk motion is represented in the averaged radius $r_o = \sqrt{r_{in} \cdot r_{out}}$ [8], the Eq. (2.2) for the disk vibrating with the surrounding fluid becomes:

$$\boldsymbol{\rho_D h_D \frac{\partial^2 w}{\partial t^2} + \frac{D^*}{r_o^4} \frac{\partial^4 w}{\partial \theta^4} = p_{r_o}} \quad \textbf{(2.14)}$$

In this Equation, D* is a parameter that depends on the geometry and material of the disk and has the same units as the stiffness D. p_{r_o} is the pressure that the fluid exerts on the disk. With the simplifications made for the model (uniform vibration in the radial direction), Eq. (2.3) can be rewritten as:

$$\boldsymbol{w = \sum_{n=\pm 2}^{\pm \infty} A_n e^{jn\theta} e^{j\omega_n t}} \quad \textbf{(2.15)}$$

The difference between Eq. (2.3) and Eq. (2.15) is also seen in the sign of n. In Eq. (2.3), which is used commonly to describe the motion of the free vibrations of the disk, only the positive value of n is considered. However in [8], both positive and negative values are considered. The sign of n indicates the direction of the travelling wave excited on the disk. With Eq. (2.14) and Eq. (2.15) natural frequencies of the disk in vacuum can be calculate if p_{r_o} is set to 0.

$$\boldsymbol{\omega^2_{|n|\geq 2, vacuum} = \frac{n^4 D^*}{\rho_D h_D r_o^4}} \quad \textbf{(2.16)}$$

These natural frequencies can be also calculated with Eq. (2.4). Comparing both equations, the value of D^* can be obtained.

It is observed that Eq. (2.15) does not consider the modes $n = \pm 1$ and n=0 which are the lowest modes for a thin disk with $r_{out} \gg r_{in}$. The mode n=0 is not considered since the fluid is considered incompressible and the radial motion of the flow is neglected. In [8] this

expression is supposed to be valid for the diametrical mode $n = \pm 1$. Even though, in that study the analytical values for this mode shape show a large error when compared to the experimental values.

Furthermore in [48, 49], the values for λ_{nm} using the complete disk equation (Eq. (2.2)) are given. If only the values with λ_{n0} are considered and the value of D^* is calibrated for $\lambda_{2\,0}$,the following relative errors for the values of λ_{n0} obtained with the simplified model (Eq. (2.14)) compared to those ones given in [48] are obtained(Table 2.1):

Table 2.1: Relative error (%) between natural frequencies in vacuum calculated with the simplified model and the proposed model in [48]

		Diametrical mode $\|n\|$				
r_{in}/r_{out}	h_D/r_{out}	1	3	4	5	6
0,05	0,04	51,17	1,87	0,28	-1,94	-4,18
0,125	0,02	62,20	-4,53	-6,23	-8,34	-10,43
0,125	**0,04**	**62,32**	**-4,76**	**-6,69**	**-9,08**	**-11,49**
0,125	0,2	58,99	-5,68	-12,87	-21,53	-30,97
0,2	0,04	66,74	-15,56	-18.95	-21,71	-24,41

Table 2.1 shows for which modes and geometries can be used the simplified model to estimate the natural frequencies of the disk in vacuum. The closest configuration to the tested disk in the experimental section is marked on Table 2.1. As shown in this table the mode $n = \pm 1$ shows a large error for all the geometries of the annular disk, therefore only the modes $|n| \geq 2$ will be considered in this simplified model. The mode $n = \pm 2$ is not shown, since this mode is used to calibrate the parameter D^* (and therefore the error is 0). For thin disks (h_D/r_{out}<0,2) with large radius compared to the inner radius (r_{in}/r_{out}<0,15), the error made with the simplified analytical model is not large for modes higher than $n = \pm 2$.

The analytical expression of a disk having contact with a fluid on its lower surface that rotates with respect to the disk is analytically solved in [8], with the mentioned

simplifications of the simplified model. Nevertheless, this situation is very difficult to be tested experimentally (level of fluid will not remain constant [51]) and subsequently no experimental results are given in [8] . Furthermore this situation is not realistic for the case of hydraulic turbomachinery, where the rotating parts are totally submerged. The present deduction is the extension of the simplified model of Kubota and Ohashi [8] for a totally confined and submerged rotating disk in a tank.

With the assumptions made for the model, Eq. (2.8) can be rewritten for $r=r_0$[8]:

$$\begin{cases} \frac{1}{r_o^2}\frac{\partial^2 U_{up}}{\partial \varphi^2_{up}} + \frac{\partial^2 U_{up}}{\partial z^2} = 0 \\ \frac{1}{r_o^2}\frac{\partial^2 U_{down}}{\partial \varphi^2_{down}} + \frac{\partial^2 U_{down}}{\partial z^2} = 0 \end{cases} \quad \textbf{(2.17)}$$

In this equation U is used instead of $\emptyset$ (and Eq. (2.7) is not considered). In this case, the boundary conditions expressed in Eq. (2.9) for the rigid walls are reduced to:

$$\begin{cases} \left.\frac{\partial U_{up}}{\partial z}\right|_{z=H_{down}+H_{up}} = 0 \\ \left.\frac{\partial U_{down}}{\partial z}\right|_{z=0} = 0 \end{cases} \quad \textbf{(2.18)}$$

And the boundary conditions expressed in Eq. (2.10) are reduced to:

$$\left.\frac{\partial U_{up}}{\partial z}\right|_{z=H_{down}} = \left.\frac{\partial U_{down}}{\partial z}\right|_{z=H_{down}} = \frac{\partial w}{\partial t} \quad \textbf{(2.19)}$$

U_{up}, U_{down} can be obtained separately, using the boundary conditions of Eq. (2.18) and Eq. (2.19) assuming the vibration of the disk as in Eq. (2.15) and using the relationship between the stationary and the rotating coordinates of the disk (Eq. (2.1)).Furthermore the orthogonal condition is considered:

$$\int_0^{2\pi} e^{j(n-s)\varphi} d\varphi = \begin{cases} 0 \; when \; s \neq n \\ 2\pi \; when \; s = n \end{cases} \quad \textbf{(2.20)}$$

The solution of the velocity potential for the "down" field, with all the mentioned conditions is given in [8]. Applying this solution, particularized for the case shown in Figure 2.1:

$$\begin{cases} U_{up}\big|_{z=H_{down}} = \sum_{n=\pm 1}^{\infty} \frac{j \cdot r_o \cdot A_n}{n} (\omega_n + n\Omega_{\mathrm{up}}) \coth\left(\frac{\mathrm{nH_{up}}}{\mathrm{r_0}}\right) \cdot \mathrm{e}^{\mathrm{jn}\varphi_{\mathrm{up}}} \mathrm{e}^{\mathrm{j}(\omega_n + n\Omega_{\mathrm{up}})\mathrm{t}} \\ U_{down}|_{z=H_{down}} = \sum_{n=\pm 1}^{\infty} \frac{j \cdot r_o \cdot A_n}{n} (\omega_n + n\Omega_{\mathrm{down}}) \coth\left(\frac{\mathrm{nH_{down}}}{\mathrm{r_0}}\right) \cdot \mathrm{e}^{\mathrm{jn}\varphi_{\mathrm{down}}} \mathrm{e}^{\mathrm{j}(\omega_n + n\Omega_{\mathrm{down}})\mathrm{t}} \end{cases} \quad (2.21)$$

Using the energy Equation in the non stationary form[51], the fluid dynamic pressure exerting to the disk can be calculated as:

$$\begin{cases} p_{up} = -\rho_F \left.\frac{\partial U_{up}}{\partial t}\right|_{z=(H_{down})} \\ p_{down} = -\rho_F \left.\frac{\partial U_{down}}{\partial t}\right|_{z=(H_{down})} \end{cases} \quad (2.22)$$

The term p_{r_o} of Eq. (2.14) can be obtained considering the pressure of the upper and lower fluid:

$$p_{r_o} = p_{up} + p_{down} \quad (2.23)$$

Substituting Eq. (2.21) in Eq. (2.22) and adding both pressures together (Eq. (2.23)), the term p_{r_o} becomes:

$$p_{r_o} = \rho_F r_o \sum_{n=\pm 1}^{\infty} \frac{A_n}{n} \cdot \left(\mathrm{e}^{\mathrm{jn}\varphi_{\mathrm{up}}} \mathrm{e}^{\mathrm{j}(\omega_n + n\Omega_{\mathrm{up}})\mathrm{t}} (\omega_n + n\Omega_{\mathrm{up}})^2 \coth\left(\frac{\mathrm{nH_{up}}}{\mathrm{r_0}}\right) + \mathrm{e}^{\mathrm{jn}\varphi_{\mathrm{down}}} \mathrm{e}^{\mathrm{j}(\omega_n + n\Omega_{\mathrm{down}})\mathrm{t}} (\omega_n n\Omega_{\mathrm{down}})^2 \coth\left(\frac{\mathrm{nH_{down}}}{\mathrm{r_0}}\right) \right) \quad (2.24)$$

With the coordinate transformation of Eq. (2.1):

$$\begin{cases} \mathbf{e^{jn\varphi_{up}} e^{j(\omega_n + n\Omega_{up})t} = e^{jn\theta} e^{j\omega_n t}} \\ \mathbf{e^{j\omega_n t} e^{jn\varphi_{down}} e^{j(\omega_n + n\Omega_{down})t} = e^{jn\theta} e^{j\omega_n t}} \end{cases} \quad \textbf{(2.25)}$$

And therefore:

$$\begin{aligned} \boldsymbol{p_{r_o}} = \boldsymbol{\rho_F r_o} \sum_{\boldsymbol{n=\pm 1}}^{\infty} \frac{\boldsymbol{A_n}}{\boldsymbol{n}} \cdot \mathbf{e^{jn\theta} e^{j\omega_n t}} \\ \cdot \left(\left(\boldsymbol{\omega_n} + \boldsymbol{n\Omega_{up}}\right)^2 \mathbf{coth}\left(\frac{\mathbf{nH_{up}}}{\mathbf{r_0}}\right) \right. \\ \left. + \left(\boldsymbol{\omega_n} + \boldsymbol{n\Omega_{down}}\right)^2 \mathbf{coth}\left(\frac{\mathbf{nH_{down}}}{\mathbf{r_0}}\right) \right) \end{aligned} \quad \textbf{(2.26)}$$

The vibration of the disk coupled with the surrounding fluid is obtained substituting Eq. (2.26) and Eq. (2.15) in Eq. (2.12):

$$\boldsymbol{\rho_D h_D \frac{\partial^2 w}{\partial t^2} + \frac{D^*}{{r_o}^4} \frac{\partial^4 w}{\partial \theta^4} - p_{r_o} = 0 \rightarrow \sum_{n=\pm 2}^{\infty} A_n e^{jn\theta} e^{j\omega_n t} \left(-\rho_D h_D \omega_n^2 + \frac{D^*}{{r_o}^4} n^4\right) - p_{r_o} = 0} \quad \textbf{(2.27)}$$

The solution of the characteristic Equation (Eq. (2.28)) gives the solution of the natural frequencies ω_n for each n (positive and negative). This Equation is:

$$\begin{aligned} \left(\left[\mathbf{coth}\left(\frac{\boldsymbol{nH_{up}}}{\boldsymbol{r_o}}\right) + \mathbf{coth}\left(\frac{\boldsymbol{nH_{down}}}{\boldsymbol{r_o}}\right) \right] \frac{\boldsymbol{\rho_F r_o}}{\boldsymbol{n}} + \boldsymbol{\rho_D h_D} \right) \boldsymbol{\omega_n^2} \\ + \left(\left[\mathbf{coth}\left(\frac{\boldsymbol{nH_{up}}}{\boldsymbol{r_o}}\right) \boldsymbol{2n\Omega_{up}} \right. \right. \\ \left. \left. + \mathbf{coth}\left(\frac{\boldsymbol{nH_{down}}}{\boldsymbol{r_o}}\right) \boldsymbol{2n\Omega_{down}} \right] \frac{\boldsymbol{\rho_F r_o}}{\boldsymbol{n}} \right) \boldsymbol{\omega_n} \\ + \left(-\frac{\boldsymbol{D}}{{\boldsymbol{r_0}}^4} \boldsymbol{n^4} + \left[\mathbf{coth}\left(\frac{\boldsymbol{nH_{up}}}{\boldsymbol{r_o}}\right) \boldsymbol{n^2 {\Omega_{up}}^2} \right. \right. \\ \left. \left. + \mathbf{coth}\left(\frac{\boldsymbol{nH_{down}}}{\boldsymbol{r_o}}\right) \boldsymbol{n^2 {\Omega_{down}}^2} \right] \frac{\boldsymbol{\rho_F r_o}}{\boldsymbol{n}} \right) = \mathbf{0} \end{aligned} \quad \textbf{(2.28)}$$

From this Equation, only the positive solution for each n is considered.

2.1.5 Analogy to the modal model

The modal model of 1 DOF consists in a mass, spring and damper. The damper is considered as a structural damping (general case) that may depend on the frequency itself [52]. Its motion Equation can be expressed as

$$\boldsymbol{m\ddot{x} + c\dot{x} + kx = F(t)} \tag{2.29}$$

Assuming a solution of type $X = xe^{j\omega t}$ when $F = fe^{j\omega t}$, the following transfer function is obtained:

$$\frac{\mathbf{1}}{\boldsymbol{-m\omega^2 + cj\omega + k}} = \frac{\boldsymbol{x}}{\boldsymbol{f}} \tag{2.30}$$

The similarity between Eq. (2.28) and the denominator of Eq. (2.30) permits the following analogies.

$$\begin{aligned} \boldsymbol{m} &= \left[\mathbf{coth}\left(\frac{\boldsymbol{nH_{up}}}{\boldsymbol{r_o}}\right) + \mathbf{coth}\left(\frac{\boldsymbol{nH_{down}}}{\boldsymbol{r_o}}\right)\right]\frac{\boldsymbol{\rho_F r_o}}{\boldsymbol{n}} + \boldsymbol{\rho_D h_D}\ ; \\ \boldsymbol{c} &= -\boldsymbol{j}\left[\mathbf{coth}\left(\frac{\boldsymbol{nH_{up}}}{\boldsymbol{r_o}}\right)\boldsymbol{2n\Omega_{up}} + \mathbf{coth}\left(\frac{\boldsymbol{nH_{down}}}{\boldsymbol{r_o}}\right)\boldsymbol{2n\Omega_{down}}\right]\frac{\boldsymbol{\rho_F r_o}}{\boldsymbol{n}} \\ \boldsymbol{k} &= \frac{\boldsymbol{D}}{\boldsymbol{{r_0}^4}}\boldsymbol{n^4} - \left[\mathbf{coth}\left(\frac{\boldsymbol{nH_{up}}}{\boldsymbol{r_o}}\right)\boldsymbol{n^2{\Omega_{up}}^2} + \mathbf{coth}\left(\frac{\boldsymbol{nH_{down}}}{\boldsymbol{r_o}}\right)\boldsymbol{n^2{\Omega_{down}}^2}\right]\frac{\boldsymbol{\rho_F r_o}}{\boldsymbol{n}} \end{aligned} \tag{2.31}$$

Fluid in rest

The effect of a still fluid in the natural frequencies of the disk is to increase the mass of the disk (added mass effect) and consequently decreases the value of the resonance frequency.

In this case, the same solution for ω_n is obtained for n positive and n negative when $|n_{pos}| = |n_{neg}|$. Substituting $\omega_{n_{pos}}, n_{pos}$ and $\omega_{n_{neg}}, n_{neg}$ in Eq. (2.15), a unique mode shape with all the points moving in phase or in counterphase (standing wave) is obtained for each pair of n.

Effect of fluid rotation

If the fluid rotates, it can be seen (Eq. (2.30)) that an extra stiffness and a complex damping term appear. The appearance of a complex damping term, causes that $\omega_{n_{pos}} \neq \omega_{n_{neg}}$. Now substituting $\omega_{n_{pos}}, n_{pos}$ and $\omega_{n_{neg}}, n_{neg}$ in Eq. (2.15), a mode shape is obtained for $\omega_{n_{pos}}$ and a mode shape is obtained for $\omega_{n_{neg}}$. Both mode shapes are complex mode shapes with all points moving in a different phase. They can be understood as travelling waves. The rotation of the travelling waves for $\omega_{n_{pos}}$ and for $\omega_{n_{neg}}$is always in countersense. According to Eq. (2.28), when the rotation speed of the surrounding fluid increases, the frequency shift between these two peaks also increases.

A physical explanation for this effect is the influence of the added mass of the fluid on a forward wave and on a backward wave. According to [8], the free vibration of an annular disk is the superposition of a forward and a backward wave, for each diametrical mode n. For the annular disk with steady surrounding fluid, the added mass effect of this fluid on the forward and on the backward wave is the same and therefore both waves will have the same natural frequency and the corresponding mode shape at this frequency will be the superposition of both waves, which is a standing wave. With a relative rotation of the surrounding fluid with respect to the disk, the added mass effect will be different for the forward than for the backward wave, since the relative velocity of the fluid with respect to the wave will be different depending on the rotating direction of the wave. This causes, that the frequency of the backward wave will be different than the frequency of the forward wave. In this case, for each diametrical mode n a pair of natural frequencies, which correspond to the forward and to the backward wave, will appear on the disk. A similar effect is shown in [53], for a fluid-conveying pipe with periodic boundary conditions.

Increasing Ω_{disk} will increase Ω_{up} & Ω_{down} and this will enhance the mentioned effect, which means to increase the difference between both natural frequencies. For higher values of Ω_{disk} than considered in this paper, some terms may be included in Eq. (2.14)[18] (due to centrifugal and Coriolis forces) and therefore the analytical solution would be modified. Furthermore, higher velocities of the disk leads to low pressure areas what could generate vapor bubbles (cavitation) [54, 55], changing the added mass effect depending on the type

and amount of cavitation [56]. Therefore, with the presence of cavitation, the solution of Eq.(2.14) becomes much more complex.

2.1.6 Validity of the simplified model

The presented simplified model which is an extension of the model proposed in [8] makes the important simplification of considering the differential coefficients of the motion of the fluid and disk negligibly small in the radial direction and that the disk and fluid vibrate uniformly in this direction. Therefore, the vibration characteristic of both fluid and disk can be represented in an averaged radius r_0. In that study experimental results confirm the analytical model proposed for the case of a standing disk, i.e. Ω_{up}=$\Omega_{\mathrm{down}} = 0$. In this study experimental results will be compared with the simplified analytical model when $\Omega_{\mathrm{up}} \neq \Omega_{\mathrm{down}} \neq 0$

Due to the simplifications made, this model can only predict the diametrical modes, i.e. when m=0. As said before, the mode $\omega_{0,0}$ is also not possible for the simplified model, since the fluid is considered incompressible and the disk vibrates uniformly in the radial direction. In [8], the simplified model is given for $|n| \geq 1$ and no geometrical characteristics are imposed on the disk. Table 2.1 shows that the assumptions introduced in the simplified model do not change substantially the results of the natural frequencies in vacuum compared to the results where the radial deformation is considered[48, 49], for modes $|n| \geq 2$ (specially for modes $|n| = 3{,}4$) and for disks with $r_{out} \gg r_{in}$.

In fact, since Eq. (2.3) is written as superposition of mode shapes n,m for $0 \leq n, m \leq \infty$, and w satisfies Eq. (2.2), each mode n, m has to satisfy separately Eq. (2.2). For some geometrical conditions of the disk (Table 2.1), some mode shapes satisfy the simplified form of Eq. (2.2) which is Eq. (2.14). Fortunately, these modes (diametrical modes with $|n| > 2$), are commonly the most relevant modes in case of hydraulic runners since they are more prompt to be excited [3, 4], and therefore they will be studied experimentally in this case.

Finally, due to the assumptions made, no influence of the radial gap can be estimated with this model. Askari in [31] shown that the radial gap ($r_{gap} = r_{casing} - r_{out}$) has no

influence in the transverse vibration of the disk when $\frac{r_{gap}}{r_{out}} \geq 0{,}2$ approximately . Therefore this model will predict the natural frequencies with more accuracy when this condition is satisfied.

2.2 Forced response of a system due to a multiple exciters under resonance

Real hydraulic runners are excited by the Rotor-Stator Interaction or RSI. The study of the dynamic behaviour involves the dynamic response (chapter 2.1) and the excitation characteristic (chapter 2.3).

Before studying the dynamic response, a general formulation of the forced response of a structure when it is excited under resonance condition ($\omega_{\mathrm{n}} = \omega_{\mathrm{excit}}$) is presented here.

2.2.1 Model for general MDOF structures. Frequency response function

In the general case a structure can be described as an assembly of an infinite number of masses, stifnesses and dampings. In this case:

$$[\boldsymbol{M}]\{\ddot{\boldsymbol{x}}\} + [\boldsymbol{C}]\{\dot{\boldsymbol{x}}\} + [\boldsymbol{K}]\{\boldsymbol{x}\} = \{\boldsymbol{F}(\boldsymbol{t})\} \qquad \textbf{(2.32)}$$

This equation considers the inertia force, the damping force and the stifness force. Assuming that initial displacement and velocities are zero and applying Laplace transformation:

$$([\boldsymbol{M}]\boldsymbol{s^2} + [\boldsymbol{C}]\boldsymbol{s} + [\boldsymbol{K}])\{\boldsymbol{X}(\boldsymbol{s})\} = \{\boldsymbol{F}(\boldsymbol{s})\} \rightarrow [\boldsymbol{Z}(\boldsymbol{s})]\{\boldsymbol{X}(\boldsymbol{s})\} = \boldsymbol{F}(\boldsymbol{s}) \qquad \textbf{(2.33)}$$

Now inverting the matrix $[Z(s)]$:

$$[\boldsymbol{H}(\boldsymbol{s})] = [\boldsymbol{Z}(\boldsymbol{s})]^{-\mathbf{1}} = \frac{\boldsymbol{adj}([\boldsymbol{Z}(\boldsymbol{s})])}{|[\boldsymbol{Z}(\boldsymbol{s})]|} \qquad \textbf{(2.34)}$$

From $|[Z(s)]| = 0$ the poles of the system are obtained. If the matrix $[Z(s)]$ has dimension N, then 2N complex valued eigenvalues (solutions of s), appearing in complex conjugate pairs are obtained.

$$[\Delta] = \begin{bmatrix} \begin{pmatrix} \boldsymbol{\sigma_1 + j\omega_1} & \cdots & \mathbf{0} \\ \vdots & \ddots & \vdots \\ \mathbf{0} & \cdots & \boldsymbol{\sigma_N + j\omega_N} \end{pmatrix} & \mathbf{0} \\ \mathbf{0} & \begin{pmatrix} \boldsymbol{\sigma_1 - j\omega_1} & \cdots & \mathbf{0} \\ \vdots & \ddots & \vdots \\ \mathbf{0} & \cdots & \boldsymbol{\sigma_N - j\omega_N} \end{pmatrix} \end{bmatrix} \quad \textbf{(2.35)}$$

For the first N poles the modal parameters σ_r and w_r are obtained. These are the damping factor and the natural damped frequency of the mode. Associated to these N eigenvalues, N eigenvectors are obtained.

$$[\boldsymbol{\theta}] = [\boldsymbol{\vartheta_1} \quad \cdots \quad \boldsymbol{\vartheta_N}] = \begin{bmatrix} \boldsymbol{\vartheta_{1,1}} & \cdots & \boldsymbol{\vartheta_{1,N}} \\ \vdots & \ddots & \vdots \\ \boldsymbol{\vartheta_{N,1}} & \cdots & \boldsymbol{\vartheta_{N,N}} \end{bmatrix} \quad \textbf{(2.36)}$$

These eigenvectors are called mode shape vectors or modal vectors.

If $[H(s)]$ is evalutated along the frequency axis jω:

$$\{\boldsymbol{X(j\omega)}\} = [\boldsymbol{H(j\omega)}]\{\boldsymbol{F(j\omega)}\} \quad \textbf{(2.37)}$$

$[H(j\omega)]$ is used to determine the response due to an harmonic excitation $\{F(j\omega)\}$.

2.3 Rotor-Stator Interaction

An unidimensional model for the Rotor-Stator Interaction is presented in [57]. When the rotating blades of the rotor pass in front of the static vanes of the stator (*Figure 2.2*) the pressure field in the gap between blades and vanes can be described as the superposition of all the combinations l,k:

$$\boldsymbol{p_{lk}(\theta, t) = A_{lk} \cdot \cos(lZ_o\theta_s + \emptyset_l) \cdot \cos(kZ_b\theta_r + \emptyset_k)\ for\ l = 1, 2, \dots, \infty\ k = 1, 2, \dots, \infty} \quad \textbf{(2.38)}$$

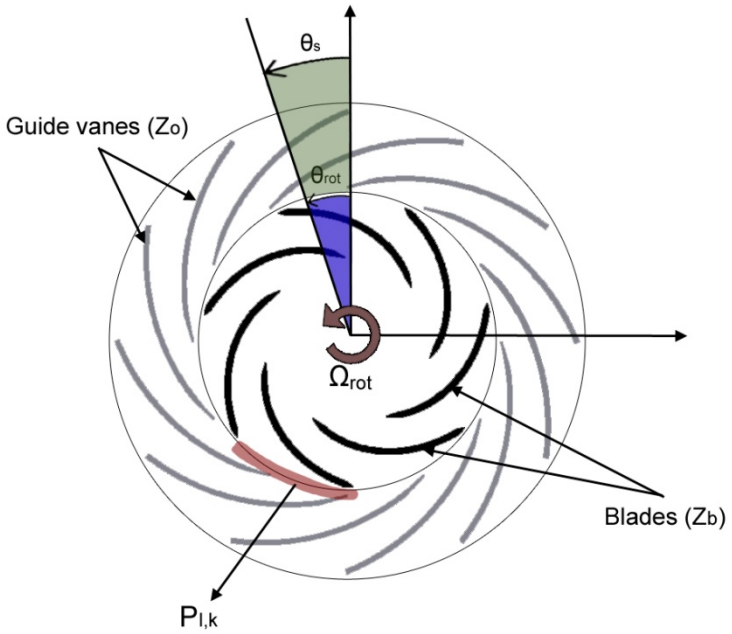

Figure 2.2: Rotor-Stator-Interaction

This pressure field can be viewed from the rotating frame or from the stationary frame. In this study, since the structural response is viewed from the rotating frame, the excitation will be also considered from the rotating frame. Transforming Eq.(2.38) in the rotating coordinate ($\theta_r = \theta_s - \Omega t$) this pressure field can be expressed as:

$$\begin{aligned} p_{l,k} &= \frac{A_{lk}}{2}\cos(lZ_o\Omega_{\mathrm{rot}}t - (kZ_b - lZ_o)\theta_r + \emptyset_l - \emptyset_k) \\ &\quad + \frac{A_{lk}}{2}\cos(lZ_o\Omega_{\mathrm{rot}}t - (-lZ_o - kZ_b)\theta_r + \emptyset_l + \emptyset_k) \\ &= \frac{A_{lk}}{2}\cos(lZ_o\Omega_{\mathrm{rot}}t - \gamma_1\theta_r + \emptyset_l - \emptyset_k) \\ &\quad + \frac{A_{lk}}{2}\cos(lZ_o\Omega_{\mathrm{rot}}t - \gamma_2\theta_r + \emptyset_l + \emptyset_k) \end{aligned} \tag{2.39}$$

From Equation (2.39) it can be seen, that the excitation shape depends on the number of guide vanes and rotating blades ($\gamma_1 = kZ_b - lZ_o$) and ($\gamma_2 = -lZ_o - kZ_b$) . This number represents the number of maximums and minimums in the pressure pulsation in a circle (Figure 2.3) and the sign of γ_1 and γ_2 indicates the rotating direction of the excitation. If it is positive, it indicates that the excitation rotates in the same direction (faster) than the rotating disk-like part. If it is negative it rotates in the opposite direction (slower).

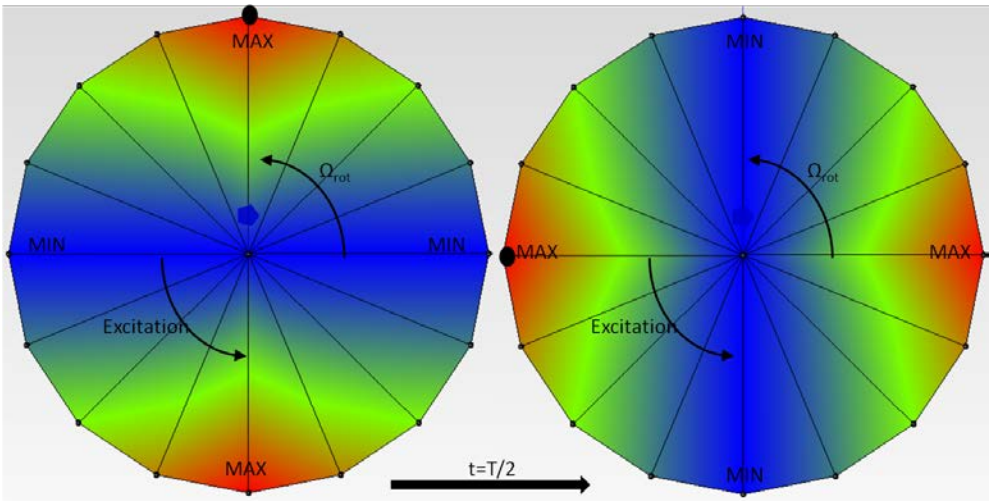

Figure 2.3: γ = +2 pressure pulsations for a rotating disk.

Usually the term of the pressure pulsation that contains γ_2 is not relevant for the RSI, since the several first mode shapes of a disk like structure have a small number of diametrical modes [57].

The excited frequency depends only on the number of guide vanes and on the rotating speed of the machine ($lZ_o\Omega_{rot}$). For higher number of harmonics (l, k) lower amplitudes A_{lk} are expected

Rotating turbomachinery components that suffer the RSI, are designed to avoid resonances during its steady state. Nevertheless, during the acceleration or deceleration of the rotor, since the rotating speed changes, a resonance can occur if the natural frequency coincides with the excited frequency and the excitation shape with the mode shape.

The frequency response function (FRF) is defined as the relationship between displacement at point ***p*** when a force is applied at point ***q*** for an arbitrary frequency ω. Considering the response in resonance of the mode n, i.e. $\omega=\omega_n$:

$$H_{pq}(j\omega_n) = \begin{bmatrix} h_{11} & \cdots & h_{1q} \\ \vdots & \ddots & \vdots \\ h_{p1} & \cdots & h_{pq} \end{bmatrix}_n = \frac{\{X\}_n}{\{F\}_n} \quad \textbf{(2.40)}$$

If only the response of the point 1 is studied:

$$X_{1,n} = [h_{11} \quad \cdots \quad h_{1q}]_n \begin{Bmatrix} F_1 \\ \vdots \\ F_q \end{Bmatrix}_n \tag{2.41}$$

2.3.1 Air

When the disk is rotating in air at lower speeds, the mode shape is a standing wave on the disk (Eq.(2.16) substituted in Eq.(2.15)). It is considered, that the disk is excited in q equidistant points with respect to the origin of angles (point 1) and that the RSI pattern is equal in magnitude for all the q points (Eq. (2.39)). The vector $[h_{11} \quad \cdots \quad h_{1q}]_n$, is obtained for each of the considered natural frequencies ω_n , using the information of the mode shape (in this case a standing wave). For the excitation $\{F\}_n$, the pattern deduced in Eq.(2.39) is introduced. Since the excitation changes its phase for each position (not all the points moving in phase or in counterphase), complex numbers have to be used to calculate the response [58]. For each of the considered natural frequencies:

$$\begin{aligned} X_{1,n} = \Theta_n \cdot \Bigg[& \cos\left(n\left(\frac{0\cdot 2\pi}{q}\right)\right) \cdot \left(\cos\left(\gamma_1\left(\frac{0\cdot 2\pi}{q}\right)\right) - \mathrm{j}\cdot\sin\left(\gamma_1\left(\frac{0\cdot 2\pi}{q}\right)\right)\right) \\ & + \cos\left(n\left(\frac{1\cdot 2\pi}{q}\right)\right) \\ & \cdot \left(\cos\left(\gamma_1\left(\frac{1\cdot 2\pi}{q}\right)\right) - \mathrm{j}\cdot\sin\left(\gamma_1\left(\frac{1\cdot 2\pi}{q}\right)\right)\right) + \cdots \\ & + \cos\left(n\left(\frac{(q-1)\cdot 2\pi}{q}\right)\right) \\ & \cdot \left(\cos\left(\gamma_1\left(\frac{(q-1)\cdot 2\pi}{q}\right)\right) - \mathrm{j}\cdot\sin\left(\gamma_1\left(\frac{(q-1)\cdot 2\pi}{q}\right)\right)\right)\Bigg] \end{aligned} \tag{2.42}$$

Θ_n is an arbitrary complex constant that depends on the mode shape considered and j is the complex unity. From Eq. (2.42), it can be deduced that to excite the structural mode ±n, the relationship between number of exciters q, excitation mode γ_1 has to be the following:

$$\boldsymbol{n = \pm\gamma_1 \pm \lambda q} \tag{2.43}$$

In Eq.(2.43), n, γ_1, q are entire and positive numbers that are defined by the structural mode, excitation shape and number of equidistant exciters respectively and λ is an arbitrary

entire number (including 0). From this equation can be deduced, that the structural mode ±n is excited with one exciter whatever the excitation shape is, as for one exciter this is not defined. When $\boldsymbol{\gamma_1 = \pm n}$ the structural mode is excited with any number of exciters q. Otherwise, when $\boldsymbol{\gamma_1 \neq \pm n}$, only for the number of exciters that accomplish Eq.(2.43) the structural mode ±n is excited.

2.3.2 Water

When the disk is rotating in water at lower speeds, two travelling waves appear for each n (Eq.(2.28) substituted in Equation (2.15)). The same assumptions made for the excitation of the rotating disk in air are assumed now. The main difference in this case, is that the structural mode shape is a travelling wave and to express $[h_{11} \quad \cdots \quad h_{1q}]_n$ also complex numbers have to be used, since generally all the points are not moving in phase or in counterphase to each other. For each of the studied mode shapes, when $lZ_o\Omega_{\mathrm{rot}}=\omega_n$:

$$\begin{aligned} X_{1,n} = \Theta_n \cdot \Bigg[& \left(\cos\left(n\left(\frac{0\cdot 2\pi}{q}\right)\right) + j\cdot\sin\left(n\left(\frac{0\cdot 2\pi}{q}\right)\right)\right) \\ & \cdot\left(\cos\left(\gamma_1\left(\frac{0\cdot 2\pi}{q}\right)\right) - \mathrm{j}\cdot\sin\left(\gamma_1\left(\frac{0\cdot 2\pi}{q}\right)\right)\right) \\ & + \left(\cos\left(n\left(\frac{1\cdot 2\pi}{q}\right)\right) + j\cdot\sin\left(n\left(\frac{1\cdot 2\pi}{q}\right)\right)\right) \\ & \cdot\left(\cos\left(\gamma_1\left(\frac{1\cdot 2\pi}{q}\right)\right) - \mathrm{j}\cdot\sin\left(\gamma_1\left(\frac{1\cdot 2\pi}{q}\right)\right)\right) + \cdots \\ & + \left(\cos\left(n\left(\frac{(q-1)\cdot 2\pi}{q}\right)\right) + j\cdot\sin\left(n\left(\frac{(q-1)\cdot 2\pi}{q}\right)\right)\right) \\ & \cdot\left(\cos\left(\gamma_1\left(\frac{(q-1)\cdot 2\pi}{q}\right)\right) - \mathrm{j}\cdot\sin\left(\gamma_1\left(\frac{(q-1)\cdot 2\pi}{q}\right)\right)\right)\Bigg] \end{aligned} \tag{2.44}$$

In this case, to excite the structural mode +n, the following equation has to be accomplished:

$$\boldsymbol{n = \gamma_1 \pm \lambda q} \tag{2.45}$$

As for the case that the disk rotates in air, for one exciter the structural mode +n is excited with any excitation shape γ_1. Nevertheless, when the disk rotates in water the structural

mode +n is excited for an arbitrary number of exciters only if $\gamma_1 = n$, which means that the excitation has to coincide with the structural mode shape in its shape and in its direction. When $\gamma_1 \neq n$, the structural mode +n is only excited if the number of exciters accomplish (2.45).

2.4 Transmission to the stationary frame

In case of hydraulic turbomachinery, it is of paramount importance to know the dynamic response of the runner under operation, which means to know the natural frequencies and mode shapes of this structure when it is confined inside the casing and rotating. Due to the inaccessibility of this structure, it is very advantageous to measure the vibration from the stationary frame or casing.

Until now, the casing has been considered as a completely rigid structure, which means that the normal velocity to the walls is zero (Eq.(2.9)). Nevertheless, real casings are not absolutely rigid and Eq.(2.9) has to be rewritten as:

$$\boldsymbol{\nabla U_{casing} \approx 0} \qquad \textbf{(2.46)}$$

If the displacement of the casing is significantly smaller than the displacement of the disk, the condition of Eq.(2.9) can be used to calculate the added mass effect of the water. Furthermore the condition expressed in Eq.(2.46) can be useful in order to measure the response of the disk with sensors placed on the casing.

The objective of this section is to present the theoretical background of the measurement of rotating systems from the stationary frame. The case of study has been presented in *Figure 2.1*. To consider the transmission to the upper cover this Figure is simplified in *Figure 2.4*.

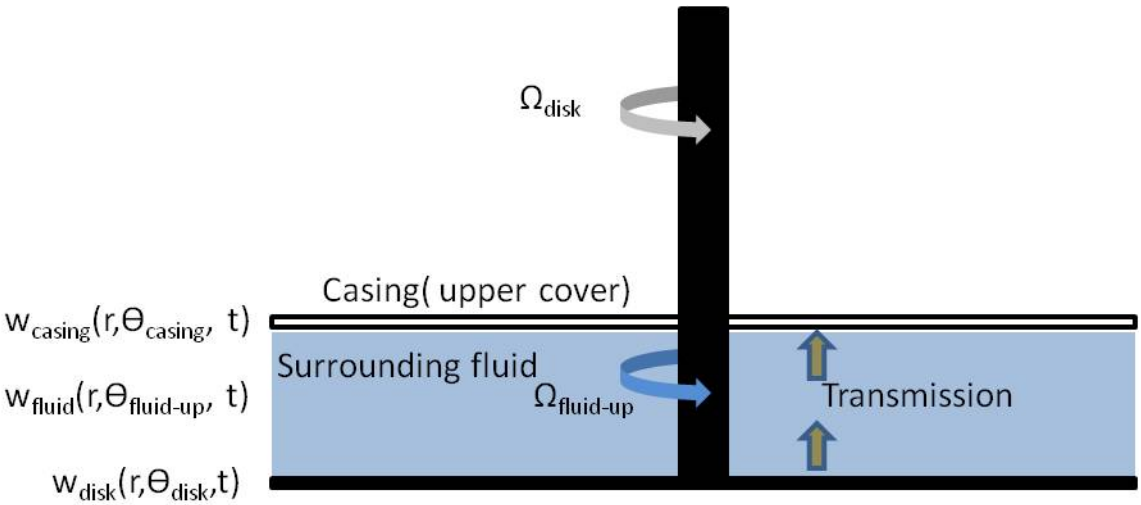

Figure 2.4: Transmission from the rotating to the stationary frame

A disk that is excited is surrounded by a fluid. In the other side the casing that covers the disk is not directly excited, but receives the vibration of the disk through the surrounding fluid.

According to the general theory presented for fluid systems and structural vibrations in a fluid [49], if a structure vibrates with frequency $\boldsymbol{\omega}$, the velocity potential of the surrounding fluid can be expressed under the hypothesis for potential flow as:

$$\boldsymbol{U = A\frac{c^2}{\omega}\eta(r,\theta)\sin(\omega t + \Psi_f)} \tag{2.47}$$

A is a dimensionless constant which specifies the amplitude of vibration, c is the speed of sound, η represents the mode shape of the fluid and Ψ is the phase angle.

The dynamic variation of the pressure in the potential flow can be described as [51]:

$$\boldsymbol{p = -\rho_F\frac{\partial U}{\partial t}} \tag{2.48}$$

2.4.1 Air

The transmission to the casing depends on the dynamic pressure in the fluid and this depends on the fluid density according to Eq.(2.48). Therefore, when the surrounding fluid is air the transmission from the rotating structure to the casing is low and therefore it is difficult to extract information of the rotating frame with sensors that measure the vibration of the casing. In this case it is desirable to use non contact sensors such as optical or proximity sensors that measure directly the vibration of the disk. It is supposed that the

transverse vibration of the disk in air under resonance can be expressed in the rotating frame as a standing wave (Eq.(2.3)) and that the sensors are measuring with no losses:

$$\boldsymbol{w_d(r,\theta_d,t) = W_{0,n}(r)\cos(n\theta_d)\cos(\omega_n t + \Psi_d)} \quad \textbf{(2.49)}$$

As mentioned before, only the transverse vibration of the modes with no nodal circles will be discussed here. Using the relation between rotating and stationary frame (Eq.(2.1)):

$$\boldsymbol{w_{d,ref\_casing}(r,\theta_c,t) = W_{0,n}(r)\cos(n(\theta_c + \Omega_{disk}t))\cos(\omega_n t + \Psi_d)} \quad \textbf{(2.50)}$$

w_{d,ref_casing} is the disk vibration but viewed from the casing with a proximity or optical sensor. Eq.(2.50) can be rewritten as:

$$\begin{aligned}\boldsymbol{w_{d,ref\ casing}(r,\theta_c,t)} &= \boldsymbol{\frac{1}{2}W_{0,n}(r)\cos((\omega_n + n\Omega_{disk})t + n\theta_c + \Psi_d)} \\ &\quad \boldsymbol{+\frac{1}{2}W_{0,n}(r)\cos((\omega_n - n\Omega_{disk})t - n\theta_c + \Psi_d)}\end{aligned} \quad \textbf{(2.51)}$$

According to Eq.(2.51), for a natural frequency in the rotating frame two natural frequencies are detected in the stationary frame:

$$\boldsymbol{\omega_{n,casing_{1,2}} = \omega_{n,disk} \pm n\Omega_{disk}} \quad \textbf{(2.52)}$$

And the phase shift between two sensors (both measuring the same physical magnitude) in the stationary frame is:

$$\boldsymbol{\Delta\alpha_{\omega_{n,casing\,1}} = +n\Delta\theta_c \ and\ \Delta\alpha_{\omega_{n,casing\,2}} = -n\Delta\theta_c} \quad \textbf{(2.53)}$$

Where $\Delta\theta_c$ is the spatial phase shift between two sensors in the peripheral direction of the casing and $\Delta\alpha$ is the phase difference between signals. In (2.52) and (2.53) only the positive value of n has to be considered.

2.4.2 Water

In this case, since the density of water is much higher than the density of air, the dynamic variation of pressure is not negligible (Equation (2.48)) and therefore information of the disk vibration can be extracted when measuring the casing.

As mentioned before, in this case the types of mode shapes with no nodal circles that appear on the disk are travelling waves. Therefore:

$$\boldsymbol{w_d(r,\theta_d,t) = W_{0,n}(r)\cos(\omega_n t + n\theta_d + \Psi_d)} \quad \textbf{(2.54)}$$

The vibration of the particles of the fluid in contact with the disk can be expressed as:

$$\boldsymbol{w_f(r,\theta_f,t) = W_{0,n}(r)\cos\left(n(\theta_f + \Omega_{\frac{disk}{fluid}}t) + \omega_n t + \Psi_f\right)} \quad \textbf{(2.55)}$$

Here is used that $\theta_d = (\theta_f + \Omega_{\frac{disk}{fluid}} t)$. If the displacement of the casing is much lower than the displacement of the disk the velocity potential in the flow can be described with the mode shape of the disk. Therefore:

$$\boldsymbol{U = A\frac{c^2}{\omega}\sin\left(\omega_n t + n\Omega_{disk/fluid}t + n\theta_f + \Psi_f\right)} \quad \textbf{(2.56)}$$

Thus the dynamic pressure that the fluid exerts on the casing can be written as:

$$\boldsymbol{p = -\rho_F\frac{\partial\emptyset}{\partial t} = A_p\sin\left((\omega_n + n\Omega_{disk/casing})t + n\theta_c + \Psi_c\right)} \quad \textbf{(2.57)}$$

A_p is the amplitude of the dynamic pressure and depends on the density of the fluid ρ_F. This pressure acts in the entire casing surface. To simplify the notation, up to now $\Omega_{disk/casing} = \Omega_{disk}$. If the frequency of the dynamic pressure (Eq. (2.57)) is well separated from the natural frequencies of the casing, then the response of the casing should be dominated by the excitation shape of the dynamic pressure. In this case the transverse vibration of a point on the casing can be expressed as:

$$\boldsymbol{w_c(r,\theta_c,t) = W_{c,n}(r)\cos((\omega_n + n\Omega_{disk})t + n\theta_c + \Psi_c)} \quad \textbf{(2.58)}$$

Which means that the relation between natural frequency viewed from the disk $\omega_{n,d}$ and viewed from the casing $\omega_{n,casing}$ is:

$$\boldsymbol{\omega_{n,casing} = \omega_{n,disk} + n\Omega_{disk}} \quad \textbf{(2.59)}$$

And the phase shift between two sensors on the casing installed at the same radius:

$$\boldsymbol{\Delta\alpha_{\omega_{n,casing}} = n\Delta\theta_c} \quad \textbf{(2.60)}$$

In this case n can be positive or negative. Compared to the case in air, in this case one frequency in the rotating frame corresponds to one frequency in the stationary frame. The lower natural frequency of the rotating frame (n>0) is translated to a higher frequency in the stationary frame as Eq.(2.59) shows. Extensively, the higher natural frequency in the rotating frame (n<0) is translated to a lower frequency in the stationary frame.

The associated mode shape observed in the casing (relative phase between sensors measuring the same magnitude) is also a travelling wave that moves in the same direction than the mode shape in the disk and with the same number of nodal diameters (Eq.(2.60)).

In case that the vibration of the disk is measured with an optical sensor that measures directly the vibration of the disk, $w_{c,n}(r) = W_{0,n}(r)$ if it is considered that there are no losses in the measurement process.

2.4.3 Validity of the deduced transmission and analytical example

The deduced Eq.(2.59) and Eq.(2.60) are valid so far the casing is not considered totally rigid and also when the casing has a negligible displacement compared to the displacement of the disk. Otherwise, the motion of the casing affects on the potential flow and this potential flow turns to a complex flow affected by the deformation shape of the casing and the deformation shape of the disk. In this case, this flow may affect also the model of the totally rigid walls described in chap. 2.1 and Eq.(2.57)-Eq.(2.60) are not valid anymore.

The displacement of the casing will be considerable if the fluid excites a frequency close to the natural frequency of the casing. Therefore if it assumed that a natural frequency of the disk is well separated from a natural frequency of the casing, the transmission will be as described. Nevertheless, casings in the real mechanical systems are usually very complex and with no peaky response, so the dynamic response of the casing itself has to be analyzed in detail in order to use the deduced equations.

In order to illustrate the mentioned effect an analytical example is made. It consists on a system with two degrees of freedom connected as shown in *Figure 2.5*.

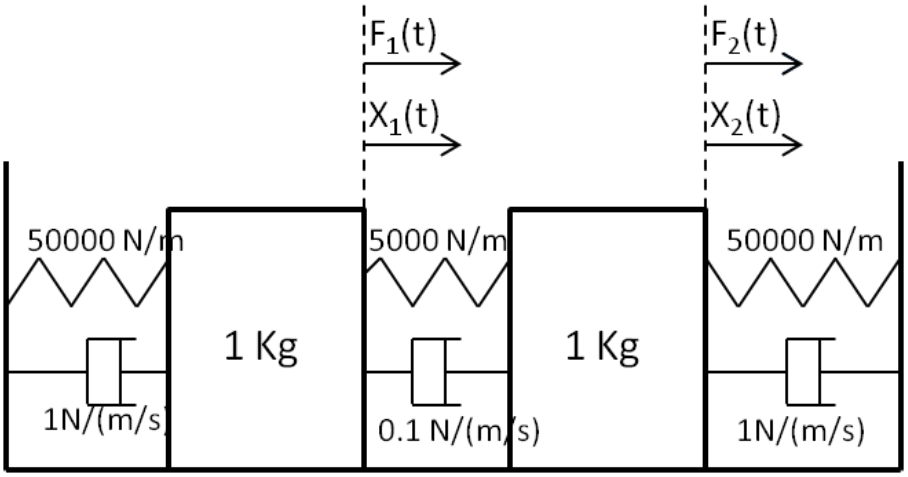

Figure 2.5: Analytical example

The corresponding natural frequencies and normalized mode shapes are:

Table 2.2: Natural frequencies and mode shapes of the analytical example

Natural frequency ($rad \cdot s^{-1}$)	Mode shape normalized
223,5	$(x_1,x_2)=(\sqrt{2}, \sqrt{2})$
245	$(x_1,x_2)=(\sqrt{2},-\sqrt{2})$

Now it is supposed that the system is excited with a sweep excitation from 0 to 1000Hz, with a mode shape different than one of the mode shapes, for example $(F_1,F_2)=(1, -2)$ changing the frequency from 1 to 1000Hz. The forced response of the system is plotted in *Figure 2.6a* and the angle between the forced vector response and the force is plotted in *Figure 2.6b*.

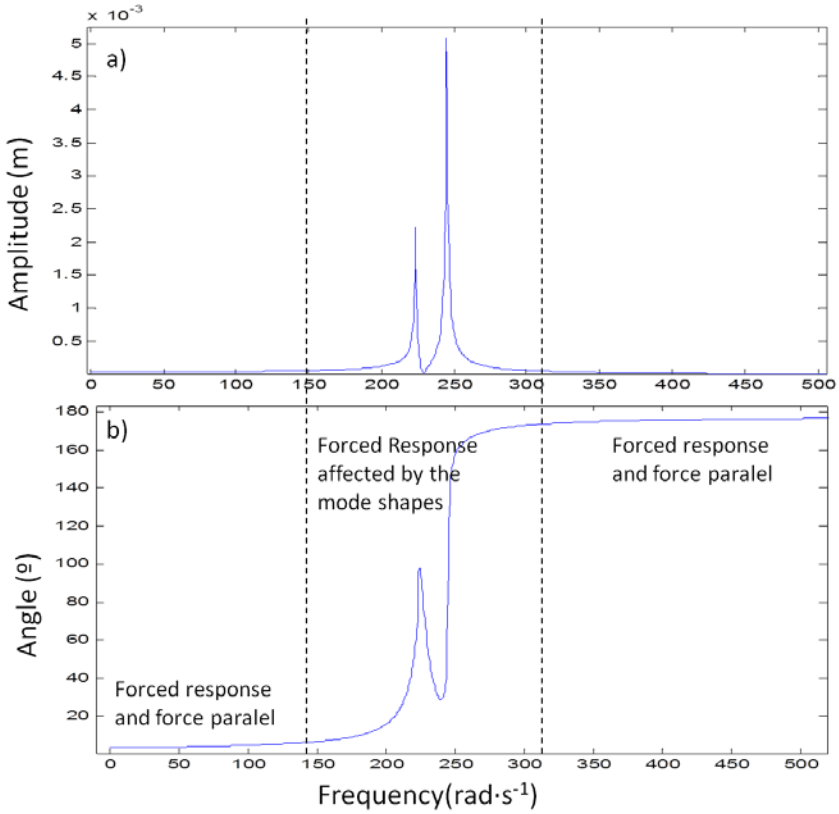

Figure 2.6: a)Forced response of the system. b) Angle between the response and the force

As shown in this figure, when the excitation frequency is not in the frequency band of the natural frequencies of the system, the response of the system is in phase or counterphase with the excitation. When the excitation frequency is in the frequency band of the natural frequencies the motion of the system is dominated by the mode shapes of the system.

With this example it is clear that if the casing is excited by the disk and the natural frequencies of the disk do not coincide with the natural frequencies of the casing, the mode shape could be theoretically measured from the casing with a phase shift that depends on the number of diametrical mode n and on the rotating speed of the disk.

Chapter 3

3. ROTATING DISK TEST RIG DESCRIPTION AND TESTS CARRIED OUT

In order to verify the main conclusions of the analytical model, an experimental setup has been developed. It consists on a disk connected to a variable speed motor. When the disk is rotating the excitation is performed from the rotating frame with piezoelectric patches (PZT's) or with a special impact device. The response is measured from the rotating frame with miniature accelerometers and from the stationary frame with different devices such as accelerometers, Laser Doppler Vibrometer or pressure sensors.

3.1 Test rig

3.1.1 Disk

The disk is made of stainless steel with an external radius r_{out} and a thickness h_D. The disk has a hole on its center in order to attach the shaft r_{int}. The disk has special holes to attach the piezoelectric patches and to screw the miniature accelerometers. The mass of the disk is approximately 7.6 Kg.

3.1.2 Casing

The casing is made by stainless steel. The ratio between the radius of the tank and the radius of the disk is $r_{casing}/ r_{out}=1.035$. Therefore the radial gap between the disk and the casing is small compared to the radius of the disk. The axial gap between the disk and the casing can be adjusted at $H_{up}/ r_{out} =0.05, 0.1, 0.15, 0.2$. For the mentioned configurations $H_{down/}/ r_{out} =0.49, 0.44, 0.39, 0.34$, which means that the disk is closer to the upper wall for all the configurations tested. A scheme of the mounted disk in the casing without the instrumentation used is shown in *Figure 3.1*.

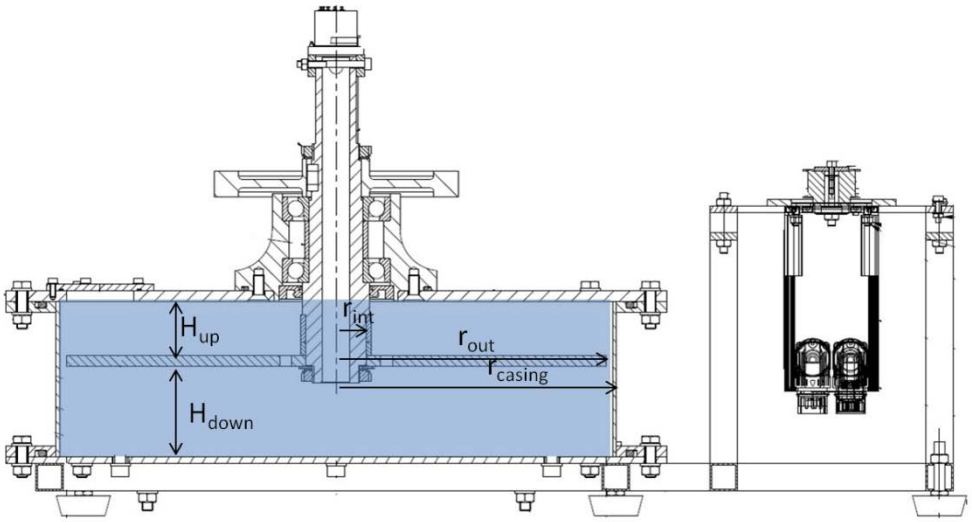

Figure 3.1: Test rig without instrumentation

In the upper cover of the casing several measurement devices can be used in order to measure the response of the rotating disk from the stationary frame. For this reason a plexiglass hole is made in order to work with the optical devices. Also five special holes are made to install pressure sensors, the impact device and a system to maintain the tank full avoiding air bubbles. An overview of the upper cover with the used sensors is shown in *Figure 3.2*.

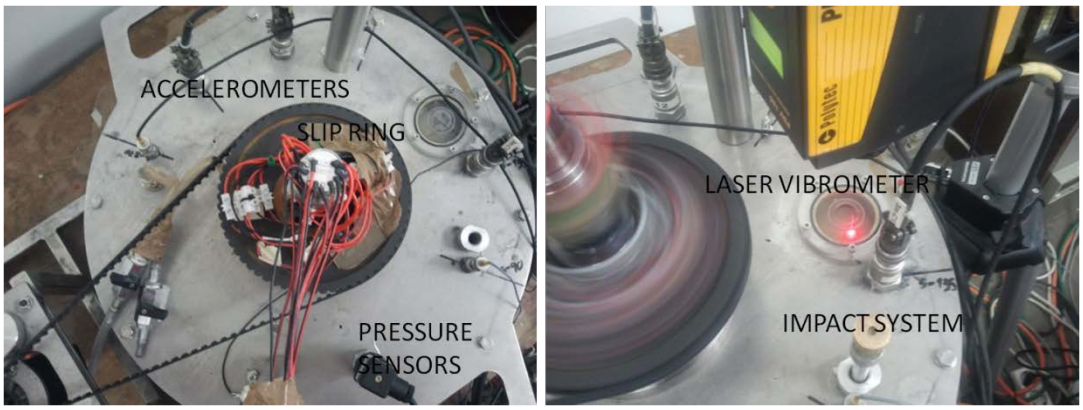

Figure 3.2: Casing of the test rig with the mounted sensors

3.1.3 Motor

The motor is a Mavilor MLV-072, which is a variable speed motor. The rotating speed is controlled and stabilized with a computer. The vibrations of the motor are isolated from the

rest of the test rig trough a silent block. The rotation of the motor is transmitted to the shaft with a cog belt with a reduction of 1/5.

When the disk is rotating in air the disk can rotate up to 10Hz. Nevertheless when the disk is rotating in water the velocity of the disk is limited to 8Hz in order to avoid damages of the motor caused by the high power consumption due to the disk-losses in water [51].

3.1.4 Slip ring

Through the slip ring Michigan S10, the excitation and response signals are transmitted from the rotating to the stationary frame. This system is mounted at the tip of the shaft (*Figure 3.2*). Ten independent circuit slip rings are used to transmit the signals. Since one channel of a sensor or exciter consist in a + and a – line, some lines have to share a common circuit. Therefore, the – terminals of the accelerometers are connected to one common point and the – terminals of the patches are connected to another common point, in order to have the maximum sensors possible on the rotating frame.

3.1.5 Data acquisition system

A Bruel&Kjaer Type 3038 module is used to acquire the signals. The maximum frequency acquisition is 25.6 KHz, much higher as needed for this study.

3.2 Instrumentation

3.2.1 Accelerometers

For the measurement of the response from the rotating frame miniature and submergible accelerometers Dytran 3006-A (sensitivity 100mV/g) have been used. They are directly screwed on the disk. It is checked that after the installation of the accelerometers on the disk the mass does not change substantially.

To measure the response from the stationary frame accelerometers Kistler 8752A50 (sensitivity 100mV/g) have been glued on the upper cover.

3.2.2 Piezoelctric patches (PZT's)

For the excitation of the disk from the rotating frame six patches PI-876A12 (61mm × 35mm) are glued on the disk. They are glued on the disk with an epoxy component LOCTITE 454.

3.2.3 Impact hammer

The impact hammer used for the tests is a Kistler 9722-A2000 (sensitivity 500uV/N). This hammer has a maximal force of 2000N, enough to excite the system. The hammer is used to impact the disk with a special device shown in *Figure 3.2* and also to impact the casing directly.

3.2.4 Laser

To measure the response of the disk from the stationary frame a Laser Doppler Vibrometer PDV-100 with adjustable sensitivity (sensitivity range of $200V/ms^{-1}$-$8V/ms^{-1}$) has been used. The Laser is mounted on a tripod without any contact to the test rig in order to avoid influences of the casing vibration.

3.2.5 Presure sensors

Pressure sensors (KRISTAL Type 4295A2V34) are installed on the stationary frame to measure the dynamic pressure due to the disk vibration. They have to be powered with 18-36Vdc and they have a sensitivity of 5V/bar in a measurement range of 0-2bar.

3.2.6 Signal generator and amplifier

The patches work in a range of -100V to 250V. For the signal generation a NI-9263 module is used. This module can generate four independent analogical outputs with an amplitude of -10V to 10V. With an amplifier OEM-835 the analogical signal is amplified by 25, so the send signal to the patch has the desired level. Also a signal for monitoring the excitation is send to the data acquisition system.

An overview of the system test rig with the instrumentation used is shown in *Figure 3.3.*

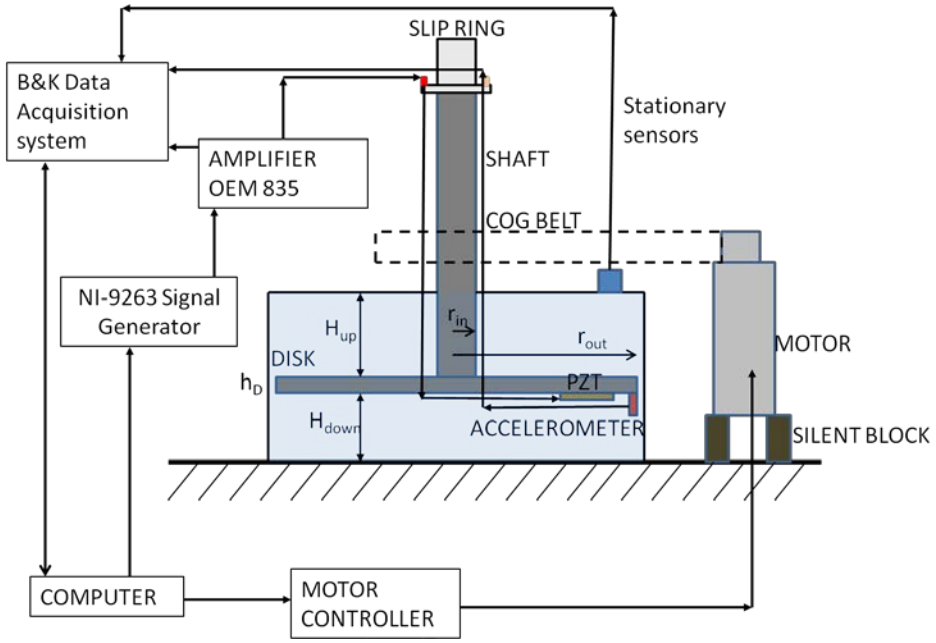

Figure 3.3: Experimental apparatus

3.3Position of the sensors

3.3.1 Rotating frame

In the rotating frame only piezoelectric patches and miniature accelerometers are placed. The nomenclature used for the accelerometers is A-X, where X is the angle related to the 0º direction in counterclockwise direction, when the disk is attached to the shaft and viewing the test rig from the top. Seven accelerometers (A-0, A-90, A-135, A-180,A-210,A-240 and A-270) have been used during the tests. Not all of them have been used simultaneously because the limited numbers of channels in the slip ring system.

The nomenclature used is the same as for the accelerometers (P-0, P-90, P-135, P-180, P-270, P-315). Only four can be used simultaneously because the limited current in the slip ring system. Two different configurations have been used for the rotating excitation: (P-0, P-90, P-180, P-270) and (P-0, P-135, P-180, P-315).

The installed patches and accelerometers on the disk are shown in *Figure 3.4*.

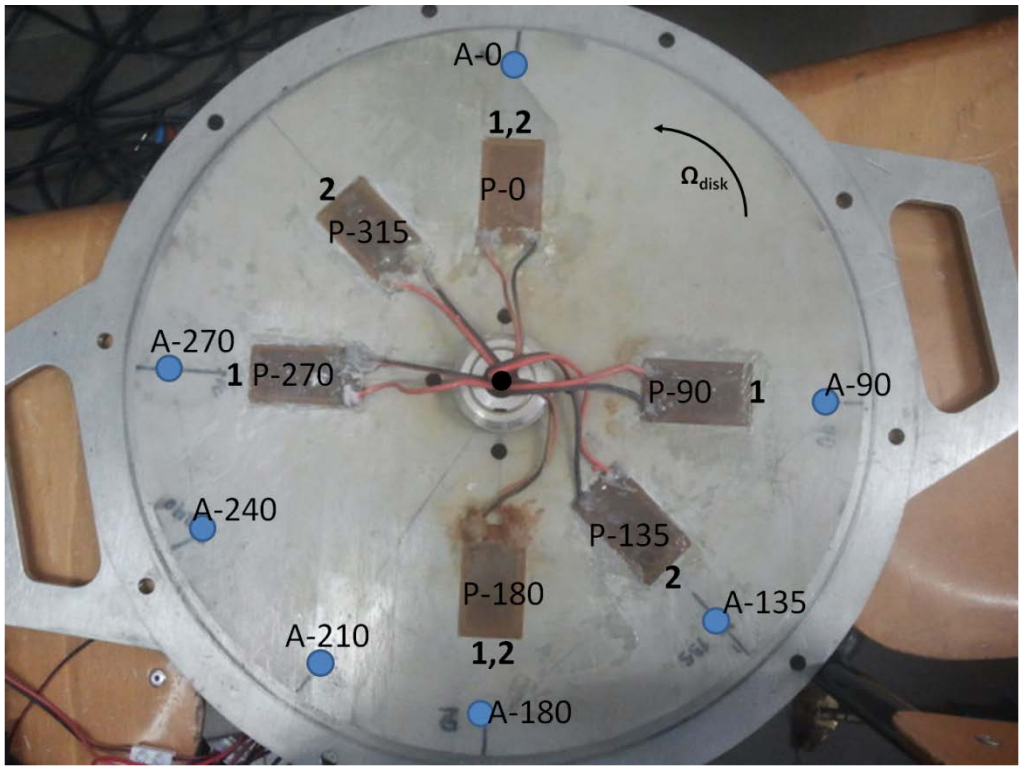

Figure 3.4: Disk with installed accelerometers and piezoelectric patches

3.3.2 Stationary frame

In the stationary frame (upper cover) pressure sensors, accelerometers and a Laser Doppler Vibrometer have been used. The accelerometer and pressure sensors are determined by its angular position with respect to its reference direction shown in Figure 3.5. Following accelerometers have been installed: AS-0, AS-45, AS-90, AS-135, AS-180, AS-210, AS-240.

In the same way, the position for pressure sensors is defined. The pressure sensors are installed farther from the centre. Three pressure sensors are installed: PRES-0, PRES-30, PRES-180.

The Laser is installed in the shown position in Figure 3.5. It is installed in the same radius than the pressure sensors.

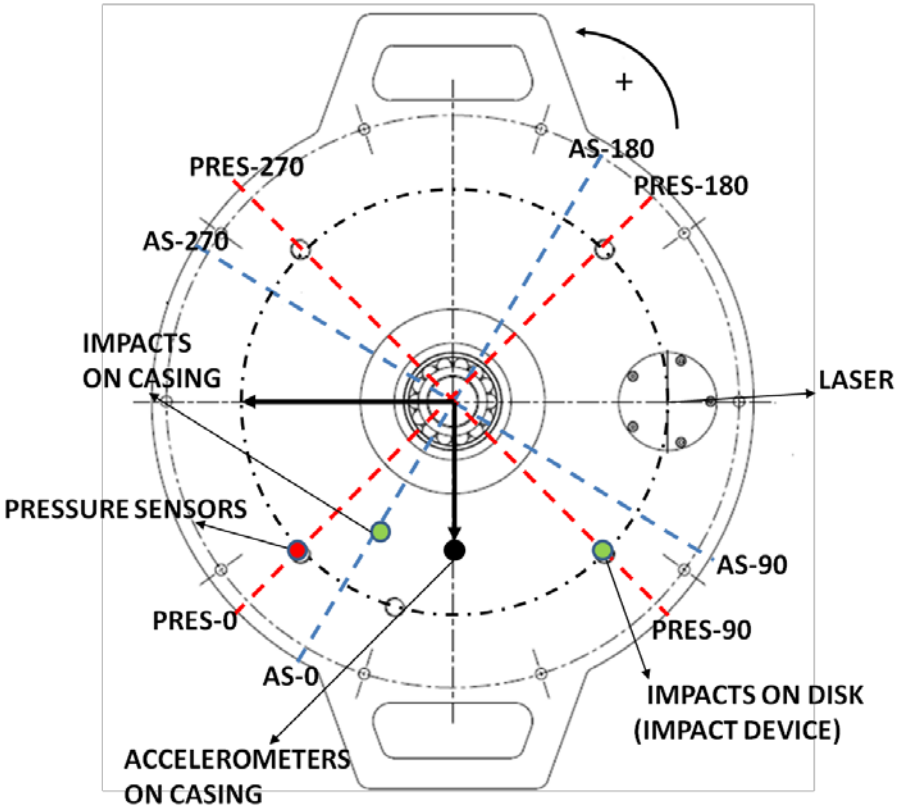

Figure 3.5: Sensors on the stationary frame

3.4Calibration

3.4.1 Accelerometers

With the calibrator Bruel&Kjaer 4294, that produces a vibration of $10m/s^2$ in a frequency of 159,2Hz, the sensitivity given by the manufacturers has been checked.

3.4.2 Laser

The maximal vibration for the Laser can be adjusted at 3 different levels, changing the sensitivity. In air and in water, this sensitivity has been checked with an accelerometer vibrating face to face with the accelerometer. The relationship between the sensitivity in air and in water is the refraction index of water which is 1.33.

Table 3.1: Sensitivity of the Laser in air and in water

Sensitivity air	Maximal velocity air	Sensitivity water	Maximal velocity water
200 (V/(m·s^{-1}))	20 mm·s^{-1}	267 (V/(m·s^{-1}))	15 mm·s^{-1}
40 (V/(m·s^{-1}))	100 mm·s^{-1}	53 (V/(m·s^{-1}))	75 mm·s^{-1}
8(V/(m·s^{-1}))	500 mm·s^{-1}	10,67(V/(m·s^{-1}))	375 mm·s^{-1}

3.4.3 Pressure sensors

Since only the dynamic pressure produced by the disk is of interest, the continuous component of the signal, which is much larger than the pressure produced by the disk vibration, has been removed applying a high-pass filter of 7Hz.

3.4.4 Piezoelectric patches (PZT's)

It is checked that, when using the same excitation signal for two different patches the response of the contiguous accelerometer is different in terms of amplitude and phase, since the excitation depends on the mounting condition of the patch. Furthermore, for the same patch the relationship force/voltage changes within the excited frequency. Therefore patches have to be calibrated, in order to make a compensated excitation shape at one desired frequency. In this case, since the response of the disk is studied under resonance condition, the calibrated frequencies are the natural frequencies of the disk. For the first several natural frequencies, patches are calibrated to make a compensated excitation shape in angle and phase.

The relation force/voltage characteristic for the piezoelectric patches changes for each patch (since it depends on the mounting condition of the patch) and with the signal frequency. To make that patches work with the same amplitude (in force) and with the desired phase to each other, they have been previously calibrated at the natural frequencies studied. Here is explained how the calibration is performed for the mode n=±2 (disk rotating in air) and configuration 1 (*Figure 3.4*). For other modes and configurations the procedure is equivalent.

First, only patch P-0 is used at one natural frequency with a peak value of 75V. $(X_{A\text{-}0(P\text{-}0)})_{fn}$ (amplitude of the vibration of accelerometer A-0 due to an excitation with P-0 at the natural frequency n) and $(\alpha_{A\text{-}0(P\text{-}0)/P\text{-}0})_{fn}$ (angle between the signal of A-0 and the signal of P-0 due to an excitation with P-0 at the natural frequency n) are measured.

When using another patch at the same natural frequency, $(X_{A\text{-}i(P\text{-}i)})_{fn}$ and $(\alpha_{A\text{-}i(P\text{-}i)/P\text{-}0})_{fn}$ are measured (i is 90º, 180º and 270º in this case). The amplitude of P-i is changed in order to accomplish $(X_{A\text{-}i(P\text{-}i)})_{fn}=(X_{A\text{-}0(P\text{-}0)})_{fn}$ for each i. Also a phase shift between signal P-i and signal P-0 is introduced to make that $(\alpha_{A\text{-}i(P\text{-}i)/P\text{-}0})_{fn}=(\alpha_{A\text{-}0(P\text{-}0)/P\text{-}0})_{fn}$. In this case the signal of P-0 is acquired as a reference, but is not really used to excite the patch P-0. In the specified case, the calibration of the patches has been done adjusting the signals of the patches, to accomplish:

$$(X_{A\text{-}0(P\text{-}0)})_{fn} = (X_{A\text{-}90(P\text{-}90)})_{fn} = (X_{A\text{-}180(P\text{-}180)})_{fn} = (X_{A\text{-}90(P\text{-}270)})_{fn} \tag{3.1}$$

$$(\alpha_{A\text{-}0(P\text{-}0)/P\text{-}0})_{fn} = (\alpha_{A\text{-}90(P\text{-}90)/P\text{-}0})_{fn} = (\alpha_{A\text{-}180(P\text{-}180)/P\text{-}0})_{fn} = (\alpha_{A\text{-}270(P\text{-}270)/P\text{-}0})_{fn}$$

The accomplishment of Eq.**(3.1)** for each f_n (f_n are the first natural frequencies of the disk), guarantee that patches are properly calibrated in amplitude and phase (**Figure 3.6**).

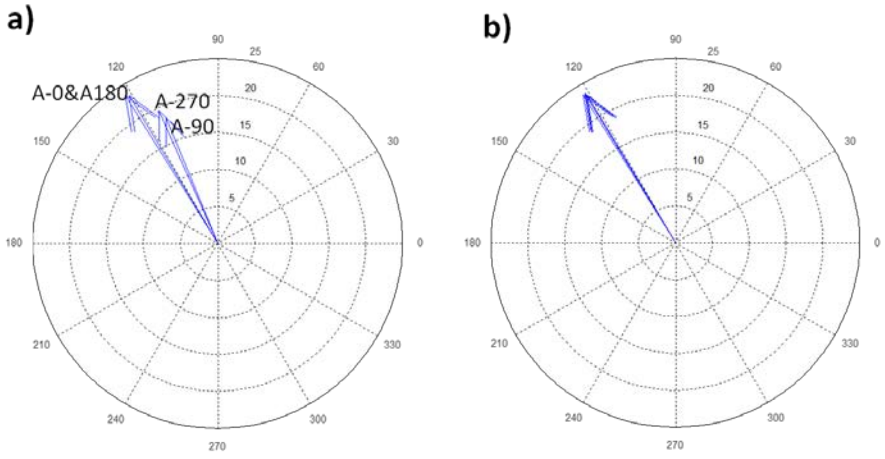

Figure 3.6: Polar plot of the sensors. a) Before calibration of PZTs b) After calibration of PZTS

After patches are calibrated, a phase shift between them (apart from the phase shift introduced for the calibration) can be introduced to make the desired excitation pattern.

3.5 Tests to be performed

Once the system is set-up at one configuration it is excited on the disk and excited on the casing to determine the dynamic response. One configuration is defined by the rotating speed of the disk, the fluid on the casing and the distance H_{up}. The combination of these parameters (*Table 3.2)* gives the possible configurations.

Table 3.2: Configurations tested

Ω_{disk}	Fluid on casing	H_{up}/r_{out}
0Hz-8Hz	Air, Water	0.05, 0.1, 0.15, 0.2

3.5.1 Excitation with hammer

For one configuration, the disk is impacted with the impact device (**Figure 3.2**). Five impacts are performed on the disk in order to get the averaged FRF.

Furthermore, the casing is also impacted (generally close to the accelerometer AS-0 as shown in *Figure 3.5*) in order to enhance the natural frequencies of the casing in front of the natural frequencies of the disk.

3.5.2 Excitation with one patch (sweep excitation)

To determine the natural frequencies and mode shapes of the disk, it is excited with one patch and with a sweep signal. Natural frequencies of the rotating disk in air and in water have to be determined. Since, the first several natural frequencies are the most relevant in the real case, cause they can be excited by RSI phenomena [8], this study is concerned in a frequency range of 0-1200Hz, which includes the three first diametrical modes of the disk with n>1. Therefore, for this disk a sweep signal from 0 to 1200Hz is used to excite the first natural frequencies of the disk in air and in water. Such a signal can be described as:

$$y = Asin(\varepsilon t(t)) \qquad for\ 0<t<t_{end} \qquad \textbf{(3.2)}$$

When a patch works with this signal, it excites all the frequency band from 0Hz to $\frac{\omega t_{end}}{2\pi}$ Hz. $\frac{\omega t_{end}}{2\pi}$ is selected as 1200Hz in this case. ε (sweep rate) has to be enough small (slow sweep) in order to have a good resolution in frequency when applying the FFT, without losing information.

In Figure 3.7, the procedure to obtain the natural frequencies of the disk is shown for one resonance and one sensor. The time signal of the excitation P-0 (Figure 3.7a) shows a slow sweep excitation. The time signal of A-0 (Figure 3.7a) shows that a resonance occur at certain time. To obtain the frequency content of these signals, a Hanning Window of 4s (resolution 0,25Hz) is applied on the time signals. Since this window is shorter than the total length of the time signals, it is translated 0,2 seconds (5% of the window length) every average. In each average, the FFT is applied in both signals and superposed to the other averages with the maximum hold method, which considers only the maximum value for each frequency. In this way the frequency content of both signals is obtained (Figure 3.7b). Using both response (A-0) and excitation (P-0) signals, the frequency response is obtained (Figure 7c). Natural frequencies are detected in precision looking at the peaks of the frequency response function (FRF). The corresponding mode shapes are obtained analyzing the relative phase of the accelerometers on the rotating frame and contrasting with the analytical model. In this way, natural frequencies and mode shapes are determined for the disk in the different situations tested.

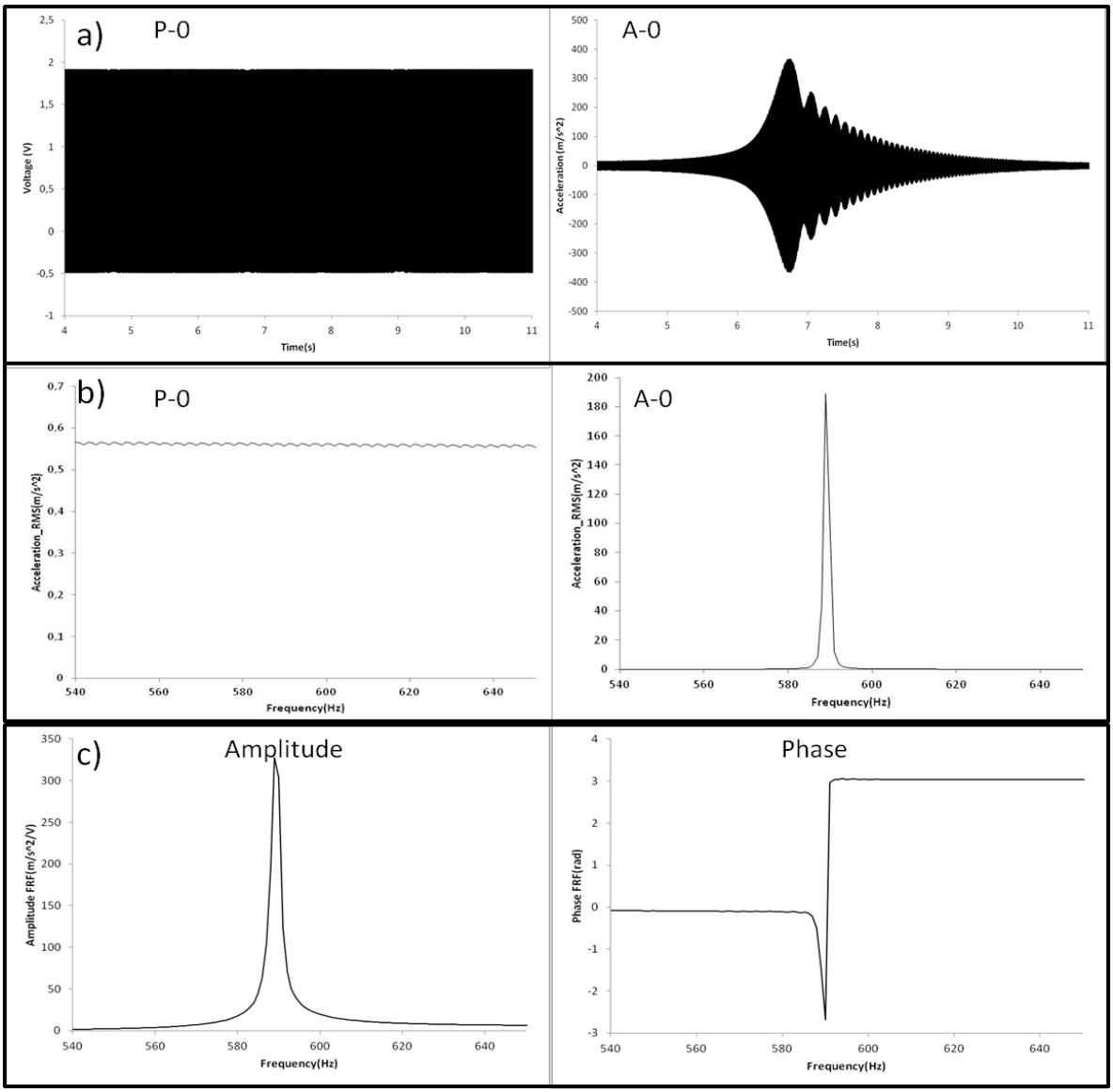

Figure 3.7: Determination of the natural frequencies of the rotating disk. a) Time signals. b) Signals after FFT. c) FRF Amplitude& Phase

3.5.3 Rotating excitation patterns with several PZT's actuators for one configuration

For H_{up}/r_{out}=0.15, Ω_{disk}=8Hz the disk is excited with different rotating excitation patterns that simulate the RSI (see chapter 2.3). Patches are calibrated in this configuration in order to make a compensated excitation shape in these frequencies (as mentioned in chapter 3.4.4). This is performed for the disk rotating in air and for the disk rotating in water. The excitation patterns that are created with four patches installed in the two different

configurations shown in Figure 3.4 are represented in Figure 3.8. The response is measured with the accelerometers screwed on the disk.

In Figure 3.8 the rotating direction of the disk is shown (viewing the disk from the top). This rotating direction is the same for all the tests performed. Adjusting the phase shift between patches the excitation shape and its rotating direction is defined (γ). The number of γ indicates the excitation shape and the sign of γ its rotating direction. Note that for some configurations and excitation shapes this rotating direction cannot be defined with the patches available. These excitations are applied for the structural modes n=±2, ±3 and ±4 as Figure 3.8 shows.

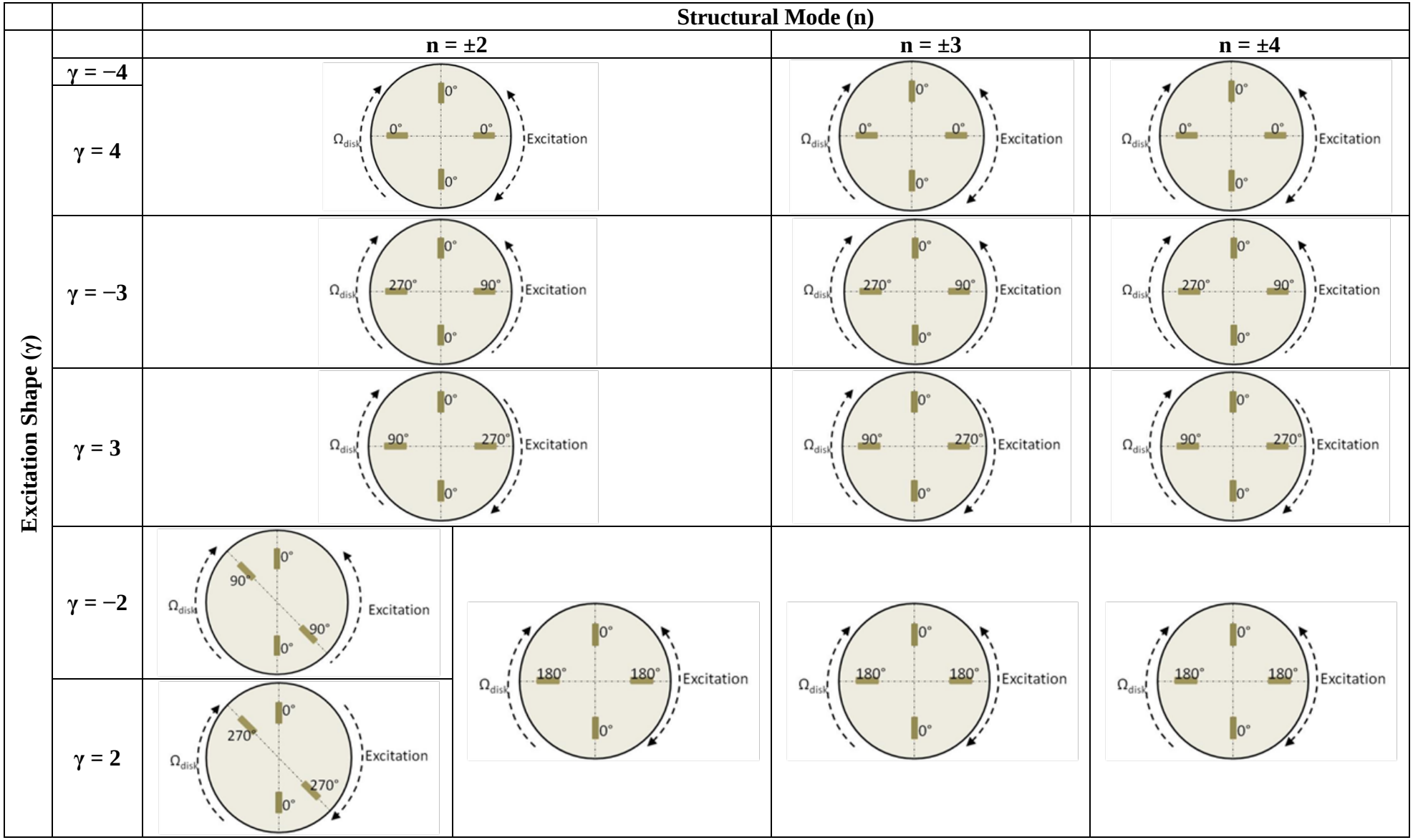

Figure 3.8: Excitation patterns created with the installed Piezoelectric Patches

As Figure 3.8 shows, with four patches attached at 90º it is not possible to define the rotating direction of the excitation for the modes n=±2 and n=±4, changing the phases between exciters. For n=±3 this direction is decided changing the phase of the patches (Figure 9). For n=±2 another configuration is tested (P-0, P-135, P-180 and P-315), that defines the rotating direction. With this configuration is also not possible to define the direction of the excitation for n=±4.

3.5.4 Rowing accelerometer on casing for one configuration

For H_{up}/r_{out}=0.05, Ω_{disk}=8Hz and water between the disk and the casing, the transmission disk-casing is studied with more detail.

For this purpose, only one accelerometer is leaved on the disk (AR-0) as a reference in the rotating frame during all the tests and five series, moving all the accelerometers placed on the casing, are performed. The disk is not stopped during the tests in order to maintain the boundary and environmental conditions as constant as possible. For each serie, the disk is excited through the impact device, excited with a sweep excitation (with the PZT P-0) and the casing impacted with the hammer. The specified positions of the accelerometers and the impact positions are shown in Figure 3.9.

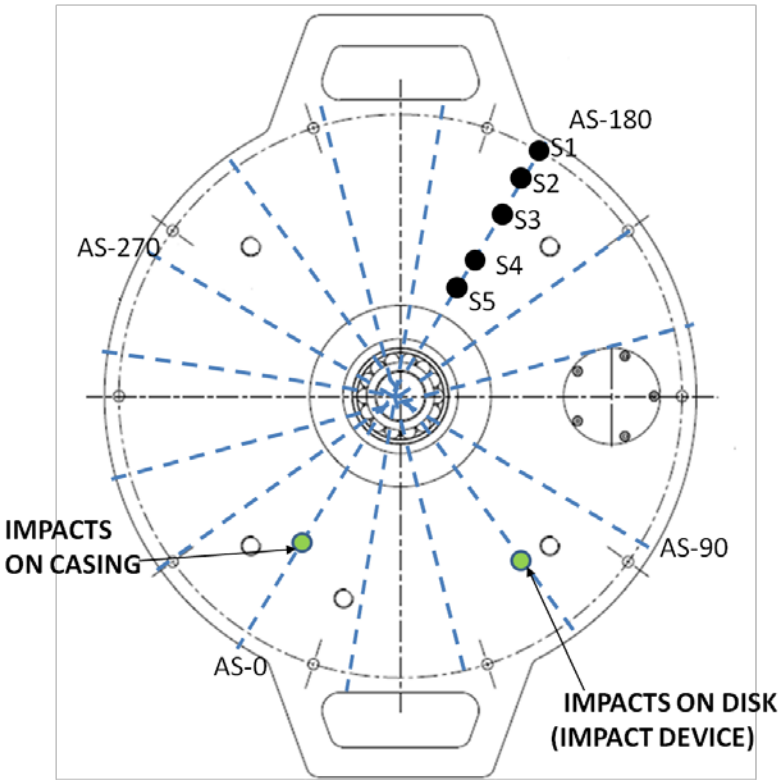

Figure 3.9: Detailed study of the transmission disk-casing. Position of the accelerometers and of the excitation points

As seen in Figure 3.9, for each serie an accelerometer every 22,5º is located excepting on the line 135º due to the interference of the plexiglass window.

Chapter 4

4. STRUCTURAL RESPONSE OF A ROTATING DISK IN WATER

This section presents the influence of the rotation when the disk is submerged and confined. Experimental, analytical and numerical results are compared together showing that the effect of the relative rotation of a heavy fluid with respect to the disk has a very important effect on the natural frequencies and mode shapes. All the results presented are for H_{up}/r_{out}=0.05, except in Chapter 4.5.5 where the natural frequencies for the other heights tested are presented.

4.1 Preliminary analysis of the rotating disk in air

To analyze the natural frequencies of the confined disk submerged in water and rotating, a previous analysis of the disk in air has been performed, in order to calibrate the parameters that refer to the geometrical and material properties of the disk. The influence of ρ_F, when the surrounding fluid is air, is negligibly small in the term of mass and stiffness (Eq. (2.30)). In this case, natural frequencies of the disk in air can be calculated as in Eq. (2.16). To determine D* from Eq. (2.16), the methodology described in Chap. 2.2.1 is used.

4.1.1 Natural frequencies of an annular plate in air

With the non rotating disk, a sweep signal excitation from 200 to 1200Hz is applied with the patch P-0. The signals of accelerometer A-0 and patch P-0 are analyzed. Figure 4.1 shows the time signals of both sensors.

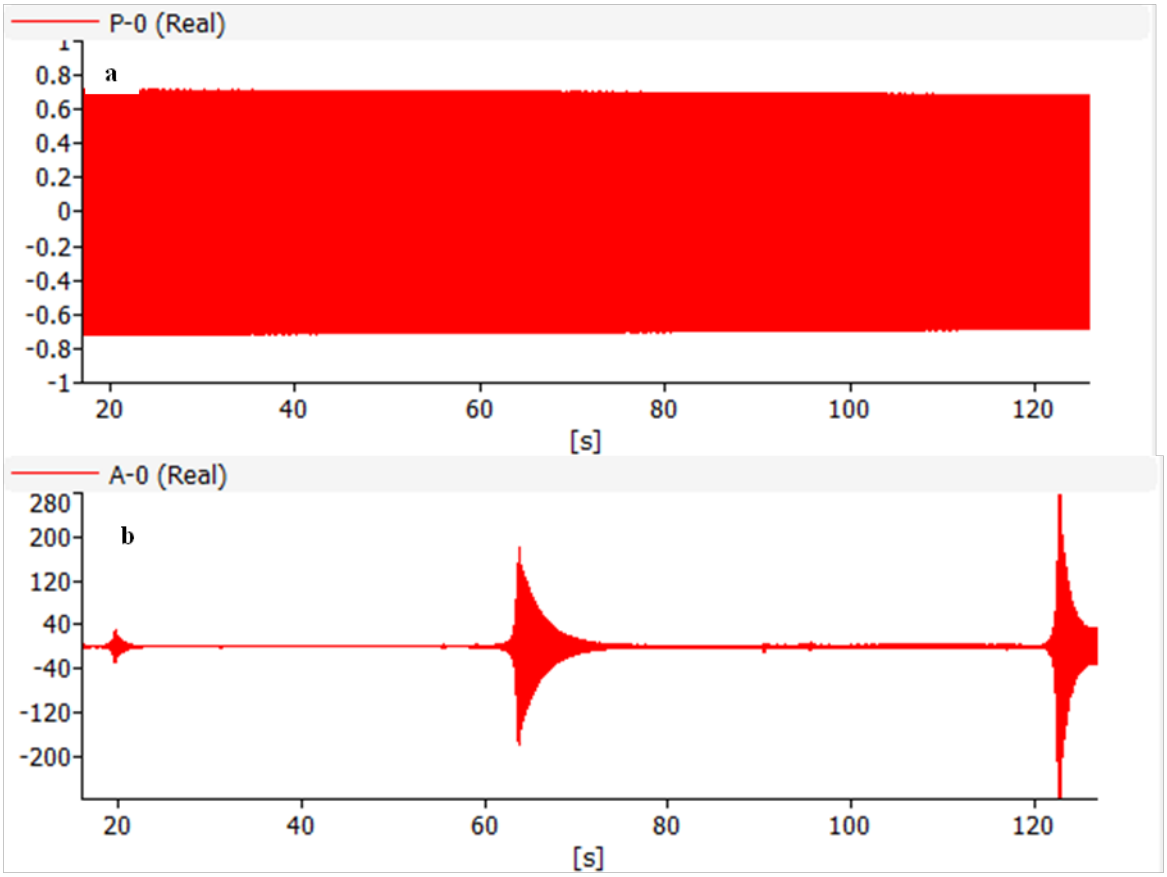

Figure 4.1: Time signals of the sweep excitation (a) and response (b)

The signal A-0 shows three local maximum when it is excited from with the patch P-0. These are the three natural frequencies of the disk below 1200Hz. To study the frequency content of these signals the procedure explained in Chapter 3.5 (Figure 3.7) is used. This procedure leads to the resulting response of the disk in the frequency domain (Figure 4.2).

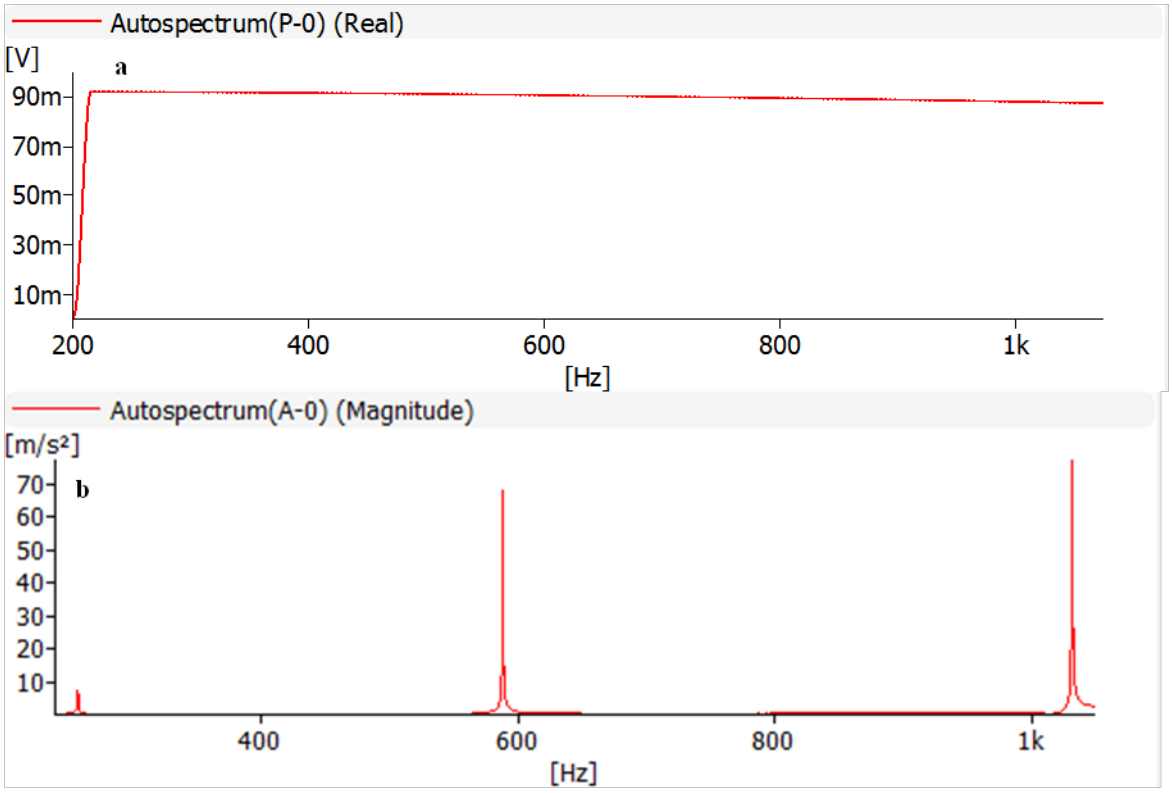

Figure 4.2: ***Autospectrum of the patch P-0 (a) and accelerometer A-0 (b) with peak hold method***

The resulting Autospectrum of the patch indicates that the disk has been excited properly from 200 to 1200Hz, since the curve is continuous for all the frequencies. From the Autospectrum of the accelerometer, the natural frequencies of the disk are obtained.

For the geometrical properties of the disk and the studied modes, the simplified analytical model can be used to predict the natural frequencies of the disk. Also a numerical FEM simulation has been performed in order to estimate the natural frequencies of the disk in air. The comparison between methods is shown in Table 4.1

Table 4.1: Natural frequencies (Hz) of the disk in air

Nodal diameters	Experimental	Analytical	Numerical	Discrepancy (analytical-experimental)	Discrepancy (numerical-experimental)
2	257,75	260,03	261,02	0,88%	1,27%
3	588,25	585,07	574,93	0,54%	2,27%
4	1031,5	1040,13	1009,7	0,84%	2,11%

The analytical model estimates D* minimizing the global error for these three modes.

4.1.2 Influence of rotation

The same excitation and the same procedure mentioned before are applied for the case that the disk is rotating. In this way, natural frequencies for the rotating case are obtained Figure 4.3 represents the variation of the natural frequencies due to rotation for the mode n=±3.

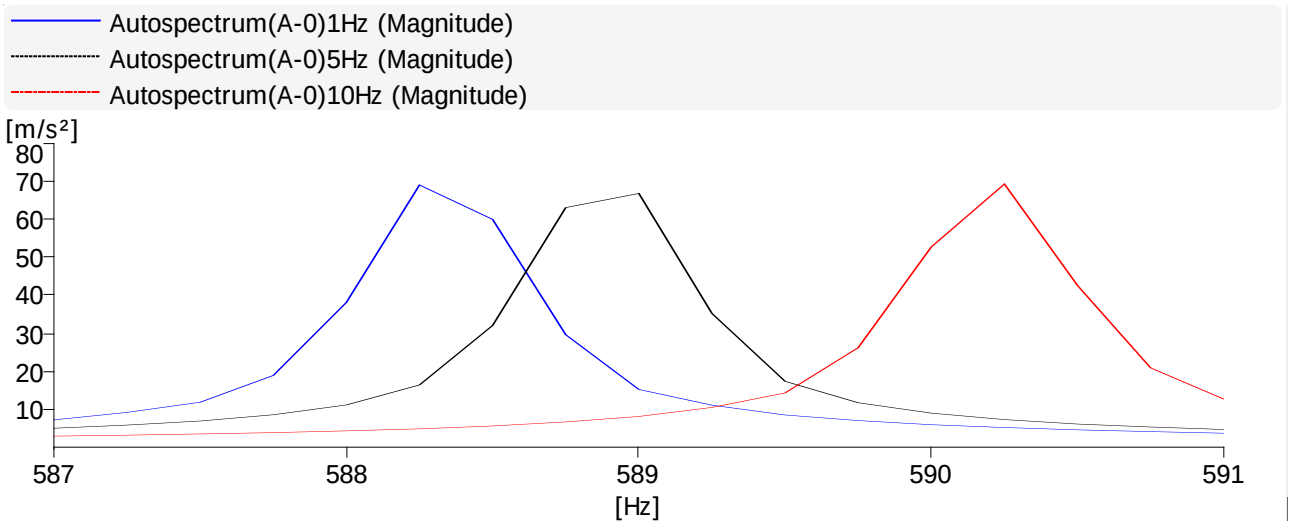

Figure 4.3: Natural frequency n=±3 for different rotating speeds

A light increase due to centrifugal effect is observed for the studied modes. The values for the modes n=±2, ±3, ±4 are represented on Table 4.2.

Table 4.2: First natural frequencies of the disk under different rotating speeds.

Mode (Hz)/rotation speed (Hz)	2ND	3ND	4ND
0	257,75	588,25	1031,5
1	257,75	588,25	1031,5
2	257,75	588,5	1031,5
3	257,75	588, 5	1031,5
4	258	588,75	1031,75
5	258,25	589	1032
6	258,5	589,25	1032,25
7	258,75	589,25	1032,5
8	259,25	589,75	1032,75
9	259,5	590	1033
10	259,75	590,25	1033,25
$\Delta\% = \frac{\omega_{10\mathrm{Hz}} - \omega_{0\mathrm{Hz}}}{\omega_{0\mathrm{Hz}}} \cdot 100$	0,78	0,33	0,17

Since the rotating speed is maximum at 10Hz, only a slight variation in the natural frequencies is observed (less than 1% compared to the non-rotating case), when analyzing the results from the rotating frame. Furthermore, due to limited resolution of the analysis (0.25Hz) some of the values appear repeated. According to the analytical model, the natural frequencies of the rotating disk in air remain constant for increasing rotating speed which is a good approach for the tested rotating speeds.

This light increase in the experimental values is considered in some studies [16, 18, 19, 44], since the centrifugal and Coriolis forces are added to the inertia forces on Eq.(2.2). Nevertheless, for a rotating speed of 10Hz (600rpm) the centrifugal effect has only a very small influence.

4.2 Added mass of infinite water

The same experimental methodology (Chap. 3.5) is performed to obtain the natural frequencies of the disk in a pool with infinite water. For the analytical model, Eq. (2.30) is used with $\Omega_{up}= \Omega_{down}=0$, $\rho_F=1000$ and H_{up} and H_{down} are set to infinite. The numerical simulation has been also developed imposing infinite surrounding water. Results are compared in Table 4.3.

Table 4.3: Natural frequencies (Hz) of the disk in infinite water

Nodal diameters	Experimental	Analytical	Numerical	Discrepancy (analytical-experimental)	Discrepancy (numerical-experimental)
2	178,5	178,28	182,43	0,12%	2,33%
3	439,1	442,07	425,41	0,67%	3,1%
4	776,7	831,78	777,67	7,09%	0,12%

4.3Effect of the radial gap

The analytical model does not consider the effect of the radial gap disk-casing in the transverse vibration. In [31] it is shown that up to certain distance, the radial gap does not have any influence in the value of the natural frequencies of the axial modes. For the present configuration two situations are compared, one with the disk with water until its lower surface and the other with water in the radial gap (Figure 4.4).

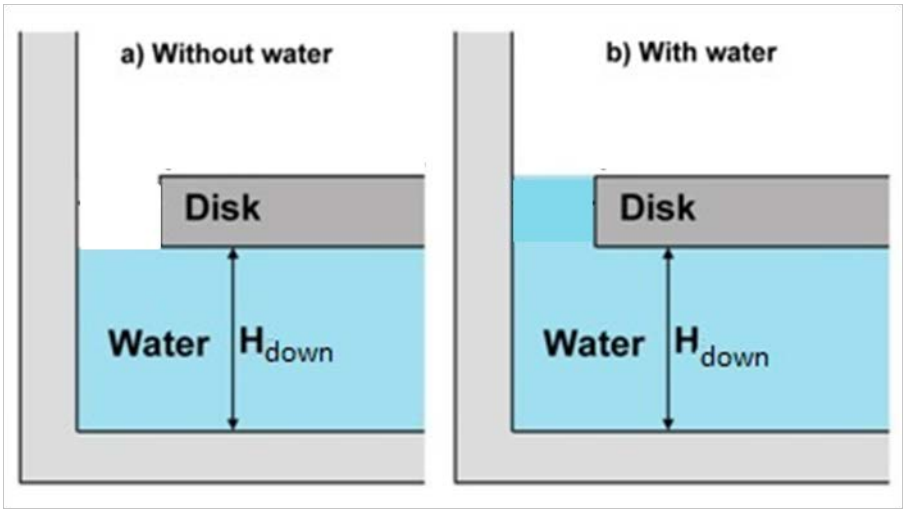

Figure 4.4: Disk without water in the radial gap(a) and with water(b)

Results of the studied modes for these two cases are shown in Table 4.4.

Table 4.4: Natural frequencies (Hz) of the disk without and with water in the radial gap (numerical simulation)

Nodal diameters	Without water	With water	Decrease
2	208,04	196,94	5,33%
3	482,47	463,67	3,90%
4	873,36	843,51	3,42%

The decrease in natural frequencies is approximately 3%-5% for this test set-up. In order to consider this effect in the analytical model, the parameter r_0 is slightly augmented to take into account the effect of the radial gap, which physically means to increase the mass of the disk and decrease the stiffness. r_0 is set to a value that minimize the averaged discrepancy in percent between numerical and analytical model for these three modes.

4.4Added mass of the disk confined

When the disk is inside the tank its natural frequencies are determined experimentally with the experimental procedures mentioned before (Chap. 3.5). In this case, for the analytical

model the value of r_0 used, is the corrected one, in order to take into account the radial gap. *Table 4.5* shows the comparison between results.

Table 4.5: Natural frequencies (Hz) of the disk confined without rotation

Nodal diameters	Experimental	Analytical	Numerical	Discrepancy (analytical-experimental)	Discrepancy (numerical-experimental)
2	127,05	122,18	134,68	3,83%	6,01%
3	321,16	345,82	336,36	7,68%	4,73%
4	642,23	694,12	645	8,08%	0,43%

4.5Effect of rotation in the natural frequencies

4.5.1 Experimental

Putting a rotating speed on the tested disk and applying the same experimental procedure, the natural frequencies of the disk for different rotating speeds are obtained. Regarding the natural frequencies, two significant changes are observed when the surrounding water rotates with respect to the disk. *Figure 4.5* shows the waterfall plot of the sweep excitation around the natural frequency of n=2 for the confined and non rotating disk and the confined and rotating disk. For the rotating case, two peaks are detected with an accelerometer placed on the disk (*Figure 4.5* c), while for the non rotating disk only one is detected (*Figure 4.5* b), as predicted in the analytical model. According to this model, these two peaks are the solution of n_{pos} and n_{neg} in Eq. (2.28), when $\Omega_{up} \neq 0$ and/or $\Omega_{down} \neq 0$.

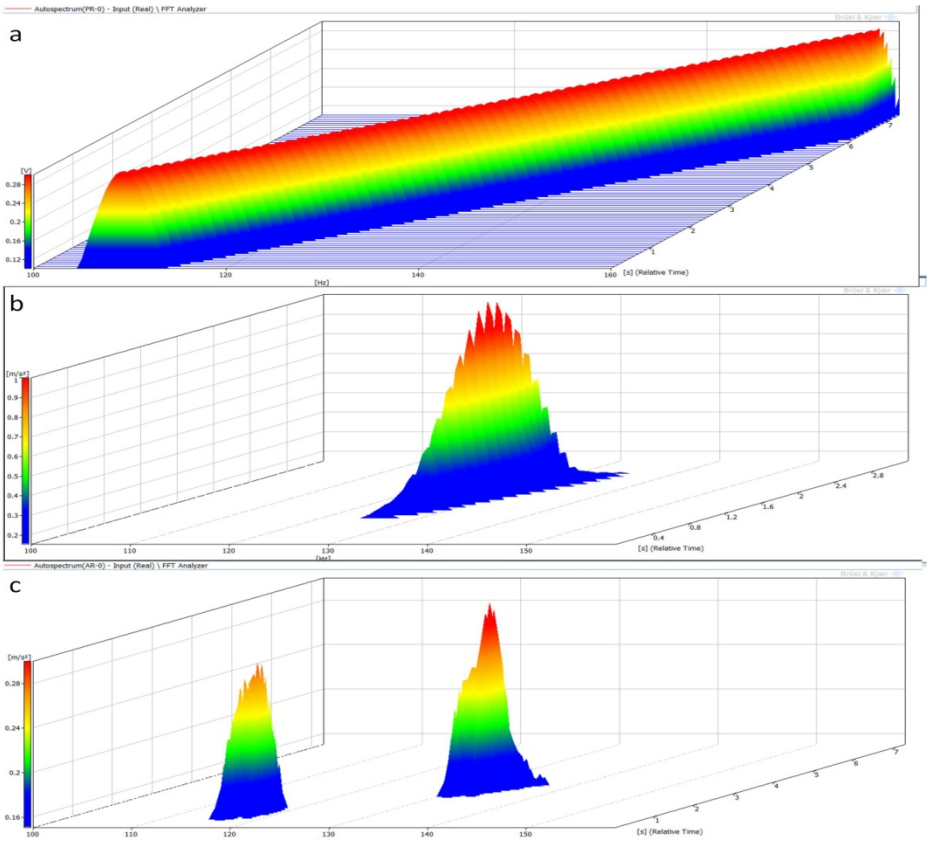

Figure 4.5: Sweep excitation (a). Non rotating case (b) and rotating case (6Hz) (c)

The other important change is observed in the mode shapes. These are experimentally determined, with the amplitude and relative phase of the sensors placed on the rotating frame (Figure 3.4). For the stationary case, since the solution of n_{pos} and n_{neg} gives the same natural frequency and the sign of n represents the direction of the travelling wave (Eq.(2.16)), when they both are added together, produce a stationary wave on the disk (normal mode shape) (*Figure 4.6a*). For the rotating case, since these solutions are different, each of the two peaks corresponds to a travelling wave travelling in opposite direction to the other (*Figure 4.6b & Figure 4.6c*).

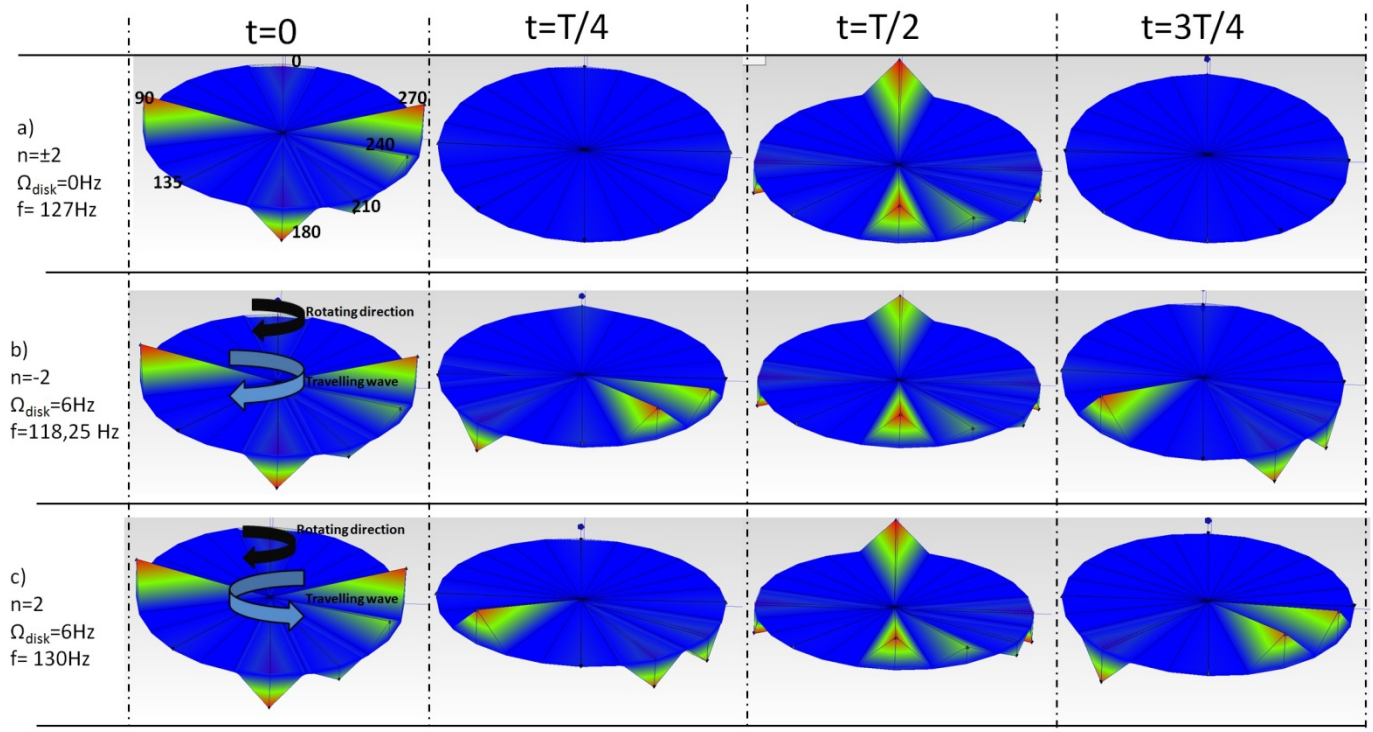

Figure 4.6: Normal mode shape (a). Complex mode shapes (b&c)

As *Figure 4.6a* shows, for the normal mode shape all the points pass through their maxima (or through zero) at the same time, while for the rotating case they pass through their maxima at different time. In this case for t=0 and t=T/2 all the sensors show their maxima and for t=T/4 and t=3T/4 they pass through zero. *Figure 4.6b* shows a wave travelling in rotating direction and Figure 4.6c shows a wave travelling in counter rotating direction. The change in the type of mode shapes can also be clearly seen in *Figure 4.7*, where the polar plot of the sensors (amplitude and phase in respect to A-0) for the represented cases in Fig. 10, is shown. The amplitude of A-0 is normalized to 1, and the phase to 0º. In *Figure 4.7a*, which correspond to the non rotating case, the mode is normal and therefore all the sensors are over the same line (phase 0º or 180º between sensors). To notice is also that they have all different amplitude In *Figure 4.7b* and *Figure 4.7c*, which correspond to the rotating case, the mode is complex, and therefore all the sensors are phase shifted to each other. Furthermore, according to Eq. (2.28), the mode shape can be described as a travelling wave with all the points having the same vibration amplitude as the vectors in the polar plot shows.

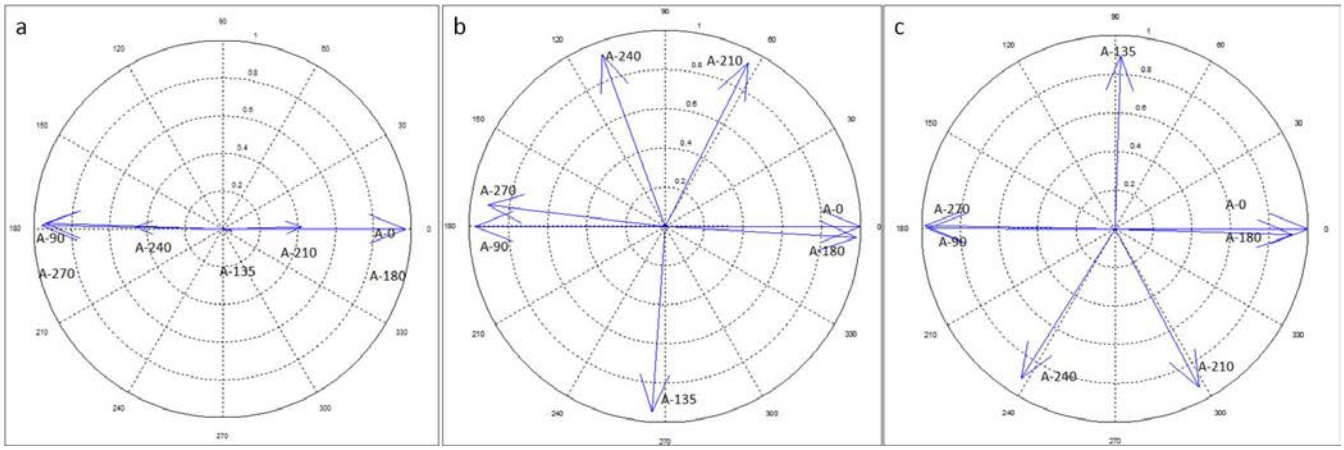

Figure 4.7: Polar plot of the accelerometers on the rotating disk. a) Ω_{disk}=0Hz,n=±2 ; b) Ω_{disk}=6 Hz,n=-2; c) Ω_{disk}=6Hz,n=2

For Eq. (2.15), the phase shift of the signal of one accelerometer A-X in respect to A-0 depends on the angle between both sensors and on the mode n, as Eq. (4.1) shows.

$$\Delta\varphi_{A-X} = |X \cdot (\pm n)| - k \cdot 360° \quad \textbf{(4.1)}$$

In Eq. (4.1), $\Delta\varphi_{A-X}$ is the phase shift of the signal of the accelerometer A-X in respect to the accelerometer A-0, and X is the angle of the accelerometer A-X in respect to A-0. k is an arbitrary entire number. *Figure 4.8* shows the experimental data for the natural frequencies studied for this rotating speed compared to the predicted by Eq. (4.1).

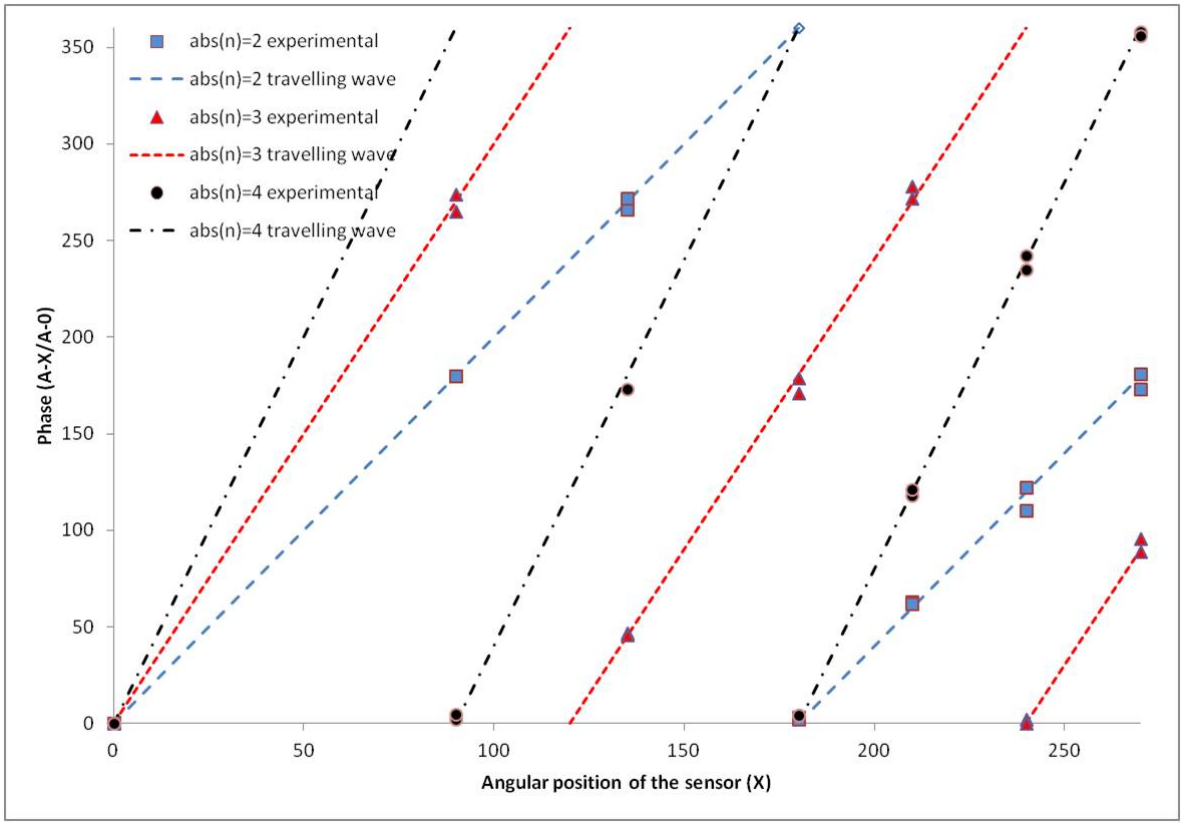

Figure 4.8: Phase of the sensors on the rotating disk for Ωdisk=6Hz

The plot shows that the phase of accelerometers can be described as a travelling wave travelling at a constant speed with respect to the disk (as modelled in Eq. (2.15)).

Doing the same procedure for all the tested rotating speeds the following natural frequencies are obtained (Table 4.6).

Table 4.6: Natural frequencies (Hz) of the disk confined with rotation (experimentally)

	Rotating speed of the disk (Hz)								
Mode	0	1	2	3	4	5	6	7	8
2-pos	127,05	123,83	122,87	119,98	120,1	119,83	118,24	118,73	117,41
2-neg	127,05	125,71	126,61	125,78	126,92	128,86	130,02	131,27	132,26
3-pos	321,16	321,225	320,883	319,19	317,77	315,89	315,46	310,13	309,11
3-neg	321,16	323,725	325,734	326,63	328,22	328,18	331,12	329,2	329,96
4-pos	642,23	634,59	628,77	623,36	619	612,47	608,92	611,24	607,89
4-neg	642,23	637,45	634,25	632,78	630,62	627,73	629,35	634,39	633,65

4.5.2 Numerical simulation

In order to contrast the analytical and the experimental model, a numerical simulation has been performed. The natural frequencies of the disk varying the rotating speed were calculated through an acoustic-structural coupling simulation in a FEM (Finite Element Method) model. This type of simulation considers the fluid as an acoustic fluid, neglecting the fluid viscosity and the rotating component of the velocity of the flow. As in the case of the analytical model, the FEM simulation considers that all the fluid is rotating at a constant speed. However, this assumption is not actually true, because all the fluid particles are not rotating at the same speed inside the tank. To determine the real rotating speed of the fluid in the tank, the viscosity of the fluid has to be considered. Therefore, a CFD (Computational Fluid Dynamics) simulation has been performed. With the CFD simulation, the real flow pattern can be obtained and an averaged rotating speed of the fluid can be estimated. Once this averaged rotating speed is obtained, it is introduced in the FEM model and the natural frequencies are determined. Detailed information of the simulation process is shown in Figure 4.9.

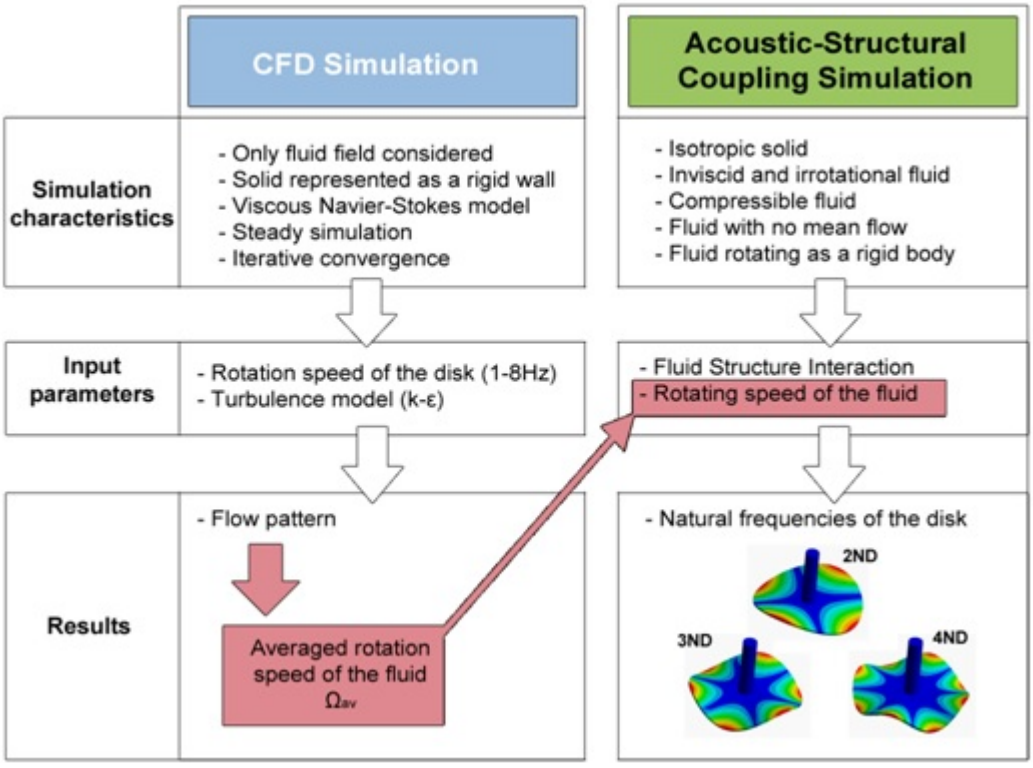

Figure 4.9: Computational simulation process

Several modal analyses have been carried out for the different rotating speeds of the disk using Ansys Workbench® software (release 14.5). The model is constructed with hexahedral elements, using SOLID185 for the solid parts and FLUID30 for the liquid elements. Nodes of the solid parts in contact with the fluid are defined as a FSI (Fluid Structure Interaction) interface. The bottom of the tank is fixed in the y direction, as well as the top of the shaft. The mesh of the FEM model including the applied boundary conditions is shown in Figure 4.10. The density of the fluid is fixed at 1000 kg/m^3 and the speed of sound was considered as 1430 m/s according to the standard data for water ([51]). The acoustic-structural coupling simulation assumes that the fluid is inviscid, irrotational, compressible and without mean flow.

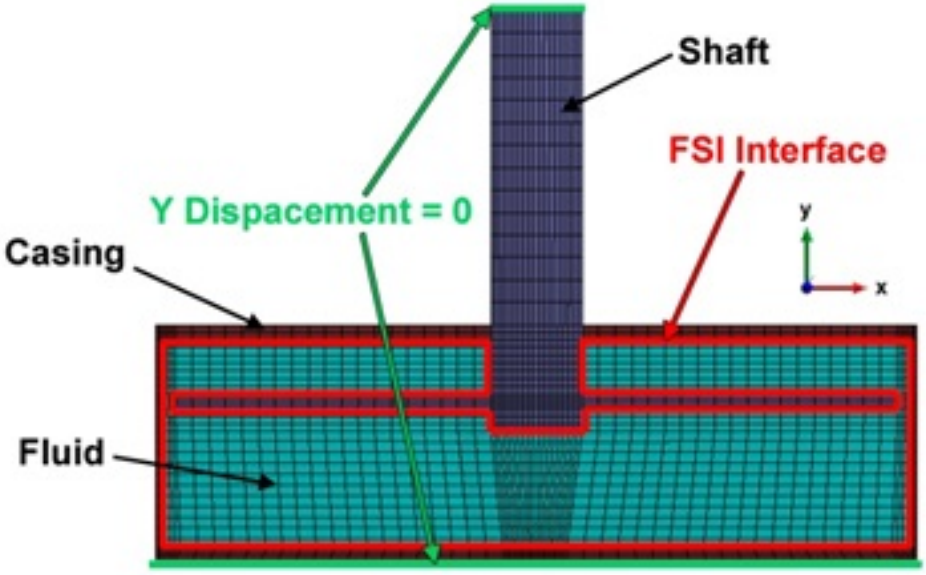

Figure 4.10: FEM model

A mesh sensitivity study was previously carried out to determine the optimal number of elements of the FEM model. The value of the natural frequency of the main mode shapes of the disk was selected as the variable to compare the element density of the mesh. The density of the mesh was changed in the axial and in the radial direction in order to consider all the possible parameters. Results obtained showed that the optimal mesh had approximately $7 \cdot 10^4$ elements and less than 1% of error over the densest mesh.

To consider the real rotating flow inside the tank CFD simulations have been performed. With these simulations, the averaged rotating speed can be estimated for the upper (Ω_{up}) and the lower field (Ω_{down}), analyzing the flow pattern that is created due to the rotation of the disk.

When the disk rotates, viscous forces appear at the surface of the disk and this fact induces movement to the fluid. Therefore, to consider viscosity in the simulations is essential to know the relative velocity of the fluid in respect of the rotating disk. For this purpose, Navier-Stokes Equations have been solved numerically using Ansys Fluent® v14.5 software. A pressure based-double precision solver was selected in order to solve the set of Equation used. Second order upwind discretization schemes were imposed on all the transport Equations solved (momentum, energy and turbulence). Simulations were run in steady state.

A 3D structured hexahedral grid was applied to the geometrical model. Only the fluid field was considered, fixing the nodes in contact with the casing as a standing wall and imposing a rotation speed in the nodes corresponding to the disk. As in the case of the FEM model, a mesh sensitivity study has been performed to ensure the model is adequately accurate. In this case, the mean velocity in a constant radius of the disc (r_o) is the selected variable to compare the results for each mesh tested. Finally, the optimal mesh has approximately $7 \cdot 10^5$ elements and less than 1% of difference between the densest mesh tested (2 million elements).

Since the fluid field is axisymetric only a section r-z will be studied. For each discretized value of the r coordinate the averaged speed is determined for the upper and the lower field (*Figure 4.11*).

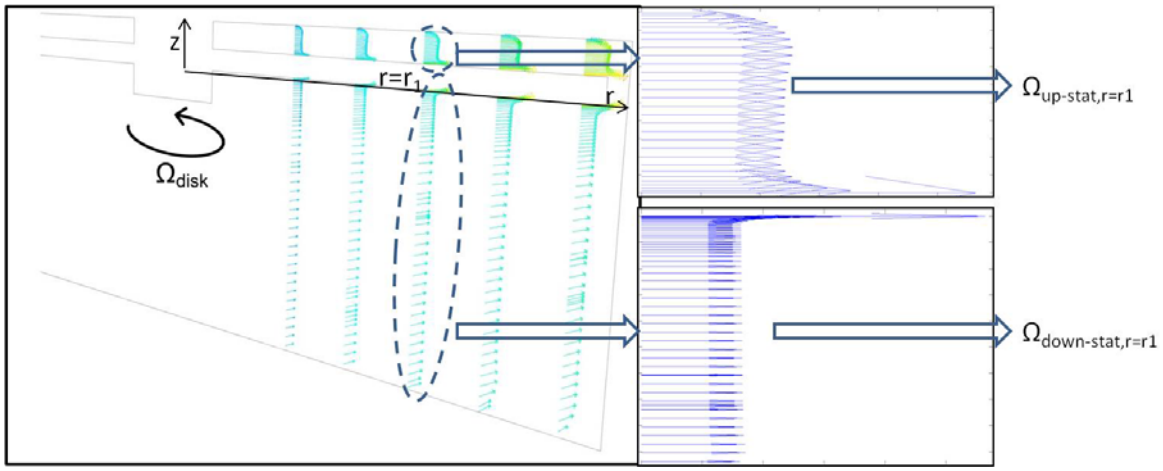

Figure 4.11: CFD result. Obtaining $\Omega_{up\text{-}stat,r=r1}$ and $\Omega_{down\text{-}stat,r=r1}$. H_{up}/r_{out}=0.05

Both values ($\Omega_{up\text{-}stat,r=r1}$ *and* $\Omega_{down\text{-}stat,r=r1}$) are averaged for all the discretized values of *r* obtaining an averaged value for $\Omega_{up\text{-}stat}$ and $\Omega_{down\text{-}stat}$ for each rotating speed of the disk. Since the values Ω_{up} and Ω_{down} of the analytical model are both referred to the rotating frame the transformation shown in Eq. (33) has to be used.

$$\Omega_{up} = \Omega_{disk} - \Omega_{up-stat} \qquad \Omega_{down} = \Omega_{disk} - \Omega_{down-stat} \tag{4.2}$$

Both values are substituted in Eq. (2.28) obtaining the natural frequencies of the disk confined for every rotating speed. These values are also used in the numerical model to correct the solutions provided. There is a linear relationship between Ω_{up}, Ω_{down} and Ω_{disk} as *Figure 4.12* shows.

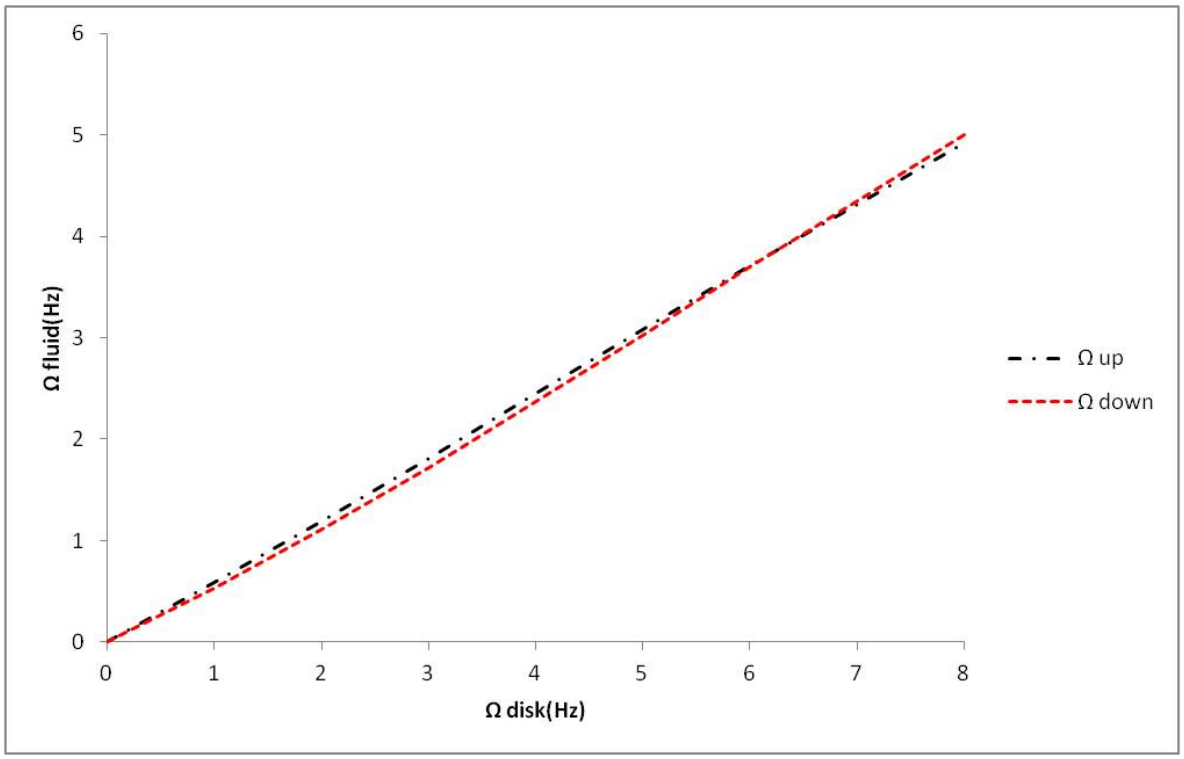

Figure 4.12: Relation between Ωdisk and Ωup (black line) and Ωdown(red line). H_{up}/r_{out}=0.05

Increasing Ω_{disk}, Ω_{up}& Ω_{down} are also increased. For other heights (varying H_{up} and H_{down}) the same procedure to obtain Ω_{up}& Ω_{down} has been performed

4.5.3 Influence of the parameters through the analytical method

In order to study analytically the different parameters that can affect the natural frequencies of the disk, avoiding the effect of the flow field the representative values $f_{center} = \frac{f_{n,pos}+f_{n,neg}}{2}$ and $f_{n,pos} - f_{n,neg}$ are represented for increasing $\Omega_{fluid} = \Omega_{up} = \Omega_{down}$. This means, to consider the fluid rotating as a rigid body in respect to the disk.

The value f_{center} is representative for the natural frequency of the non rotating case and $f_{n,pos} - f_{n,neg}$ is representative for the distance between the two natural frequencies obtained for each n.

The effect of the diametrical mode n is seen in *Figure 4.13*. Other properties (fluid, disk and confinement) are fixed with the test rig parameters. For increasing rotating speed f_{center} remains nearby constant for the represented velocities of Ω_{fluid}**.** There is a light decrease (of less than 1%), which is higher for lower modes. The value $f_{n,pos} - f_{n,neg}$ increases always linearly with increasing Ω_{fluid}, since the added mass effect difference for the forward and for the backward wave increases. For higher n, this increase is higher (*Figure 4.13 b*) since the travelling wave speed for these modes is higher.

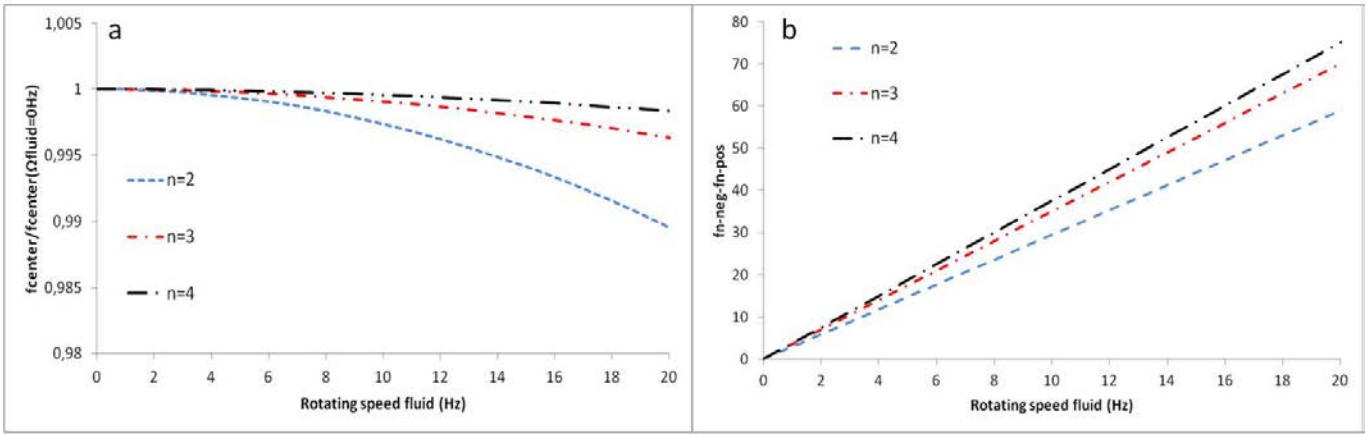

Figure 4.13: a) Effect of n in fcenter and b) effect of n in $f_{n\text{-}neg}$-$f_{n\text{-}pos}$

The effect of confinement is seen in *Figure 4.14*. The mode n, is fixed to 2.The ratio H_{down}/r_{out} is set to 0.49 and the distance H_{up} is varied. For a closer distance to the tank the decrease in f_{center} is higher (*Figure 4.14*a). The difference between the two natural frequencies $f_{n,pos} - f_{n,neg}$ is also higher when the disk is closer to the rigid wall (*Figure 4.14*b).

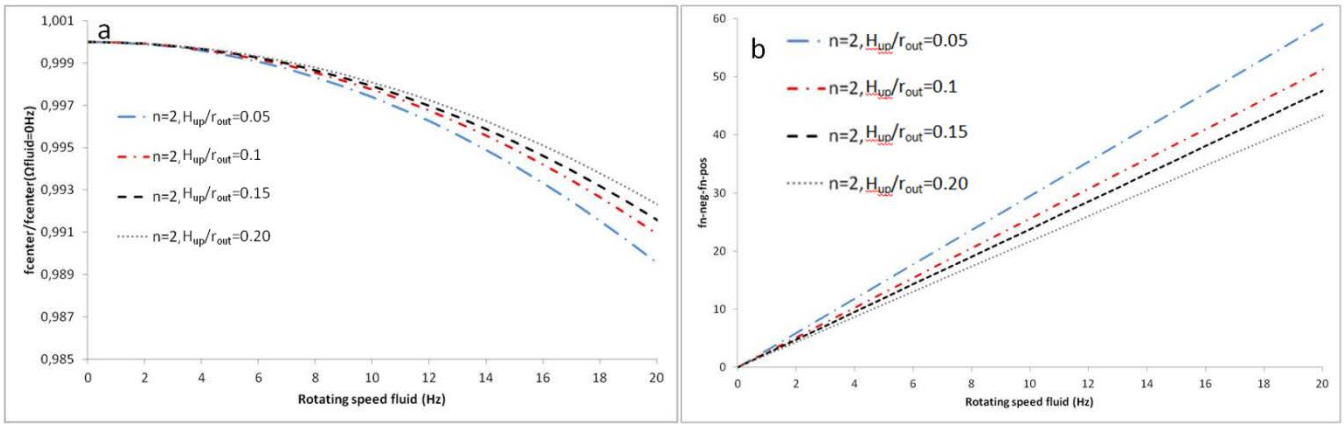

Figure 4.14: a) Effect of confinement in fcenter and b) effect of confinement in fn-neg-fn-pos

4.5.4 Comparison within methods

As *Figure 4.15* shows, the trend of f_{center} is to be constant when increasing the rotating speed for the tested rotating speeds according to the analytical and the numerical model. For the experimental values a slight decrease is observed maybe due to a small misalignment of the mechanical system that is not considered in the numerical and analytical model.

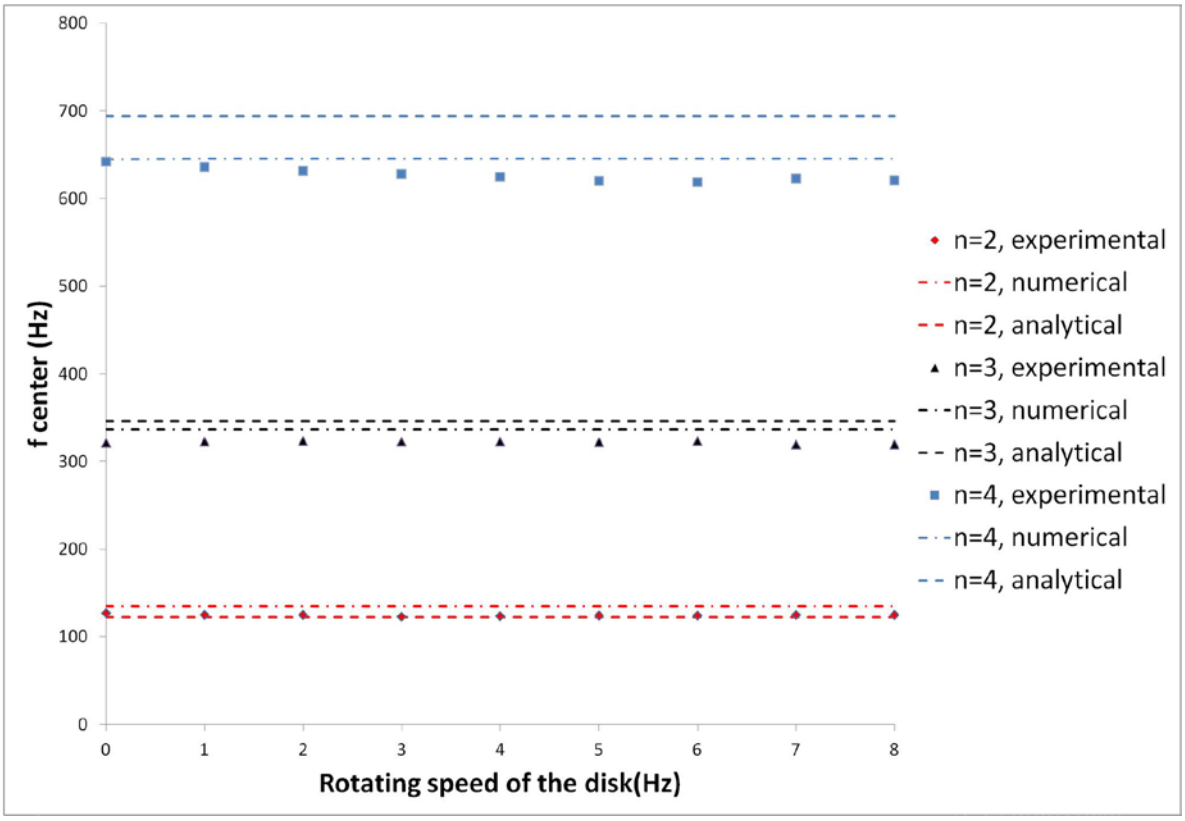

Figure 4.15: f_{center} for n=2,3,4

The other representative values calculated are $f_{n,neg}$ - $f_{n,pos}$, which are represented in *Figure 4.16*. These values show the deviation between both natural frequencies obtained for each n. A linear trend, which is predicted with the analytical model is also observed in the experimental and numerical results. When increasing the rotating speed of the disk, the distance between $f_{n,neg} - f_{n,pos}$ increases linearly.

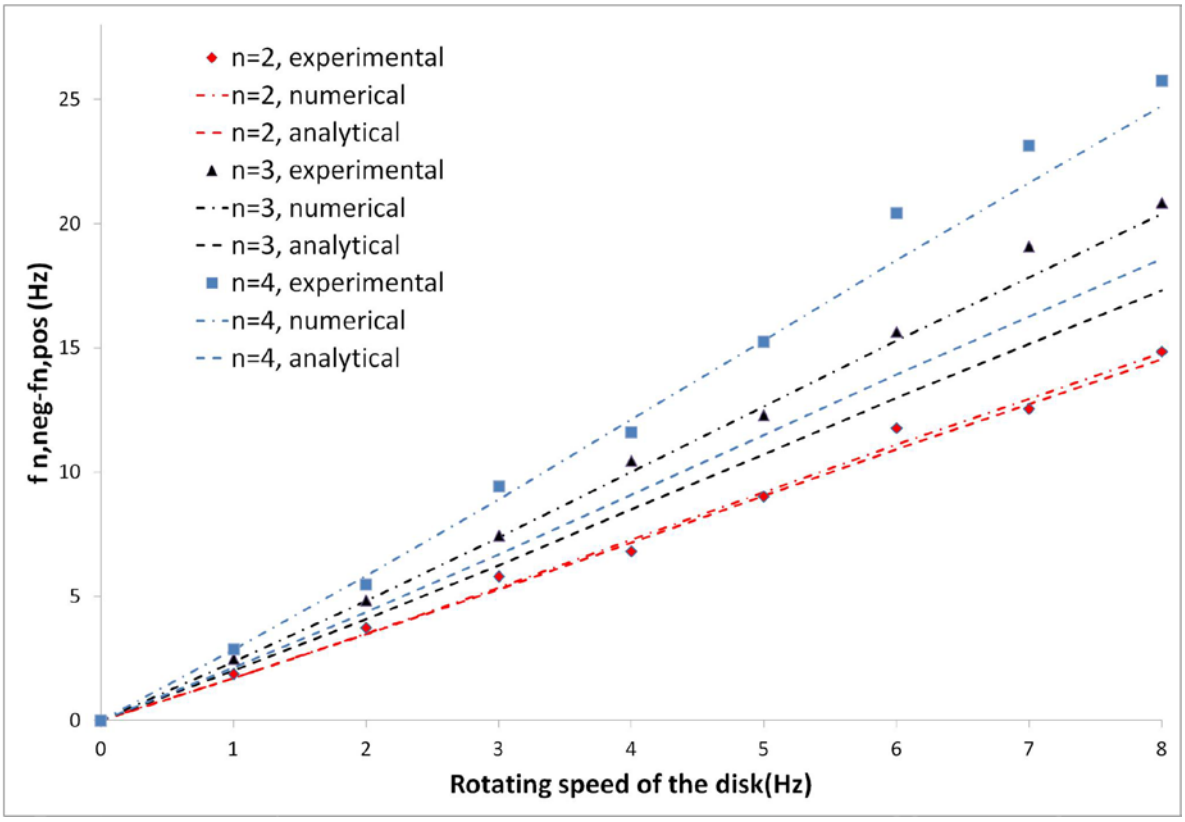

Figure 4.16: $f_{n,neg} - f_{n,pos}$ for n=2,3,4

4.5.5 Tests with other heights

For the other heights tested (H_{up}/ r_{out} =0.1, 0.15, 0.2), the natural frequencies are also obtained experimentally and contrasted with analytical and numerical methods. The modes n=±4 are not presented because generally, not clear experimental results have been obtained. Only in few configurations the structural modes n=4 and n=-4 are detected with the accelerometers on the rotating frame.

The reason of this behavior is the increasing added mass effect when the disk is closer to the wall [8]. For H_{up}/r_{out}=0.05, natural frequencies are lower than for the other configurations tested. The mode n=±4 for these other heights is located on a frequency band, where the response of the casing is very high and complicated (not peaky response) and therefore not pure modes of the disk appear. In these cases the response of the casing itself has to be considered. This topic will be threatened with more detail in Chapter 6.

Figure 4.17 shows the value f_{center} for the different heights. This value is representative for the non rotating case, where the proximity of the upper cover increases the added mass effect. For this reason, increasing H_{up} has the effect of increase the natural frequencies.

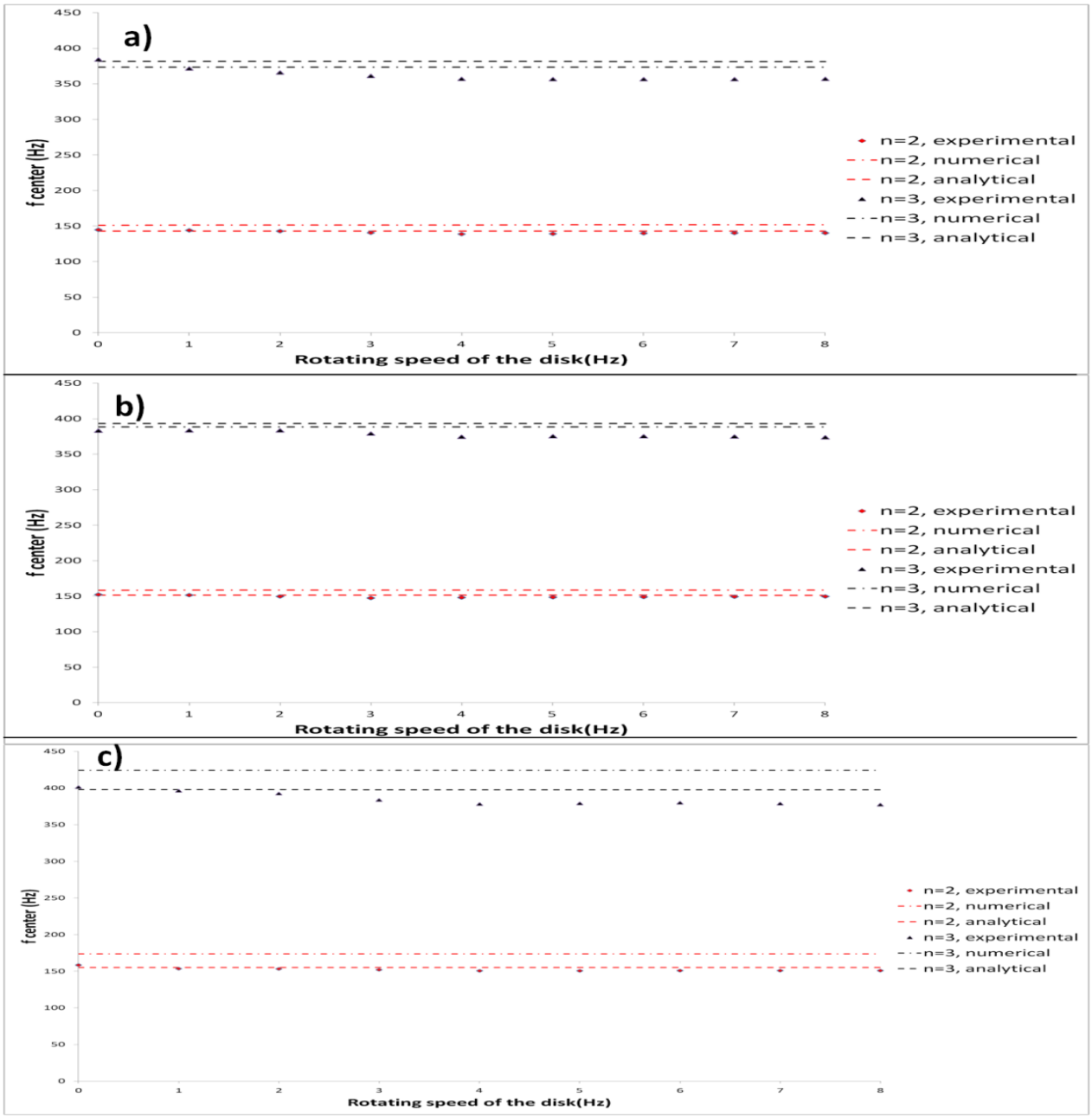

Figure 4.17: f_{center} for a) H_{up}/r_{out}=0.1.b) H_{up}/r_{out} =0.15. c) H_{up}/r_{out} =0.2

The difference $f_{n,neg}$ - $f_{n,pos}$ for the same heights is plotted in *Figure 4.18.* In this case increasing H_{up} has the effect of reduce sligthly this difference as shown analytically in *Figure 4.14.*

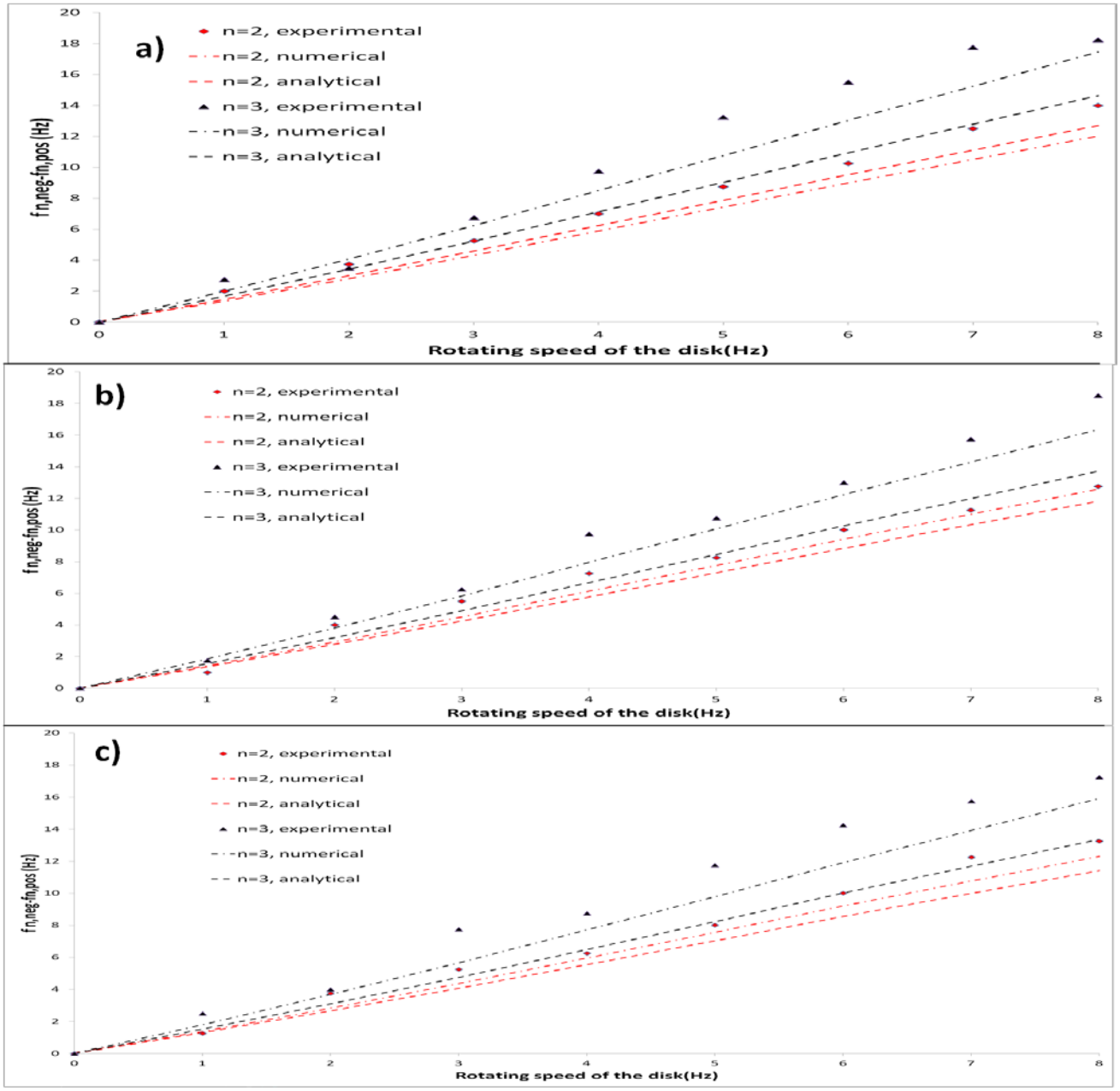

Figure 4.18: $f_{n,neg}$ - $f_{n,pos}$ for a) H_{up}/r_{out}=0.1.b) H_{up}/r_{out} =0.15. c) H_{up}/r_{out} =0.2

4.5.6 Comparison with air

Figure 4.19 shows the effect of the surrounding fluid for H_{up}/r_{out}=0.05. For the tested rotating speeds the effect of air is to increase very slight the natural frequencies. In water for each n, two natural frequencies appear for the rotating disk. The increase/decrease with respect the value for the still case is much higher than in air.

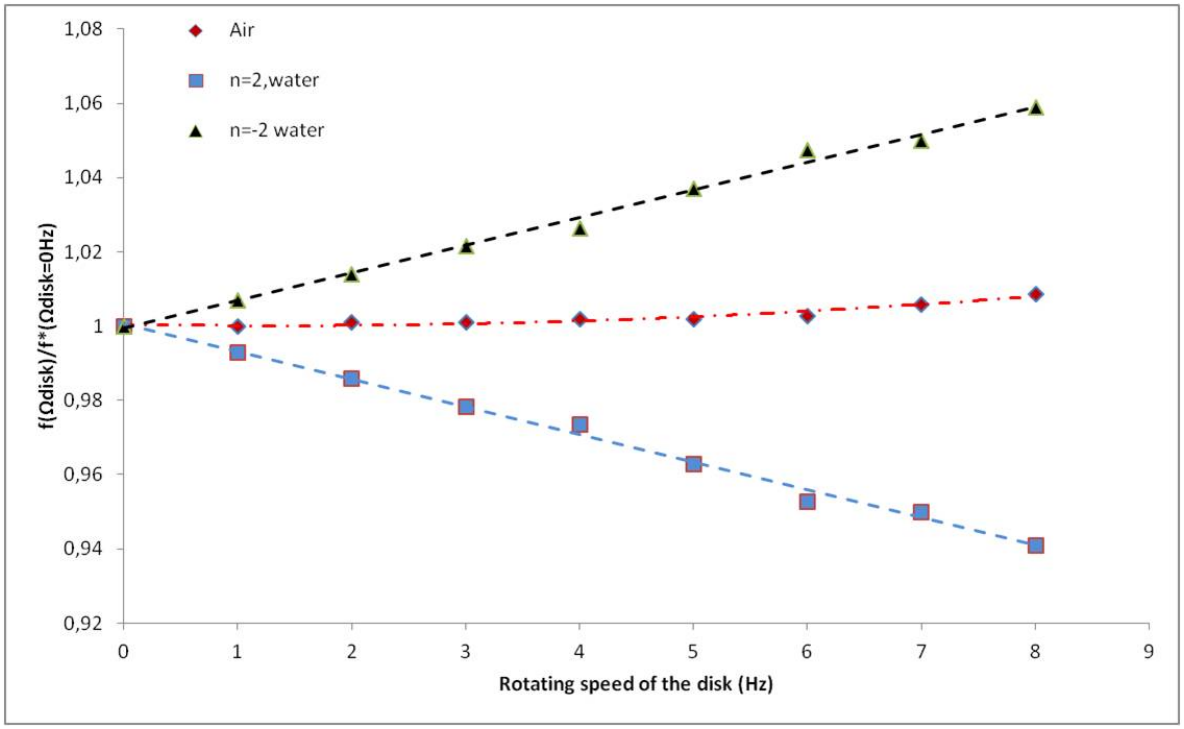

Figure 4.19: Effect of the rotating speed of the disk in air and in water (n=±2)

In air f*(Ω_{disk}=0 Hz) is directly the value of the natural frequency measured for Ω_{disk}=0 Hz. In water, since a slight drop in the experimental values of $\frac{f_{n-pos}+f_{n-neg}}{2}$ is observed, this value is used as the reference value f*(Ω_{disk}=0 Hz).

4.6 Partial conclusions

The natural frequencies and mode shapes of a rotating disk submerged in water and confined have been studied in this chapter. The effect of rotation of the surrounding water has been determined as a fundamental change not only in the natural frequencies, but also in the mode shapes. Even for low rotating speeds of the disk (0-8Hz), which is in range of actual hydraulic turbomachinery, the surrounding water has a great influence in the value of the natural frequencies and in the nature of the mode shapes.

While for a rotating disk in air only one natural frequency (observed from the rotating frame) for each n (number of nodal diameters) is detected, when the disk is rotating in water two peaks appear. The center of these two peaks remains nearby constant and equal

to the non rotating case (for low rotating speeds). Nevertheless the difference in frequency between them increases linearly with the rotating speed.

This phenomenon is not only important for the prediction of the value of the natural frequency itself, but also for the change in the mode shape. While for the non rotating case, the mode shapes of the disk observed from the rotating frame are normal mode shapes(standing wave), for the case that the disk is rotating in water the mode shapes have a complex pattern(travelling wave). For each n (number of nodal diameters in the mode shape), there is a first peak (lower frequency) travelling in the rotating direction of the disk and a second peak (higher frequency) travelling in the opposite direction. This is proven experimentally. This conclusion could be important when analyzing the dynamic behavior of real hydraulic turbomachinery under operation, since hydraulic runners behave as disk-like structures for lower frequencies and there are excited with a combination of rotating excitation patterns.

Experimental results have been compared and validated with an analytical model and numerical FEM model. For these two models the averaged rotating speed of the fluid with respect to the disk has been calculated using the results of a CFD simulation for every rotating speed of the disk. Introducing the averaged rotating speed in the analytical and numerical model the natural frequencies of the disk are predicted with good accuracy.

Chapter 5

5. DYNAMIC BEHAVIOUR OF THE ROTATING DISK IN AIR AND IN WATER

Once the natural frequencies and mode shapes of the rotating disk, in air and submerged in water, have been studied in detail, the next step is to study the dynamic behavior of the rotating disk considering the RSI excitation. To study the response of the disk due to a real excitation pattern several PZTs have been used. PZT are used to create different rotating excitation patterns that simulate the RSI. The dynamic behavior of the disk in air and in water, due to these excitations patterns, is studied. The configuration used to perform these tests is H_{up}/r_{out} =0.15 and Ω_{disk}=*8Hz*.

5.1 Dynamic behaviour of the rotating disk in air due to an RSI excitation

The disk is excited with a sweep signal passing through the resonance with the excitation patterns presented in Figure 3.8. As Figure 5.1 shows, for n=±2 when the disk is excited with the pattern γ =±2 the resonance is amplified and when it is excited with γ =±4 is eliminated (as predicted in Eq.(2.43)). Note that for the symmetric-position of patches the excitation direction for γ=±2 and γ =±4 cannot be defined. For the same structural mode, the disk is excited with the non-symmetric position of the PZT. In this case the direction of excitation can be defined for γ =±2. As Figure 5.1 shows, both excitations amplify the amplitude of resonance, as the mode shape is a standing wave on the disk.

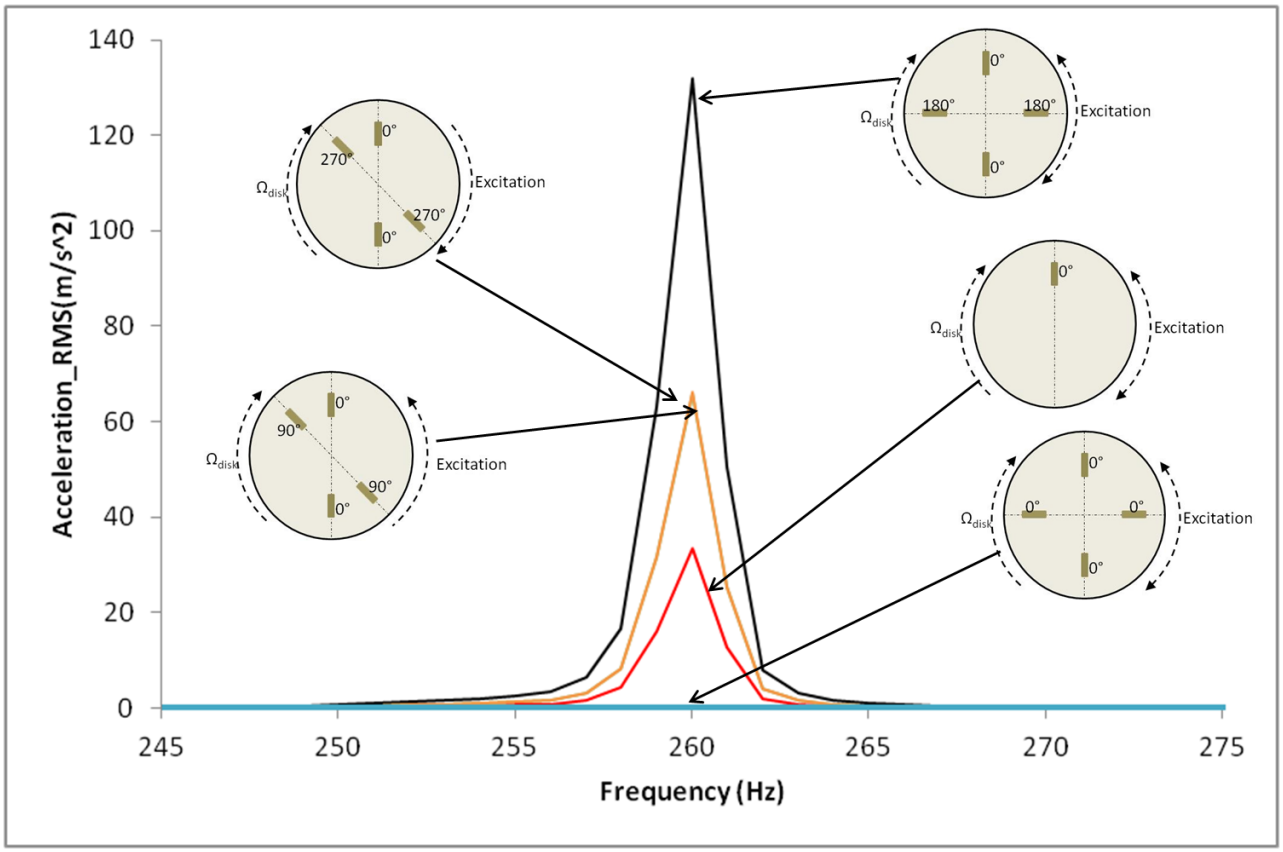

Figure 5.1: Resonances around n=±2 (experimental) for the disk rotating in air (Ω_{disk}=8Hz). Different excitation patterns.

The rest of resonance amplitudes divided by the amplitude of resonance due to one patch excitation (red line in Figure 5.1) are presented in Table 5.1 compared with the analytical results.

Table 5.1: Amplification of the resonances ($A_\gamma/A_{1\text{-PATCH}}$) of the rotating disk in air (Ω_{disk}=8Hz) due to the different excitation patterns. Analytical, experimental and error.

Excitation shape(γ)							
γ=2	γ=-2	γ=3	γ=-3	γ=4	γ=-4		Structural mode(n)
2 1,981 1%	2 1,971 1,5%	0 0,003 -	0 0,004 -	0 0,003 -		n=±2	
4 3,942 1,5%							
0 0,003 -		2 2,005 0,3%	2 2,008 0,4%	0 0,005 -		n=±3	
0 0,017 -		0 0,003 -	0 0,001 -	4 4,042 1,1%		n=±4	

A difference of less than 1,5% between the analytical model and experimental results is obtained for all the experimented cases. From the experimental results can be extracted that patches are feasible to excite a thick disk in air and that RSI excitation can be studied and simulated (or attenuated) with PZTs. It is found that for each mode n, only one resonance (from the rotating system) is produced and amplified when the excitation shape γ coincides with the structural mode shape n, with no matter of the direction of rotation of excitation. For the other excitation shapes γ, with the positions of the exciters used, the amplitude of resonance is almost 0.

5.2Dynamic behaviour of the rotating disk in water due to an RSI excitation

Again the same experimental procedure explained in Chapter 3.5.3 is applied when the disk is rotating in water. Figure 5.2 shows the excitation of the structural modes n=+2 and n=-2 with different excitation patterns.

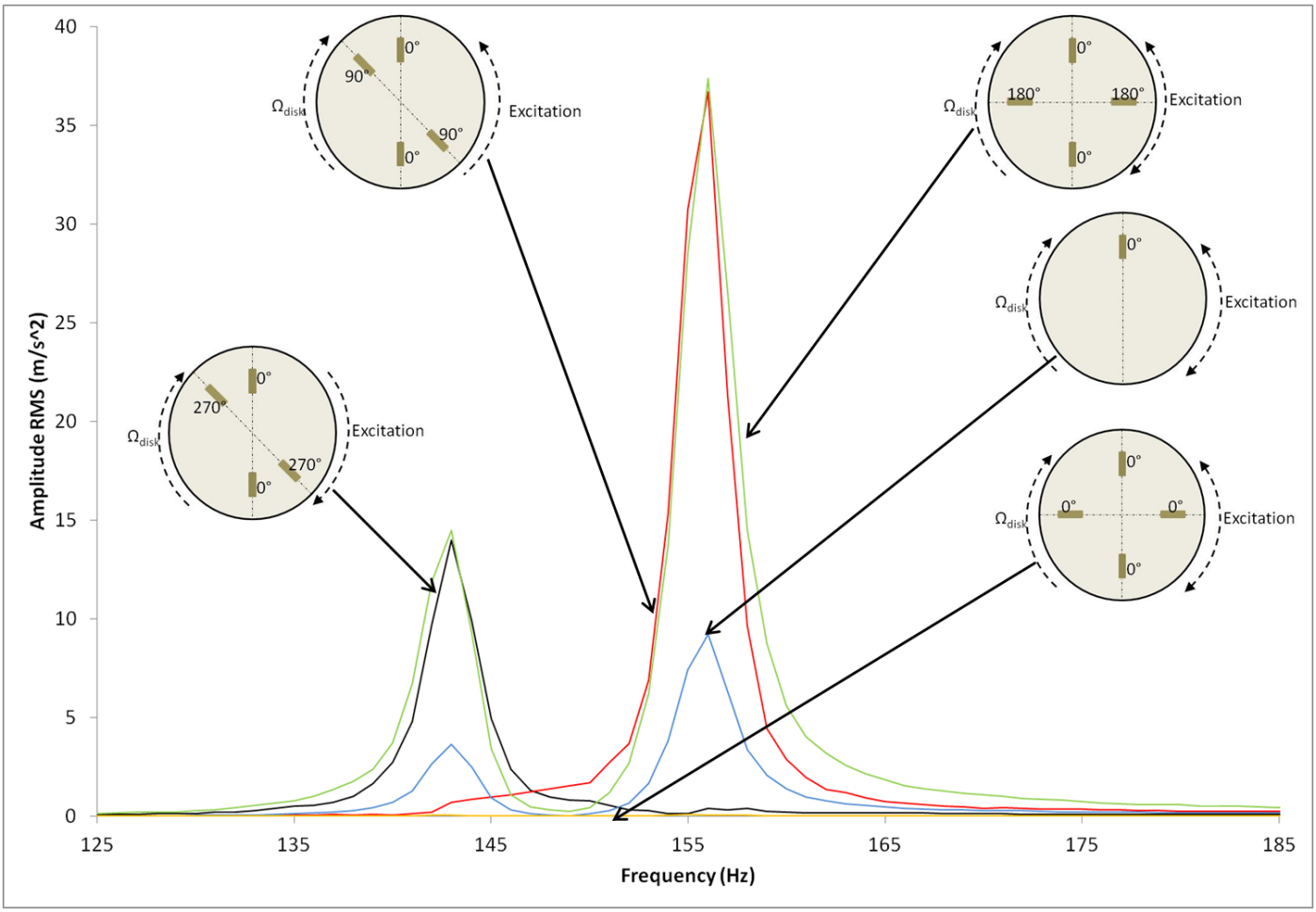

Figure 5.2: Resonances around n=2 and n=-2 (experimental) for the disk rotating in water (Ω_{disk}=8Hz). Different excitation patterns.

In this case, when the disk is excited with one patch, the two resonances (n=2 and n=-2) are detected from the rotating frame. For the excitation γ=±2 without defining the rotating direction of the excitation, both resonances are amplified. When γ is different than ±2, the amplitude of the resonance is almost 0 as predicted in Eq.(2.44) for the position of exciters used. Only one resonance appears if the rotating direction of the excitation is defined. In the

case of the non-symmertric position of patches this direction is defined (Figure 3.8) and it can be checked that to excite the structural mode n=2 the excitation γ=2 is necessary. For the same structural mode the excitation γ=-2 eliminates the resonance. The same conclusion is achieved for the structural mode n=-2, which needs an excitation shape γ=-2 to be amplified. The rest of resonance amplitudes compared to the case of one patch excitation are presented in Table 5.2 compared with the results of the analytical model.

Table 5.2: Amplification of the resonances ($A_\gamma/A_{1\text{-PATCH}}$) of the rotating disk in water (Ω_{disk}=8Hz) due to the different excitation patterns. Analytical, experimental and error.

<table>
<tr><td colspan="6">Excitation shape(γ)</td><td></td></tr>
<tr><td>γ=2</td><td>γ=-2</td><td>γ=3</td><td>γ=-3</td><td colspan="2">γ=4 γ=-4</td><td></td></tr>
<tr><td>4
3,852
3,7%</td><td>0
0,120
-</td><td rowspan="2">0
0,007
-</td><td rowspan="2">0
0,008
-</td><td colspan="2" rowspan="2">0
0,003
-</td><td>n= + 2</td></tr>
<tr><td colspan="2">4
3,983
0,4%</td><td>n= + 2</td></tr>
<tr><td>0
0,033
-</td><td>4
3,991
0,2%</td><td rowspan="2">0
0,003
-</td><td rowspan="2">0
0,004
-</td><td colspan="2" rowspan="2">0
0,015
-</td><td>n= - 2</td></tr>
<tr><td colspan="2">4
4,101
3%</td><td>n= - 2</td></tr>
<tr><td colspan="2">0
0,003
-</td><td>4
4,023
0,5%</td><td>0
0,092
-</td><td colspan="2">0
0,007
-</td><td>n= + 3</td></tr>
<tr><td colspan="2">0
0,002
-</td><td>0
0,025
-</td><td>4
3,965
0,9%</td><td colspan="2">0
0,005
-</td><td>n= - 3</td></tr>
<tr><td colspan="2">0
0,005
-</td><td>0
0,009
-</td><td>0
0,007
-</td><td colspan="2">4
4,152
3,8%</td><td>n= + 4</td></tr>
<tr><td colspan="7">Structural mode(n)</td></tr>
</table>

0 0,003 -	0 0,008 -	0 0,017 -	4 4,102 2,6%	n= - 4	

A difference of less than 4% between methods is obtained for all the tested cases. From experimental results can be extracted that patches are feasible to excite a thick disk in water and that the RSI can be studied and simulated (or attenuated) with PZT. To notice is that the disk has two natural frequencies for each mode ±n (viewed from the rotating system) when it rotates in water. These are detected when excited with one patch. The resonance is amplified only in case that the excitation shape γ coincides with the structural mode n in magnitude and rotating direction. Both resonances are amplified when the rotating direction of the excitation shape is not defined. For other excitation patterns (n≠γ), with the used exciters, both resonances are eliminated.

5.3Partial conclusions

The dynamic behavior of a thick disk rotating in air and inside a casing filled with water has been analyzed experimentally and analytically. The disk has been excited with several rotating excitation patterns simulating the rotor-stator interaction (RSI) excitation.

For an accurate analysis of the disk behavior both exciters and sensors measuring the response were located on the disk (rotating frame). For the excitation several PZT actuators attached to the disk were used. PZTs do not affect the mass of the disk and do not perturb the flow of water produced by the rotation of the disk inside the casing. PZT actuators have been used several times to excite thin rotating disks in air and from the stationary frame, but never to excite a thick disk submerged in water and confined inside a casing. Experiments presented have demonstrated that it is feasible to use PZT actuators in thick structures in air and submerged in water. This is interesting because PZTs could be used to determine the dynamic response of disk-like structures, such as turbomachinery impellers in actual operating conditions.

The dynamic behaviour of the rotating disk in water at one natural frequency depends on the excitation shape and also on the rotating direction of the excitation. When the excitation is fixed on the rotating frame, the response at the two natural frequencies of the corresponding diametrical mode is amplified. However when the excitation spins in the

same direction of the disk only the lower natural frequency is excited, which corresponds to the travelling wave travelling in the same direction as the disk. When the excitation spins in the opposite direction only the higher natural frequency is excited, which corresponds to the travelling wave travelling in the opposite direction. If the excitation shape does not coincide with the diametrical mode considered, the response at both natural frequencies is almost zero (for the studied configuration of patches). When the disk rotates in air, only the excitation shape affects the dynamic response. If the excitation shape coincides with a diametrical mode, the response of the disk is amplified at the corresponding natural frequency, with no matter of the rotating direction of the excitation (rotating with the disk, counterwise or standing). These results are obtained experimentally and using the analytical model.

Chapter 6

6. DETECTION FROM THE STATIONARY FRAME

Until now, the dynamic behavior of the rotating disk has been studied from the rotating frame. To complete the research, this chapter threats with the transmission of the motion of the disk into the stationary frame, i.e. in this section will be discussed how natural frequencies and mode shapes of the rotating disk can be detected from the stationary frame.

6.1Detection of the disk natural frequencies in air

When the disk is rotating in air, it is much easier to detect natural frequencies of the rotating disk from the stationary frame with optical or proximity sensors that measure the vibration directly from the disk than with accelerometers that measure the casing vibration. This is because the dynamic pressure in the gap between both does not excite the casing with enough amplitude, since it depends on the density of the fluid between the disk and the casing.

According to *Equation (2.52)* one natural frequency in the rotating frame is seen from the stationary frame as two natural frequencies:

$$\boldsymbol{\omega_{n,casing}}_{1,2} = \boldsymbol{\omega_{n,disk} \pm n\Omega_{disk}} \quad \text{(2.52)bis}$$

And with a phase difference *Equation (2.53):*

$$\Delta\boldsymbol{\alpha_{\omega_{n,casing\,1}}} = +\boldsymbol{n\Delta\theta_c}\ \boldsymbol{and}\ \Delta\boldsymbol{\alpha_{\omega_{n,casing\,2}}} = -\boldsymbol{n\Delta\theta_c} \quad \text{(2.53)bis}$$

Figure 6.1 shows the Time-Frequency plot using Wavelets [59] of the sensors in the rotating frame when it is passing through the resonance n=3. The disk is excited with the piezoelectric patch PR-0. As shown in this figure, the electrical signal send to the patch is constant for the frequency band excited. In this case it excites the frequencies from 560 to 660 Hz as *Figure 6.1a* shows. Approximately at 590Hz the excitation passes through the mode n=3 and the resonance is clearly detected with the accelerometer AR-0(*Figure 6.1b*).

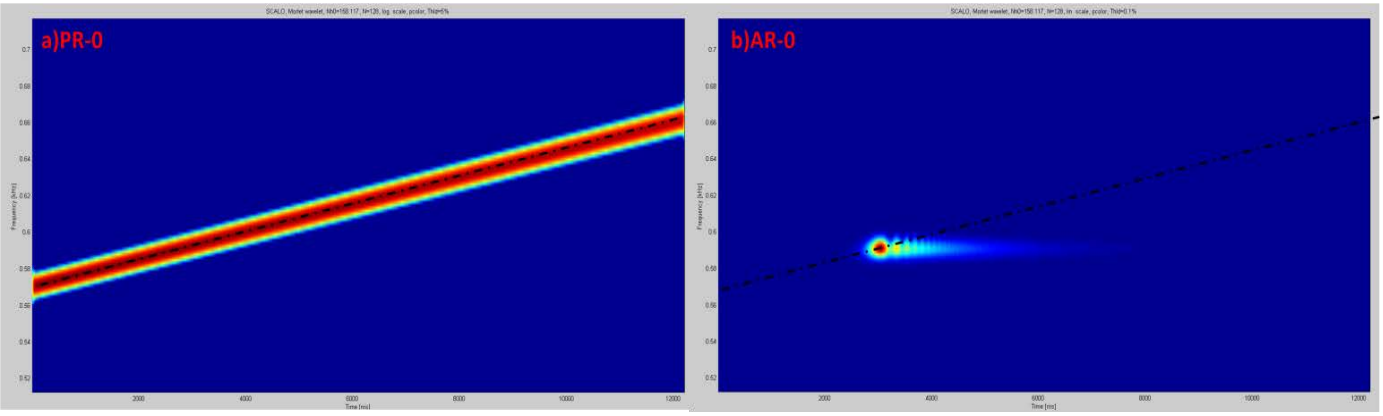

Figure 6.1: a) Excitation characteristic with one patch (PR-0) b) Response detected from the rotating system (AR-0)

At the same time, the resonance is analyzed with sensors on the stationary frame (*Figure 6.2* and *Figure 6.3*). *Figure 6.2* shows the detection with the pressure sensor (PRES-0) and the accelerometer on the casing (AS-180).

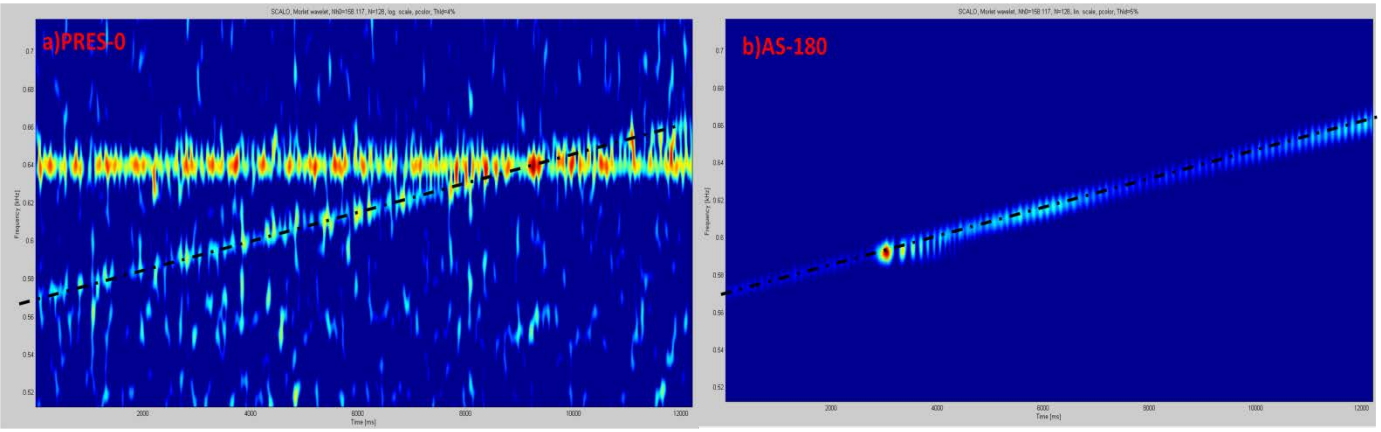

Figure 6.2: a) Detection with pressure sensor (PRES-0) b) Detection with an accelerometer on the casing (AS-180)

With the pressure sensor, which is representative of the excitation that comes from the fluid between disk and casing, nothing clear is seen since in this case, this fluid is air. For the accelerometer AS-180 the peak is detected. This seems to be contradictory to the analytical explanation developed, since two peaks should be seen with a sensor in the stationary frame. Nevertheless, the explanation of this peak is not the transmission through the fluid but through the mechanical system, i.e. the vibration of the disk is transmitted to the casing through the bearings on the shaft. In this case, the axial component of the mode n=3 is

transmitted to the stationary frame through the mechanical part (pure axial transmission) and the natural frequency in the rotating frame does appear as two natural frequencies in the stationary frame.

The detection with the Laser, which is directly pointing on the disk, is shown in *Figure 6.3*.

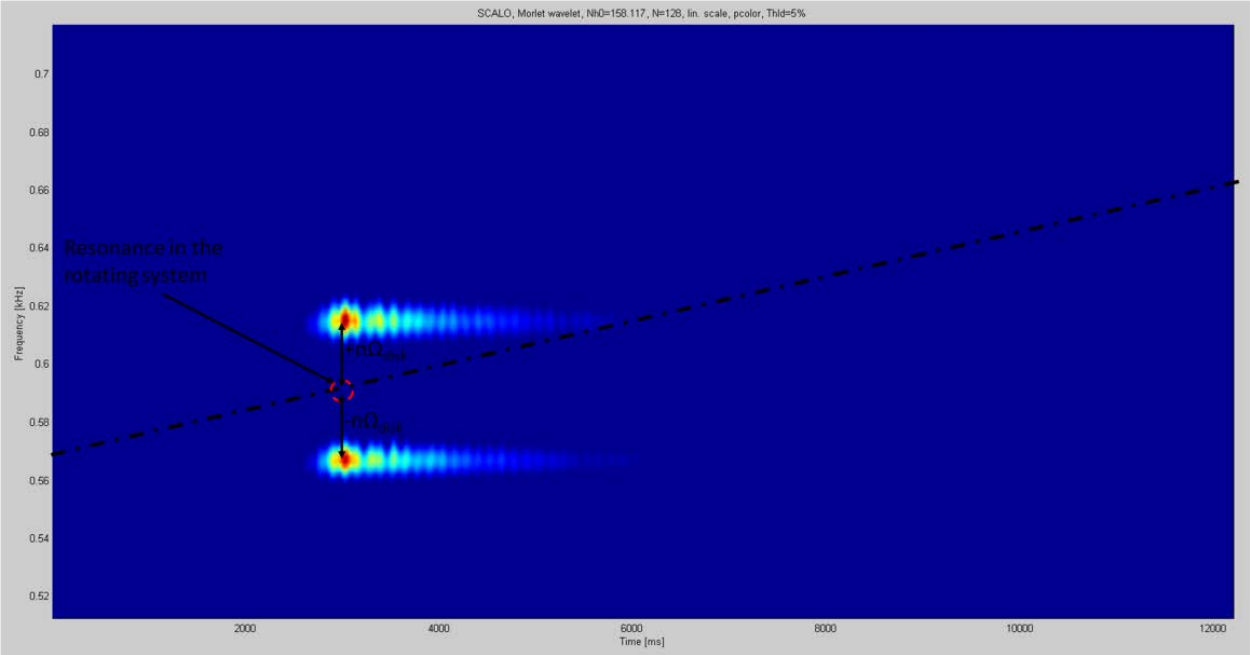

Figure 6.3: Detection of the resonance with the Laser

In this case two clear peaks are detected with the Laser separated at $\pm n\Omega_{disk}$ from the natural frequency detected from the stationary frame. To see the amplitudes of the resonance with the different sensors, the peak hold method is used [58].

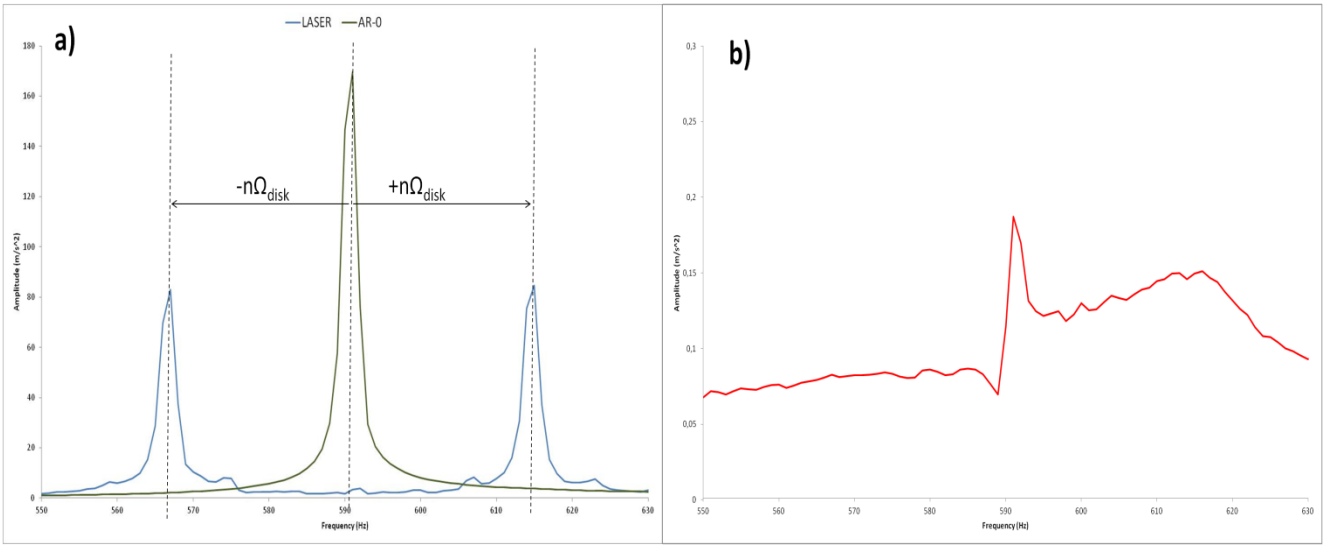

Figure 6.4: Amplitude of the resonance with the peak hold method. a) Laser and AR-0 b)AS-180

As seen in *Figure 6.4* the amplitude of the Laser vibration in the two peaks is approximately the half of the amplitude measured with the accelerometer AR-0 as predicted by *Equation (2.51).* It is not exactly the half since the Laser is not pointing exactly in the same radial position (the Laser is located 5mm closer to the center). The amplitude detected with the accelerometer AS-180 is much lower and approximately 1/1000 of the amplitude detected from the rotating frame, which means that the transmission through a stiff system as the shaft bearings and casing is very low. Therefore, to use the Laser or other non contact sensors measuring directly the disk is very advantageous if it is desired to measure the response of the rotating system when the fluid between the rotating and the stationary system is air.

6.2Detection of the disk natural frequencies and mode shapes in water

In this case, since the fluid between the disk and casing has a high density, the dynamic pressure caused by the vibration of the disk excites the casing with an excitation shape that is determined by the mode shape of the disk. When the disk is rotating in water, the mode shapes of the disk for each number of diametrical nodes n are a pair of travelling waves (Chapter 4); the lower one, travelling in the same direction than the disk and the upper one,

travelling in counter disk direction. These are transmitted only as one frequency in the stationary frame. Considering the sign of n, these natural frequencies are (*Equation (2.59)bis*):

$$\omega_{n,casing} = \omega_{n,disk} + n\Omega_{disk} \qquad (2.59)bis$$

In this section it will be discussed if it is possible to determine not only the natural frequency but also the mode shape. Therefore the equation of the casing vibration is also considered. If it is considered that the casing vibration is dominated by the disk vibration (see Chapter 2):

$$\mathbf{w_c}(\boldsymbol{r}, \boldsymbol{\theta_c}, \boldsymbol{t}) = \boldsymbol{W_{c,n}}(\boldsymbol{r}) \mathbf{cos}((\boldsymbol{\omega_n} + \boldsymbol{n\Omega_{disk}})\boldsymbol{t} + \boldsymbol{n\theta_c} + \boldsymbol{\Psi_c}) \qquad (2.58)bis$$

6.2.1 Laser

Under the assumptions that the Laser beam is pointing directly on the disk (properly focused) and that the motion of the casing is negligible in front the motion of the disk it can be considered that the amplitude detected is the same as the amplitude of vibration detected with a sensor on the rotating frame located in the same radial position, but with a frequency shift (*Equation (2.58)*). In the experimental test rig, analyzing the time signal with wavelets in the time-frequency domain the following diagram is obtained:

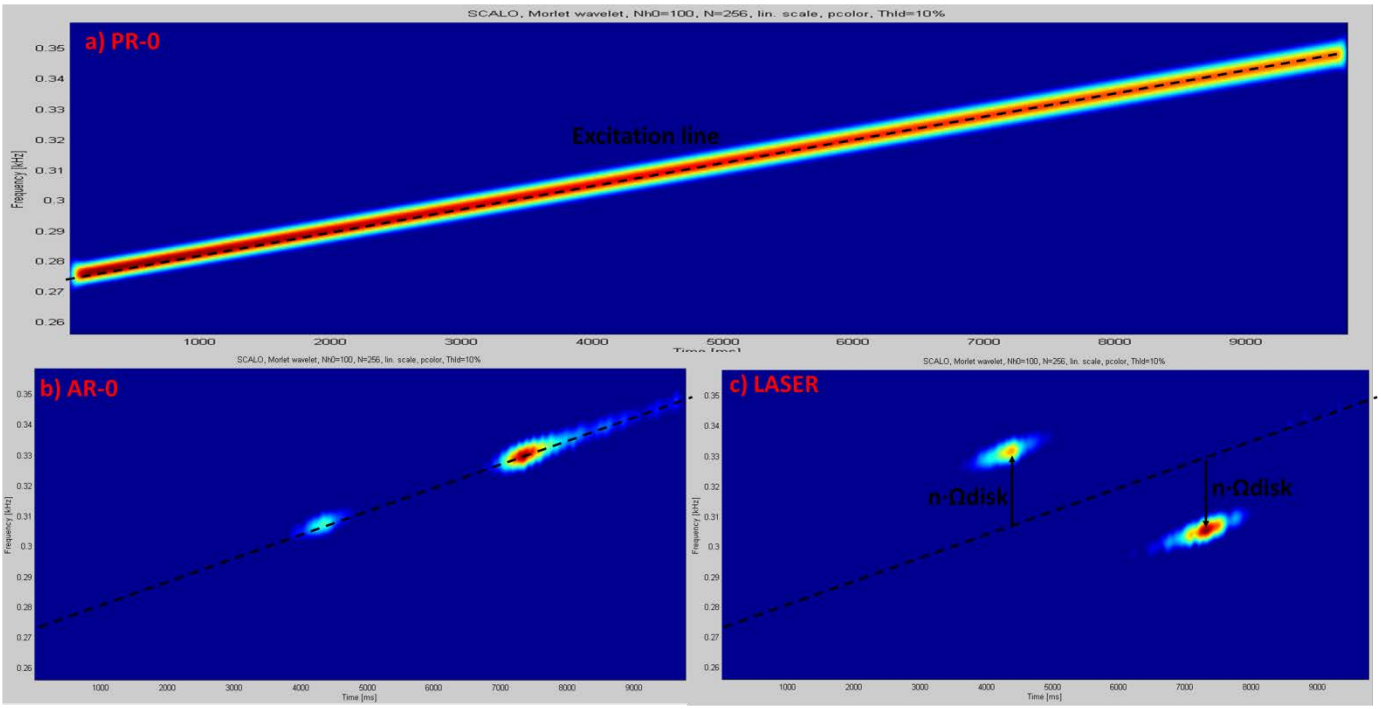

Figure 6.5: a) Excitation characteristic with a sweep excitation (PR-0) b) Response detected from the rotating system (AR-0) c) Response detected with the LASER

As predicted by *Equation (2.59),* one natural frequency in the rotating frame is transmitted to one natural frequency in the stationary frame. The lower natural frequency of the rotating frame (n-positive) is transmitted to a higher natural frequency in the stationary frame and the higher natural frequency of the rotating frame (n-negative) is transmitted to a lower natural frequency in the stationary frame. Using the peak hold method the amplitude of the resonance can be evaluated.

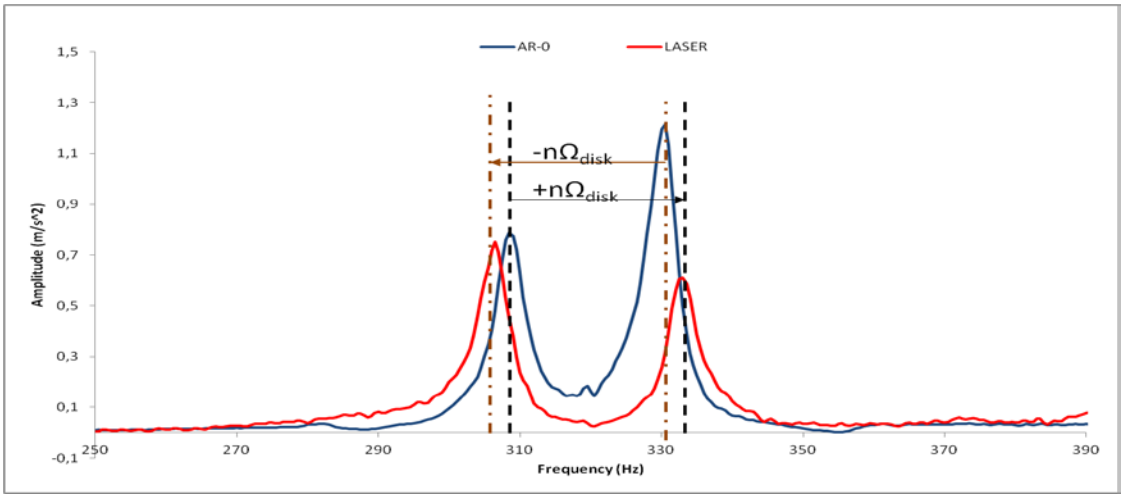

Figure 6.6: Amplitude of resonance of the modes n=3 and n=-3 with the accelerometer AR-0 and LASER

Since the Laser is pointing directly on the disk, the amplitude of the resonance detected by this sensor is approximately the same amplitude as detected with the accelerometer on the rotating frame. From the experimental point of view, it is a very hard task to focus the Laser properly. Also the transparency of the water is very important to have a good measurement. Otherwise the Laser sensor will also measure the vibration of the water and not the vibration of the disk surface as desired.

According to the manufacturer the Laser beam should look as thin as possible on the target surface. If the target (the rotating part) is not visible, it is not possible to see if the beam is a small spot or not as required to make a good measurement. In this case, a reference sensor in the rotating frame is necessary to compare the response.

6.2.2 Pressure sensors

The same resonance is detected from the stationary frame by means of pressure sensors. The shift in frequency, predicted by *Equation* (2.59), is also seen in this case:

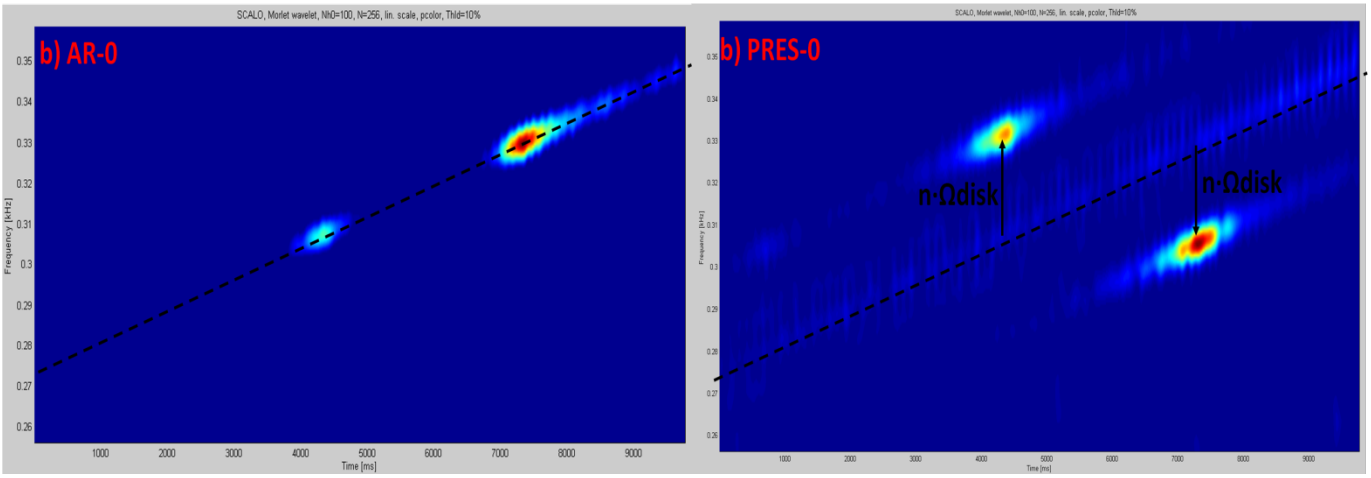

Figure 6.7: a) Response detected from the rotating system (AR-0) b) Response detected with the pressure sensor

Three pressure sensors are installed on the disk as mentioned in Chapter 3.3.2. The phase between them for one mode should be

$$\Delta\boldsymbol{\alpha} = \boldsymbol{n}\Delta\boldsymbol{\theta_c} \qquad \text{(2.60)bis}$$

In this case, with the peak hold method the following amplitudes and phases relative to the sensor PRES-0 are obtained for the modes n=3 and n=-3.

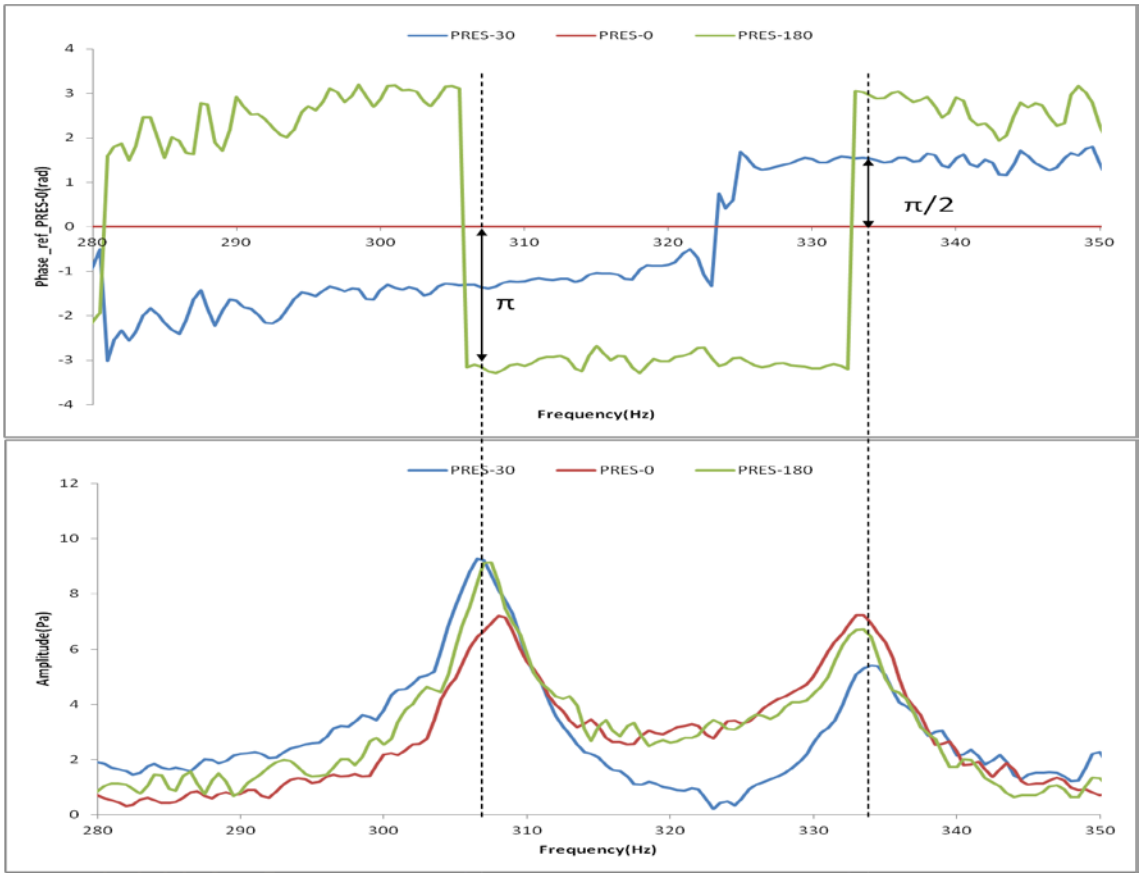

Figure 6.8: Amplitude of the pressure sensors and phase with respect to pressure sensor "PRES-0"

As predicted by *Equation (2.60)*, the phase shift between the pressure sensors correspond to the modes n=±3. In both peaks the phase of two sensors at 180º (PRES-0 and PRES-180) is π rad according to *Equation (2.60).* For this reason, with these two sensors, the direction of the travelling wave cannot be determined. Considering two sensors at 30º from each other (PRES-0 and PRES-30) the phase shift should be ±90º or ±π/2 rad. In the first peak a phase shift of **-π/2** is observed, which means that the wave is travelling in direction from PRES-0 to PRES-30. This correspond to a travelling wave rotating in the opposite direction than the disk, corresponding to the mode n=-3 in the rotating frame. In the second peak a phase shift of π/2 is observed, which indicates the mode n=3 in the rotating frame.

6.2.3 Accelerometers

When the same case of study is measured with accelerometers placed on the casing, also the same frequency modulation is observed (*Figure 6.9)*

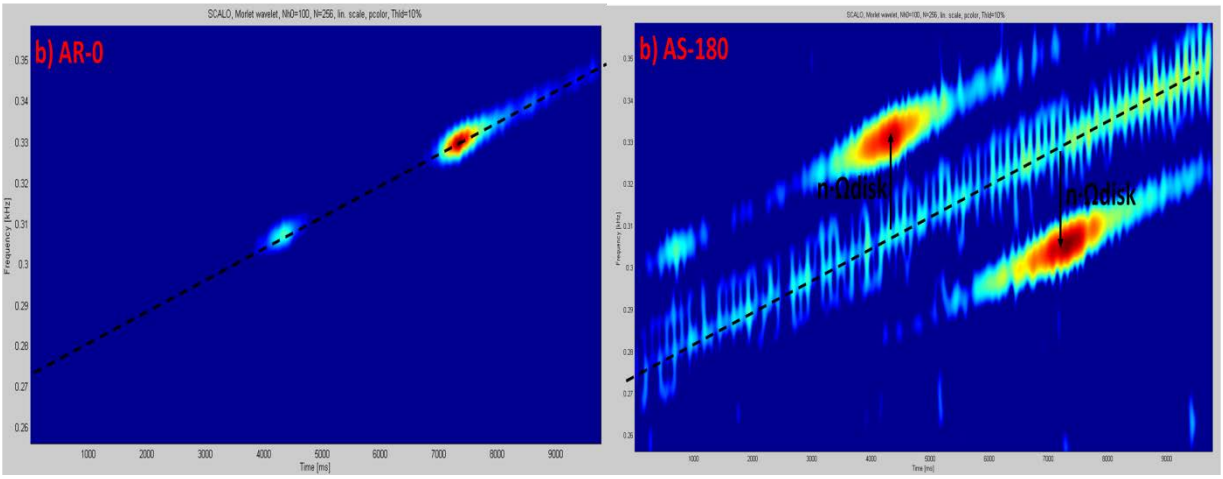

Figure 6.9: a) Response detected from the rotating system (AR-0) b) Response detected from the stationary frame (AS-180)

With the peak hold method, the amplitude of the resonance is studied from the rotating frame and from the stationary frame (*Figure 6.10*).

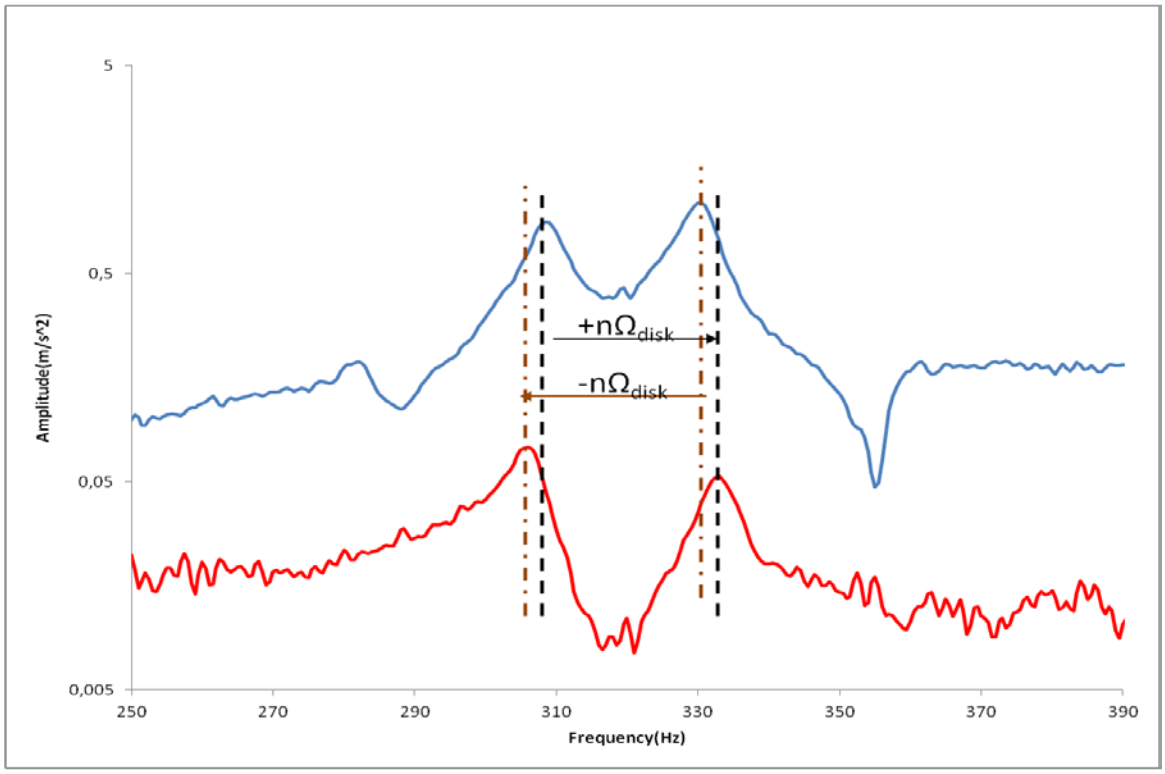

Figure 6.10: Amplitude of resonance of the modes n=3 and n=-3 with the accelerometer AR-0 (blue line) and AS-180 (red line)

From this figure it can be appreciated that the amplitude of the resonance detected with the accelerometer is much lower as when it is detected with the Laser In this case, what AS-180 measures is the forced response of the upper cover that is excited with the water. Therefore, the response of the accelerometers on the stationary system depends not only on the amplitude of vibration in the rotating frame but also on the fluid between disk and casing and on the stiffness of the cover itself. For an absolutely rigid cover, this amplitude would be 0 (see chap. 2). If the cover is not absolutely rigid, then the natural frequencies of the rotating system can be theoretically detected with the accelerometers placed on it.

Analyzing the phase shift of three sensors (*Figure 6.11*), with the same relative position to each other as the pressure sensors, the same phase shift is obtained as in those sensors (*Figure 6.8*)

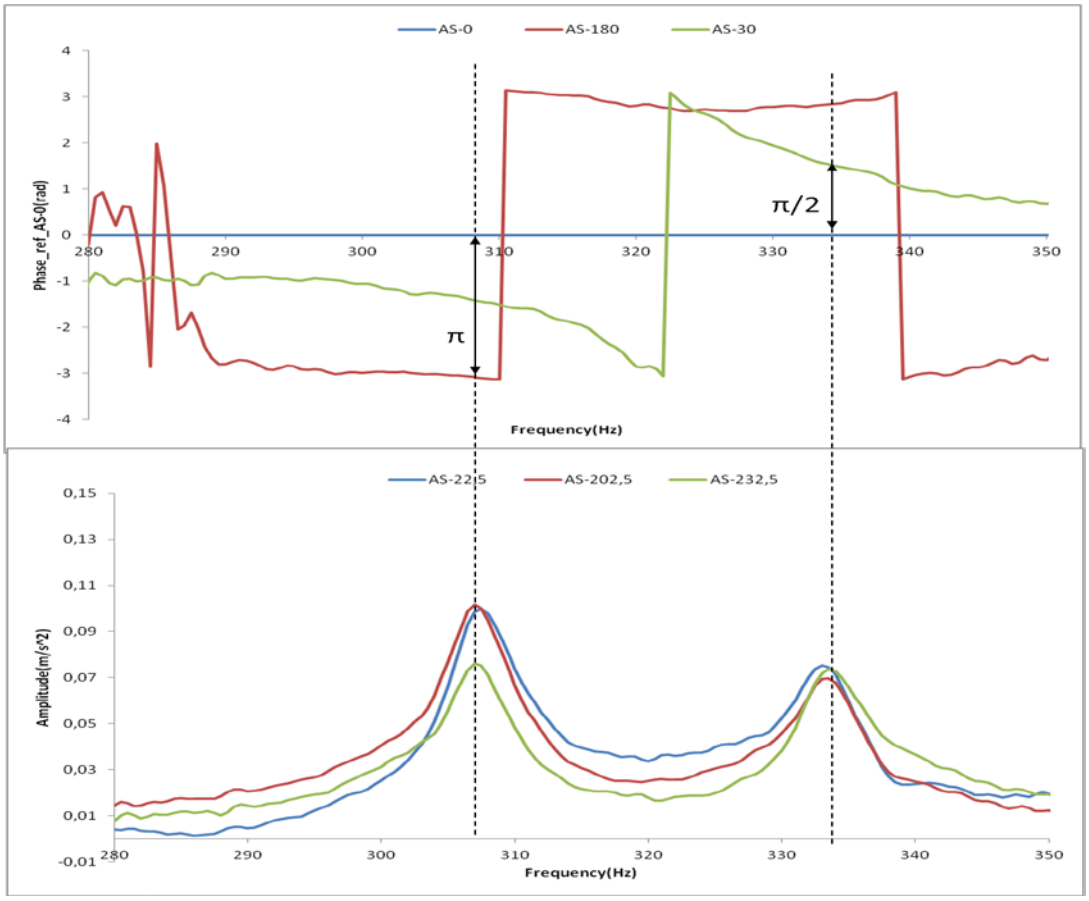

Figure 6.11: Amplitude of the accelerometers on the stationary frame and phase with respect to accelerometer "AS-0"

6.2.4 Detailed response of the casing for one configuration

To have a better view of the mode shape viewed from the casing when the disk is rotating in water, several accelerometers have been used in different series, performing the rowing accelerometer method and hitting the disk for each serie. Detail of the accelerometer positions and impact positions is shown in Figure 3.9.

This experimentation has been performed for H_{up}/r_{out}=0.05 and non rotating disk (Ω_{disk}= 0Hz) and for the same H_{up} and disk rotating at 8Hz (Ω_{disk}= 8Hz).

In the non rotating disk case, the modes n=±2; ±3 of the disk (stationary waves) can be clearly seen.

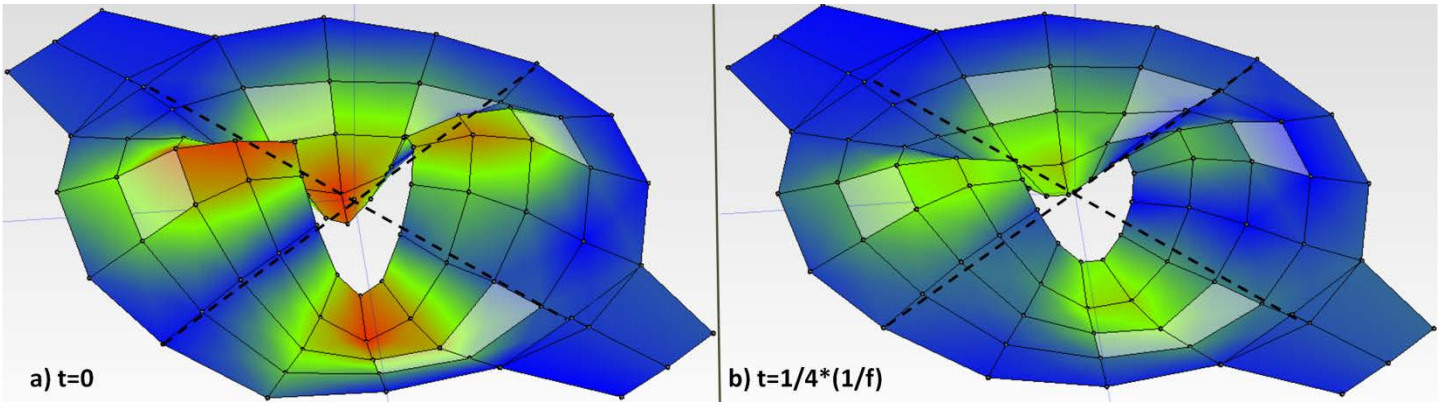

Figure 6.12: Mode n=±2 detected from the casing. Ω_{disk}=0Hz

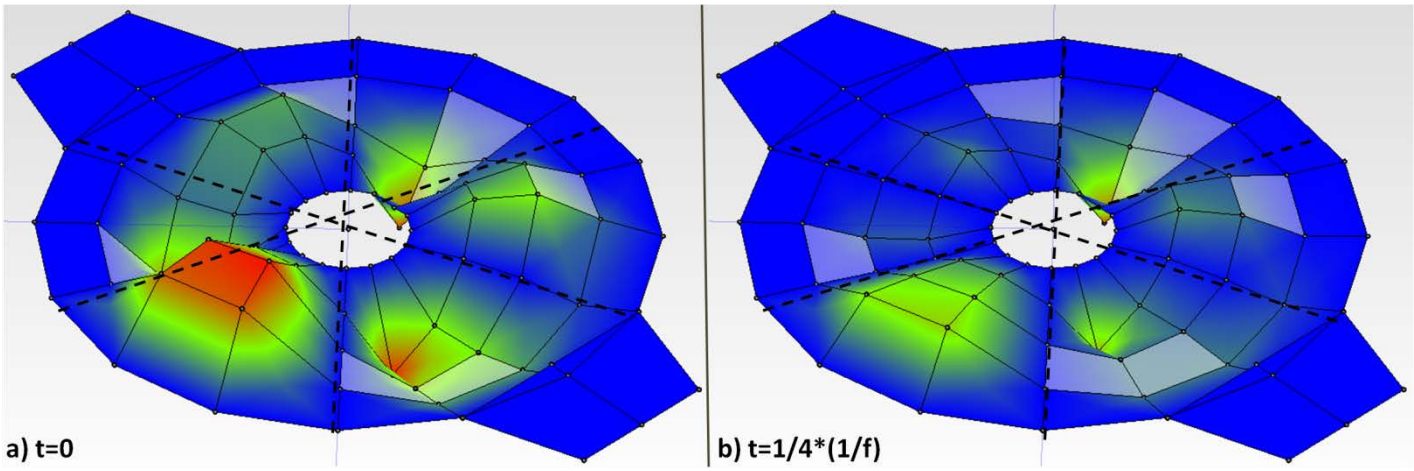

Figure 6.13: Mode n=±3 detected from the casing. Ω_{disk}=0Hz

As seen in both cases, the nodal diameters do not rotate in time, and this indicates the presence of standing waves on the disk with all the points moving in phase or in counterphase to each other.

When the disk is rotating, as predicted by *Equation (2.16)* two travelling waves appear for each diametrical node n. The lower frequency from the rotating frame, which corresponds to the higher frequency in the stationary frame *(Figure 6.5)*, rotates in the same direction than the disk. The higher frequency from the rotating frame, which corresponds to the lower frequency in the stationary frame, rotates in the opposite direction than the disk.

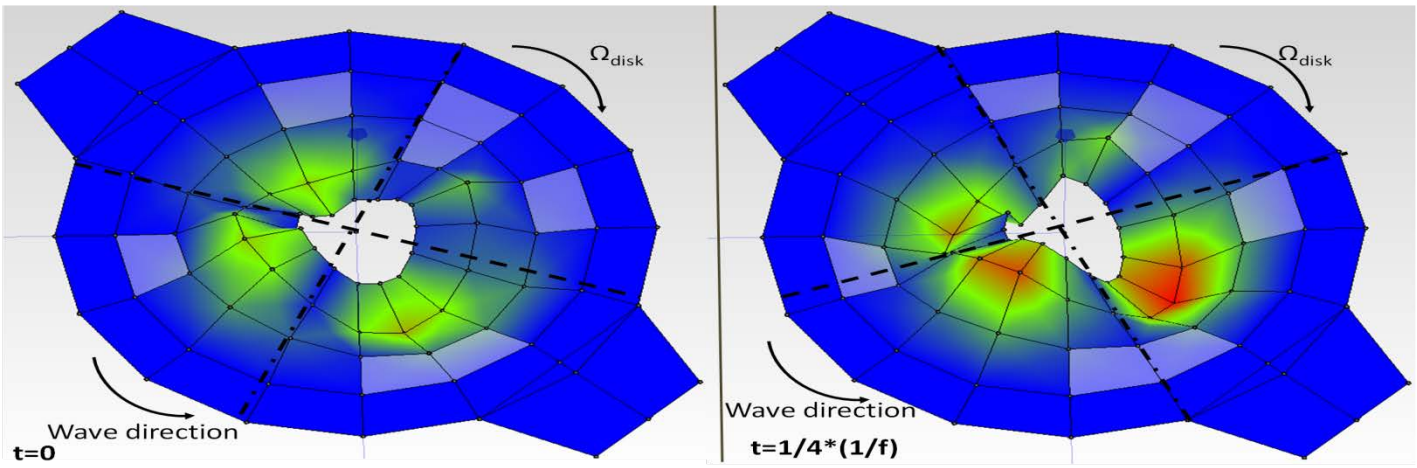

Figure 6.14: Mode n= -2 detected from the casing. Ω_{disk}=8 Hz

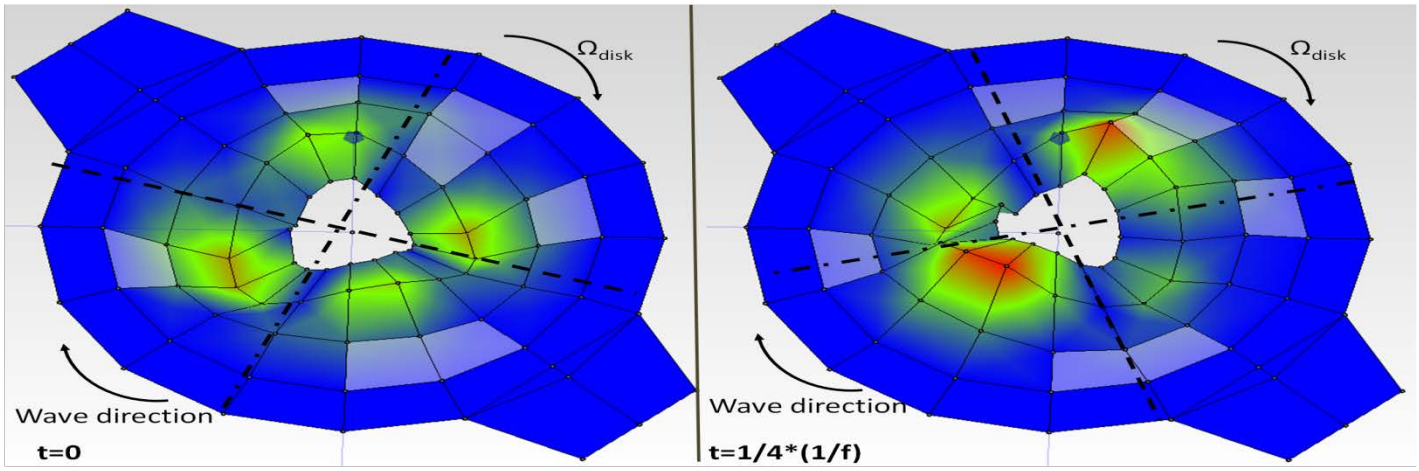

Figure 6.15: Mode n=2 detected from the casing. Ω_{disk}=8 Hz

As seen in *Figure 6.14* the nodal diameters rotate in counter direction than the disk. In ¼ of the period they have rotated approximately 45º. This mode is the mode n=-2 of the rotating frame which correspond to the lower frequency in the stationary frame for this pair of modes. *Figure 6.15* shows the higher frequency (mode n=2).

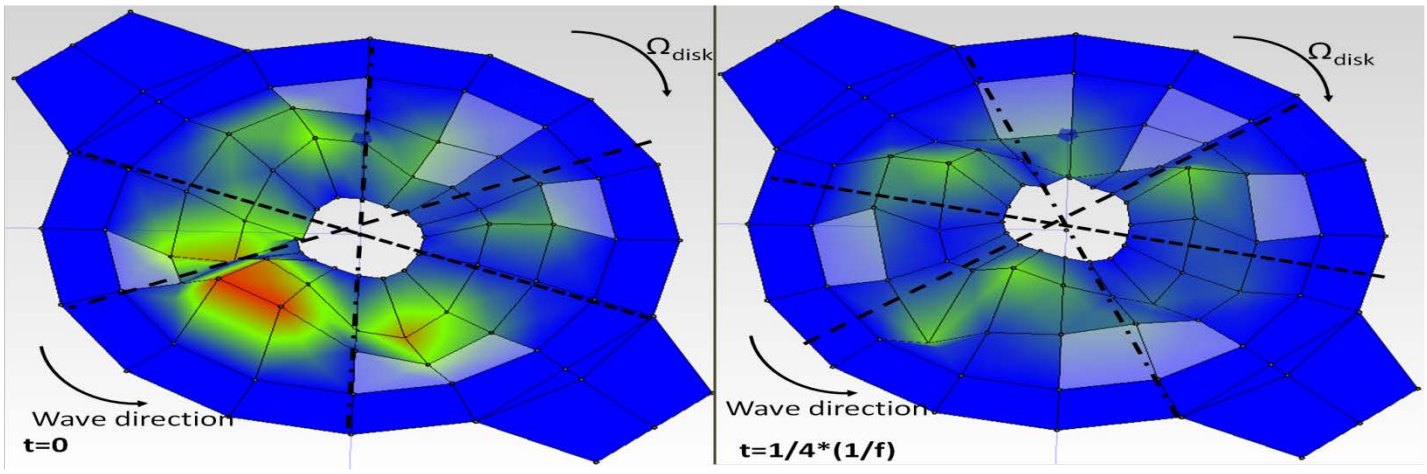

Figure 6.16: Mode n= -3 detected from the casing. Ωdisk=8 Hz

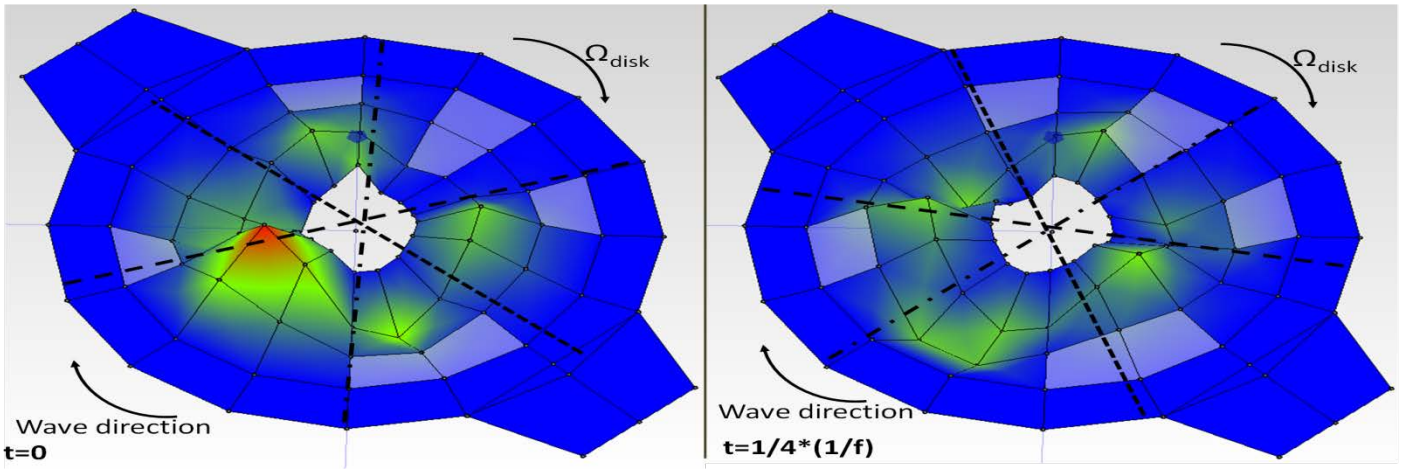

Figure 6.17: Mode n=3 detected from the casing. Ωdisk=8 Hz

As seen in *Figure 6.16* the nodal diameters rotate in counter direction than the disk. In ¼ of the period they have rotated approximately 30º. This mode is the mode n= -3 of the rotating frame which correspond to the lower frequency in the stationary frame (first peak in *Figure 6.11). Figure 6.15* shows the mode shape corresponding to the second peak in *Figure 6.11* (mode n=3).

6.2.5 Influence of the casing

As mentioned in Chap. 2.4, it is possible to see the mode shape from the casing so far the response of the casing is not high (compared to the disk response) in the frequency band of the natural frequencies of the disk. This happens in the studied test rig for the modes n=±2 and n==±3 (at least for H_{up}/r_{out}=0.05). As *Figure 6.18* shows, for these two pair of modes the response of the casing is low and the mode shape is well transmitted to the upper cover (as justified in chap. 2.4.3 and shown experimentally in *Figure 6.14-Figure 6.17*)

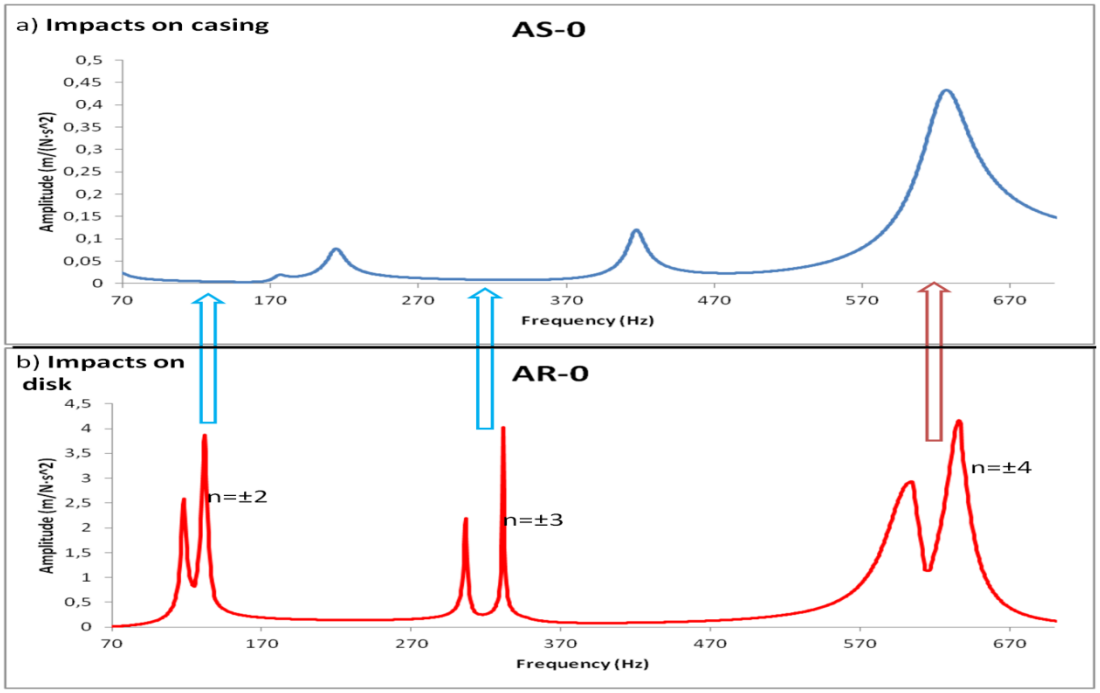

Figure 6.18:a) Response of the casing due to an impact on the casing b) Response of the disk due to an impact on the disk

Nevertheless for the pair of modes n=±4 there is a high response of the casing and the mode shape is not recognisable from the stationary frame as shown in *Figure 6.19.*

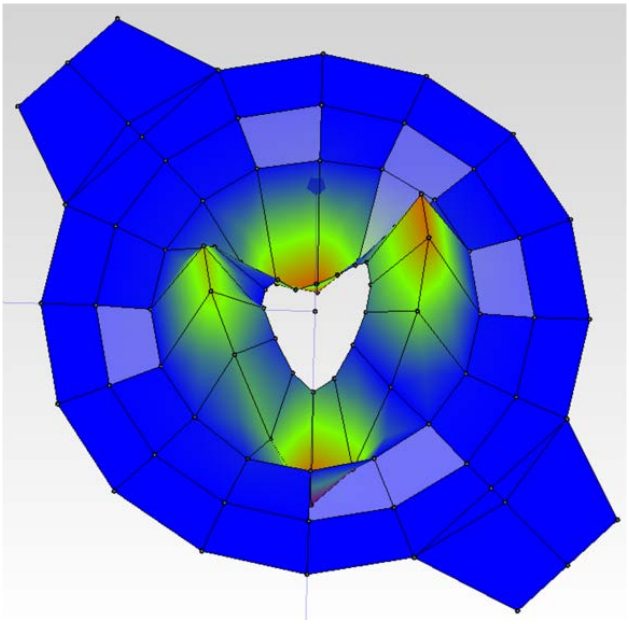

Figure 6.19: Transmission of the mode n=-4 to the casing

In this case the transmission of the mode n= -4 is not transmitted as a n=-4 in the casing, but as a n=±2, since in this frequency band the casing is dominated with the peak shown in Figure 6.18a, which has this kind of mode shape.

6.3 Partial conclusions

In this chapter, the detection of the natural frequencies and mode shapes of a rotating disk-like structure from the stationary frame has been studied experimentally and contrasted with the analytical model. The case of a disk that rotates in air (where the effects of the surrounding fluid can be neglected) has been analyzed in other researches but no studies have been found analyzing the same topic for a rotating disk-like structure surrounded by a heavy fluid (such as water). Only the diametrical modes, characterized by the number of nodal diameters n, which are the most relevant in case of turbomachinery components, are discussed here.

Analyzing the rotating disk in air for one natural frequency in the rotating frame, simultaneously two natural frequencies are detected in the stationary frame shifted $\pm n\Omega_{disk}$ from the natural frequency detected in the rotating frame.

In water, the lower natural frequency in the rotating frame, which is a travelling wave rotating in the same direction than the disk, is transmitted to a higher frequency in the

stationary frame (frequency shift of $+n\Omega_{disk}$). The higher natural frequency in the rotating frame, which is a travelling wave rotating in counter direction than the disk, is transmitted to a lower frequency in the stationary frame (frequency shift of $-n\Omega_{disk}$). This has been proved using a time-frequency analysis with wavelets.

Not only the transmission of the natural frequencies has been studied, but also the transmission of the mode shapes. Experimental results have shown that a mode shape is transmitted from the rotating to the stationary frame if the response of the casing at the considered natural frequency is not relevant in comparison to the response of the disk. This has been checked with several types of sensors placed on the stationary frame, such as accelerometers, pressure sensors and Laser.

Chapter 7

7. CONCLUSION AND FUTURE WORK

7.1Conclusions and contributions

A complete study of the dynamic behaviour of a rotating disk submerged in water has been performed. First the natural frequencies of the rotating disk in air and in water have been determined. The disk has been also excited with rotating excitation patterns that simulate the rotor-stator interaction excitation (RSI), that occurs in many turbomachinery components. The response of the disk has been analyzed from the rotating and from the stationary frame. The following conclusions and contributions have been achieved.

Excitation and measurement of the response have been performed from the rotating frame through a slip ring system. It has been demonstrated that PZT actuators are feasible to excite thick and submerged structures.

In air, for the tested speeds (10 Hz), only a slight increase of less than 1% is observed when analyzing the natural frequencies from the rotating frame.

The effect of rotation of the surrounding water has been determined as a fundamental change not only in the natural frequencies, but also in the mode shapes. Even for low rotating speeds of the disk (0-8Hz), which is in range of actual hydraulic turbomachinery, the surrounding water has a great influence in the value of the natural frequencies and in the nature of the mode shapes.

In air, each diametrical mode of the rotating disk corresponds to a standing wave. In water, for each diametrical mode, there is a first peak (lower frequency) which corresponds to a travelling wave, moving in the rotating direction of the disk and a second peak (higher frequency) which corresponds to a travelling wave, moving in the opposite direction.

The dynamic response of the rotating disk in water at one natural frequency depends on the excitation shape and also on the rotating direction of the excitation. When the excitation is fixed on the rotating frame, the response at the two natural frequencies of the corresponding diametrical mode is amplified. However when the excitation spins in the

same direction of the disk only the lower natural frequency is excited, which corresponds to the travelling wave travelling in the same direction as the disk. When the excitation spins in the opposite direction only the higher natural frequency is excited, which corresponds to the travelling wave travelling in the opposite direction. If the excitation shape does not coincide with the diametrical mode considered, the response at both natural frequencies is almost zero (for the studied configuration of patches). When the disk rotates in air, only the excitation shape affects the dynamic response. If the excitation shape coincides with a diametrical mode, the response of the disk is amplified at the corresponding natural frequency, with no matter of the rotating direction of the excitation (rotating with the disk, counterwise or standing).

In air one natural frequency in the rotating frame is transmitted into two natural frequencies in the stationary frame. In water the lower natural frequency of the corresponding mode n is transmitted to a higher frequency in the stationary frame and the higher natural frequency is transmitted to a lower frequency in the stationary frame. The frequency shift between both systems depends on the rotating speed of the disk and on the diametrical mode n (frequency shift $\pm n\Omega_{disk}$).

A mode shape of the disk can be viewed from the casing with different kind of sensors, if the casing has not a relevant response (compared to the disk) in the frequency band of the considered natural frequency of the disk.

All the experimental results have been validated with the analytical model presented and with numerical FEM simulation

7.2Future work

In order to investigate the dynamic behavior of more complex mechanical systems including rotating disk-like structures such as impellers, some points have to be studied in detail.

On one side, the effect of rotation in more complex structures such as bladed-disk structures has to be studied. Particularly when these structures are submerged in water, the effect of rotation in the natural frequencies could be very important.

On the other side, the effect of non rigid casings has to be analyzed in detail since this affects not only in the natural frequency prediction of the rotating structure but also on the transmission and detection of these natural frequencies from the stationary frame.

REFERENCES

[1] G. Jacquet-Richardet, M. Torkhani, P. Cartraud, F. Thouverez, T. Nouri, M. Herran, C. Gibert, S. Baguet, P. Almeida, L. Peletan, Rotor to stator contacts in turbomachines.Review and application, Mechanical Systems and Signal Processing, 40 (2013) 401-420.
[2] V.N. Shlyannikov, B.V. Iltchenko, N.V. Stepanov, Fracture analysis of turbine disks and computational-experimental background of the operational decisions, Engineering Failure analysis, 8 (2001) 461-475.
[3] E. Egusquiza, C. Valero, X. Huang, E. Jou, A. Guardo, C. Rodriguez, Failure investigation of a large pump-turbine runner, Engineering Failure analysis, 23 (2012) 27-34.
[4] H. Ohashi, Case study of pump failure due to rotor stator interaction, International Journal of Rotating Machinery 1, (1994) 53-60.
[5] H. Tanaka, Vibration behavior and dynamic stress of runners of very high head reversible pump-turbines, IAHR Symposium, Belgrade Yugoslavia, section U2.
[6] H. Ohashi, Vibration and oscillation in hydraulic machinery, Avebury Technical Press, 1991.
[7] J. Raabe, The design, use, and function of hydromechanical, hydraulic and electrical equipment, in, VDI-Verlag GmbH, 1985.
[8] Y. Kubota, H. Ohashi, A study on the natural frequencies of hydraulic pumps, 1st ASME Joint International Conference on Nuclear Engineering, (1991) 589-593.
[9] E. Egusquiza, Comportament dinámic de máquines hidráuliques, Edicions UPC, Barcelona, 2003.
[10] C. Nicolet, N. Ruchonnet, F. Avellan, One-Dimensional Modeling of Rotor Stator Interaction in Francis Pump-Turbine, 23rd IAHR Symposium - Yokohama, (2006).
[11] G. Jacquet-Richardet, G. Ferraris, P. Rieutord, FREQUENCIES AND MODES OF ROTATING FLEXIBLE BLADED DISC-SHAFT ASSEMBLIES: A GLOBAL CYCLIC SYMMETRY APPROACH, Journal of Sound and Vibration, 191 (1996) 901-915.
[12] F. Ehrich, Handbook of rotor dynamics, McGraw Hill, 1991.
[13] C.G. Rodriguez, E. Egusquiza, X. Escaler, Q.W. Liang, F. Avellan, Experimental investigation of added mass effects on a Francis turbine runner in still water, Journal of Fluids and Structures, 22 (2006) 699-712.
[14] X. Huang, Contribution to the Dynamic Response of Hydraulic Turbomachinery Components, in: CDIF, UPC, Barcelona, 2011.
[15] Q.W. Liang, C.G. Rodríguez, E. Egusquiza, X. Escaler, M. Farhat, F. Avellan, Numerical simulation of fluid added mass effect on a francis turbine runner, Computers and Fluids, 36 (2007) 1106-1118.
[16] T.K. Ahn, C.D.M. Jr, Mode Identification of a Rotating Disk, Experimental Mechanics, 38 (1998) 250-254.
[17] X. Wang, Z. Huang, Feedback Control and Optimization for Rotating Disk Flutter Suppression with Actuators Patches, AIAA Journal, 44 (2006) 892-900.
[18] H.F. Bauer, W. Eidel, Transverse vibration and stability of spinning circular plates of constant thickness and different boundary conditions, Journal of Sound and Vibration, 274 (2007) 877-895.

[19] L. Pust, L. Pesek, Vibration of circular bladed disk with imperfections, Journal of Bifurcation and Chaos, 10 (2011) 2893-2904.
[20] S.A. Tobias, R.N. Arnold, The Influence of Dynamical Imperfection on the Vibration of Rotating Disks, Proceedings of the Institution of Mechanical Engineers, 171 (1957) 669-690.
[21] J.A.N. Hengstler, Influence of the Fluid-Structure Interaction on the Vibrations of Structures, in, ETH Zurich, Zurich, 2013.
[22] W. Campbell, The protection of steam turbine disk wheels from axial vibration, Transactions of the ASME, 46 (1924) 272-280.
[23] H. Lamb, R.V. Southwell, The vibrations of spinning discs, Proceedings of the Royal Society London, 99 (1921) 272-280.
[24] R.V. Southwell, On the free transverse vibrations of a uniform circular disc clamped at its centre and on the effects of rotation, Proceedings of the Royal Society London, 101 (1922) 133-153.
[25] J.W. Heo, J. Chung, Vibration analysis of a flexible rotating disk with angular misalignment, Journal of Sound and Vibration, 274 (2004) 821-841.
[26] L. Pust, L. Pesek, Vibration of imperfect rotating disk, Applied and Computational Mechanics, 5 (2011) 205-216.
[27] M.K. Kwak, Vibration of circular plates in contact with water, Journal of Applied Mechanics, 58 (1991) 480-483.
[28] H. Lamb, On the vibrations of an elastic plate in contact with water, Proceedings of the Royal Society of London, A 98 (1921) 205-216.
[29] C.G. Rodriguez, P. Flores, F.G. Pierart, L.R. Contzen, E.Egusquiza, Capability of structural-acoustical FSI numerical model to predict natural frequencies of submerged structures with nearby rigid surfaces, Computers&Fluids, 64 (2012) 117-126.
[30] C. Harrison, E. Tavernier, O. Vancauwenberghe, E. Donzier, K. Hsu, A. Goofwin, F. Marty, B. Mercier, On the response of a resonating plate in a liquid near a solid wall, Sensors and Actuators A: Physical, 134 (2007) 414-426.
[31] E. Askari, K.-H. Jeong, M. Amabili, Hydroelastic vibration of circular plates immersed in a liquid-filled container with free surface, Journal of Sound and Vibration, 332 (2013) 3064-3085.
[32] C. Rodriguez, Feasibility of on board measurements for Predictive Maintenance in Large Hydraulic Turbomachinery, Doctoral Thesis, 2006.
[33] R. Parker, J.F. Watson, Interaction effects between blade rows in turbomachines, Proceedings of the Institute of Mechanical Engineers, 186 (1972) 331-340.
[34] R.P. Dring, H.D. Joslyn, L.W. Hardin, J.H. Wagner, Turbine rotor-stator interaction, ASME Journal of Engineering for Power, 104 (1982) 729-742.
[35] Y. Kubota, T. Susuki, H. Tomita, T. Nagafuji, T. Okamura, Vibration of rotating bladed disc excited by stationary distributed forces, Bulletin of the JSME, 26 (1985) 1952 – 1957.
[36] T. Iino, K. Kasai, An analysis of unsteady flow induced by interaction between a centrifugal impeller and a vaned diffuser, Transactions of the Japan Society of Mechanical Engineers, 51 (1985) 154 – 159.
[37] N. Arndt, A. Acosta, C.E. Brennen, T.K. Caughey, Rotor-stator interaction in a diffuser pump, ASME Journal of Turbomachinery, 111 (1989) 213 – 221.

[38] A. Zobeiri, J.-L. Kueny, M. Farhat, F. Avellan, Pump-turbine Rotor-Stator Interactions in Generating Mode: Pressure Fluctuation in Distributor Channel, 23rd IAHR Symposium - Yokohama, (2006).
[39] Z. Yang, S. GUo, J. Yang, Y. Hu, Electrically forced vibration of an elastic plate with a finite piezoelectric actuator, Journal of Sound and Vibration, 321 (2009) 242-253.
[40] O. Gomis-Bellmunt, F. Ikhouanne, D. Montesinos-Miracle, Control of a piezoelectric actuator considering hysteresis, Journal of Sound and Vibration, 326 (2009) 383-399.
[41] C.C. Cheng, C.C. Lin, An impedance approach for vibration response synthesis using multiple PZT actuators, Sensors and Actuators A 118 (2005) 116-126.
[42] E.M. Sekouri, Y.-R. Hu, A.D. Ngo, Modeling of a circular plate with piezoelectric actuators, Mechatronics, 14 (2004) 1007-1020.
[43] T. Yan, X. Xu, J. Han, R. Lin, B. Ju, Q. Li, Optimization of Sensing and Feedback Control for Vibration/Flutter of Rotating Disk by PZT Actuators via Air Coupled Pressure, Sensors, 11 (2011) 3094-3116.
[44] H. Mehdigholi, Forced vibration of rotating discs and interaction with non-rotating structures, in: Imperiall College of Science, Technology and Medicine London, 1991.
[45] M.Amabili, M.K. Kwak, Free vibrations of circular plates coupled with liquids: Revising the Lamb problem, Journal of Fluids and Structures, 10 (1996) 743-761.
[46] M.Amabili, G.Forsali, M.K. Kwak, Free vibrations of annular plates coupled with fluids, Journal of Sound and Vibration, 191 (1996) 825-846.
[47] M.Amabili, Effect of finite fluid depth on the hydroelastic vibration of circular and annular plate, Journal of Sound and Vibration, 193 (1996) 909-925.
[48] A.W. Leissa, Vibration of Plates, Goverment Printing Office, Washington (USA), 1969.
[49] R. Belvins, Formulas for natural frequency and mode shape, Krieger Publishing Company, 1984.
[50] C.C. Liang, Y.S. Tai, P.L. Li, Natural frequencies of annular plates having contact with fluid, Journal of Sound and Vibration, 228 (1999) 1167-1181.
[51] F. White, Fluid mechanics, McGraw-Hill, 1979.
[52] D.J. Ewins, Modal testing theory and practice, Research Studies Press, 1984.
[53] K. Singh, A.K. Mallik, Wave propagation and vibration response of a periodically supported pipe conveying fluid, Journal of Sound and Vibration, 54 (1977) 55-66.
[54] G.M. Wood, L.K. Knudsen, F.G. Hammitt, Cavitation Damage Studies With Rotating Disk in Water, Journal of Fluids Engineering, 89 (1967) 98-109.
[55] J. Zhiye, EXPERIMENTAL INVESTIGATION ON CAVITATION AND CAVITATION EROSION WITH ROTATING DISK, in: American Society of Mechanical Engineers, Fluids Engineering Division (Publication) FED, 1985, pp. 31-39.
[56] O. De La Torre, X. Escaler, E. Egusquiza, M. Farhat, Experimental investigation of added mass effects on a hydrofoil under cavitation conditions, Journal of Fluids and Structures, 39 (2013) 173-187.
[57] C. Nicolet, N. Ruchonnet, F. Avellan, One-Dimensional Modeling of Rotor Stator Interaction in Francis Turbine, in: 23rd IAHR Symposium, Yokohama, 2006.
[58] W. Heylen, Modal Analysis Theory and Testing, Katholieke Universiteit Leuven, Leuven, 2007.
[59] F. Anger, P. Flandin, P. Gonçalves, O. Lemoine, Time-Frequency Toolbox, in: C.a.R. University (Ed.), 1996.